# Distinguishing mature and immature trees allows to estimate forest carbon uptake from stand structure

Samuel M. Fischer[1,2], Xugao Wang[3], and Andreas Huth[1,2,4]

[1]Helmholtz Centre for Environmental Research – UFZ, Dept. of Ecological Modelling, Permoserstr. 15, 04318 Leipzig, Germany.

[2]Osnabrück University, Institute of Environmental Systems Research, Barbarastr. 12, 49076 Osnabrück, Germany.

[3]Chinese Academy of Sciences, Institute of Applied Ecology, PO Box 417, Shenyang 110016, China.

[4]German Centre for Integrative Biodiversity Research (iDiv) Halle-Jena-Leipzig, Puschstr. 4, 04103 Leipzig, Germany.

**Correspondence:** Samuel M. Fischer (samuel.fischer@ufz.de)

**Abstract.** Relating forest productivity to local variations in forest structure has been a long-standing challenge. Previous studies often focused on the connection between forest structure and stand-level photosynthesis (GPP). However, biomass production (NPP) and net ecosystem exchange (NEE) are also subject to respiration and other carbon losses, which vary with local conditions and life history traits. Here, we use a simulation approach to study how these losses impact forest productivity and reveal themselves in forest structure. We fit the process-based forest model Formind to a $25\ \mathrm{ha}$ inventory of an old-growth temperate forest in China and classify trees as "mature" (full-grown) or "immature" based on their intrinsic carbon use efficiency. Our results reveal a strong negative connection between the stand-level carbon use efficiency and the prevalence of mature trees: GPP increases with the total basal area, whereas NPP and NEE are driven by the basal area of immature trees. Accordingly, the basal area entropy – a structural proxy for the prevalence of immature trees – correlated well with NPP and NEE and had a higher predictive power than other structural characteristics such as Shannon diversity and height standard deviation. Our results were robust across spatial scales ($0.04$-$1\,\mathrm{ha}$) and yield promising hypotheses for field studies and new theoretical work.

**Keywords:** carbon balance, carbon use efficiency, forest structure, modelling, primary production

## 1 ~~Introduction~~

## 1 Introduction

Understanding the drivers of forest productivity is key for assessing forests' ability to provide ecosystem services (e.g. carbon sequestration or commercial wood production) and to gauge their resilience against disturbances and global change (Costanza et al., 1998; Anav et al., 2015; Jha et al., 2019; Sheil and Bongers, 2020). Forests' net primary production (NPP) may be affected via two pathways: carbon supply, i.e., gross primary production (GPP), and carbon losses due to respiratory costs and other limiting factors (Wiley and Helliker, 2012). Forest structure (e.g. density, species composition, age and size distribution; McElhinny et al., 2005) can be both a factor and result of processes acting on either of these pathways (Waide et al., 1999; Forrester and Bauhus, 2016; Sheil and Bongers, 2020). For example, denser forests may exhibit a larger total leaf area and hence higher stand productivity. Conversely, high productivity of individual trees may lead to denser forests. Hence, identifying the connection between forest structure and productivity is key for a comprehensive understanding of forest productivity.

Several studies have established links between forest structure and carbon supply (Waide et al., 1999; Forrester and Bauhus, 2016). For example, GPP is expected to benefit from higher diversity via improved exploitation of ecological niches and reduced competition, and vertically stratified forests may allow for more efficient light use due to denser leaf packaging (Forrester and Bauhus, 2016; Bohn and Huth, 2017). Nonetheless, it has proven difficult to identify clear relationships between forest structure and NPP (Chisholm et al., 2013), as diverse factors, ranging from resource availability to the impact of biotic agents, affect forest dynamics on different procedural levels (Forrester and Bauhus, 2016), and NPP is not only subject to supply-related but also loss-related factors. A unified framework for forest productivity therefore also needs to address the corresponding role of losses. This is the subject of this study.

A tree's ability to utilize acquired carbon to form biomass can be expressed through its carbon use efficiency ($\mathrm{CUE} = \mathrm{NPP}/\mathrm{GPP}$). In the absence of shading by larger plants, the CUE is expected to decline with tree size, as larger trees have a higher demand for respiration and non-structural carbon (Collalti et al., 2020b; Binkley, 2023). Such respiratory losses and other, external, factors may induce site-dependent tree size maxima, at which biomass accumulation is significantly reduced. The resulting decline of NPP with forest age is well documented on the stand level (Gower et al., 1996; Tang et al., 2014; Collalti et al., 2020a), but the extent at which loss-induced limitations drive variations of NPP on the local scale is less understood (Chisholm et al., 2013; Rödig et al., 2018). This, however, would be necessary for a mechanistic understanding of the impact of loss-related factors in comparison to supply-related factors.

To evaluate the impact of loss-induced limitations on forest productivity, we suggest a simple classification framework: we divide trees into full-grown (below: "mature") and growing ("immature") trees based on their intrinsic optimal CUE, i.e., the CUE the trees could attain if their GPP was not limited by competition. We consider trees as mature if intrinsic loss-related factors limit their CUE even under otherwise optimal growth conditions. Consequently, tree maturity and competition are distinct processes reducing stand-level forest productivity.

Forest productivity may be considered on different procedural levels: GPP, representing forests' photosynthetic capacity; NPP, denoting their total wood production after respiratory losses; and the net ecosystem exchange (NEE), measuring the

total forest carbon sequestration in the presence of emissions from deadwood decomposition and soil respiration. Studying the impact of loss-induced growth limits, we focused on three questions:

1. How do GPP, NPP, and NEE depend on the prevalence of mature and immature trees?
2. How can these relationships be linked to forest structure and expressed via easily measurable forest characteristics?
3. On which spatial scales can these relationships be observed?

To answer these questions, local carbon fluxes must be identified. Though NPP may be estimated from forest inventory data, field data for GPP and NEE, e.g. from eddy covariance measurements, are typically only available for larger scales (about $10\,\mathrm{ha}$). Similarly, it can be difficult to determine which trees have reached the mature stage. These challenges can be addressed with process-based forest models, which reproduce the forest dynamics under controlled reference conditions and provide full insight into carbon fluxes as well as the state and growth limitations of each tree.

There is a broad variety of forest models covering diverse sets of processes potentially impacting forest dynamics (Bugmann and Seidl, 2022). Depending on their respective main use cases, the models differ in their spatial resolution, their representation of vertical forest structure, physiological detail, and consideration of abiotic (e.g. soil conditions, weather, fire) and biotic (e.g. browsing, bark beetle attacks) factors (Merganičová et al., 2019; Bugmann and Seidl, 2022).In this study, we used the individual-based forest gap model FORMIND (Bohn et al., 2014; Fischer et al., 2016). The model features submodels on regeneration, competition, growth, and mortality and has been applied to study forest dynamics and carbon fluxes in a variety of both temperate and tropical forests (Fischer et al., 2016). As the model represents individual trees and the forest's vertical leaf distribution explicitly, FORMIND is particularly suited for studying the relationship between forest structure and forest productivity (Bohn and Huth, 2017). At the same time, the gap model approach of aggregating the impacts of individual trees at the local level leads to relatively high computational efficiency in large-scale simulations (Shugart et al., 2018).

We parameterized the model to mimic the dynamics of a species-rich old-growth temperate forest in Changbaishan, China. Located in a natural reserve, this forest offers unique opportunities to study long-term forest dynamics without biases introduced by human interventions. We addressed the research questions by computing GPP, NPP, and NEE on different spatial scales ($0.04\,\mathrm{ha}$ and $1\,\mathrm{ha}$) and setting them into relation with the basal area of mature and immature trees as well as different measures for structural diversity. For question (2), we suggest the DBH entropy, a measure for the diversity of tree heights, as a general proxy for the prevalence of immature trees and therefore also forest productivity.

## 2 Materials and Methods

We applied a data-driven modelling approach (Fig. 1) to analyze the relationship between forest structure and forest productivity. We fitted the process-based forest model FORMIND to forest inventory data from Changbaishan, China, and data on species' traits and allometric relationships. Using the model, we then linked forest productivity to the prevalence of mature trees and other forest characteristics. Below we describe the individual steps in detail.

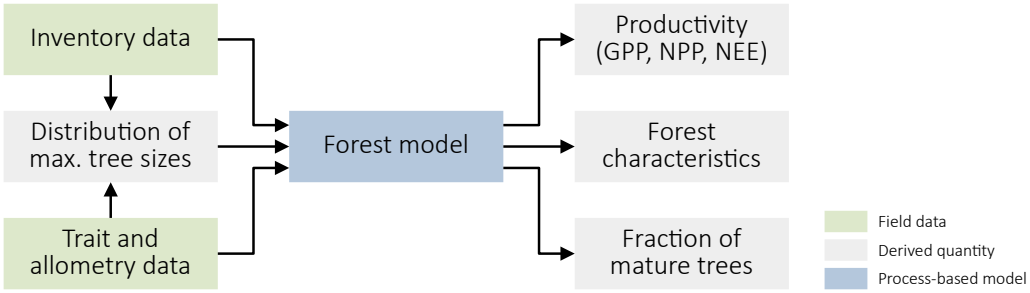


**Figure 1.** Summary of our approach. We use forest inventory data and data on species' traits and allometric relationships to derive the distribution of maximal plant sizes and parameterize a process-based forest model. This model, in turn, yields productivity metrics (GPP, NPP, and NEE) and different forest characteristics, including the fraction of mature trees.

### 2.1 Field data

We based our analysis on forest inventory data from an old-growth temperate forest in the Changbaishan National Nature Reserve in northeastern China. The surveyed area consists of $25\,\mathrm{ha}$ of conifer/broad-leaf mixed forest with $47$ species, a total biomass of $302\,{}^{\mathrm{t\,ODM}}/_{\mathrm{ha}}$ (Piponiot et al., 2022). The inventory data contain the position, diameter at breast height (DBH) and species of each tree with $\mathrm{DBH} \geq 1\mathrm{cm}$ for the census years $2004$, $2009$, and $2014$. Each tree is uniquely identified with an ID number. For trees that had multiple stems at breast height, we focused on the main stem (maximal DBH) in our analysis and we disregarded minor stems.

In addition to the inventory data, we used information on traits and allometry of the species from field measurements. These data included DBH-dependent heights, crown radii and crown base heights. Furthermore, the dataset included the species' wood densities and shade tolerance types ("light demanding", "mid-tolerant", or "shade tolerant"). Not all of these data were available for all species; we provide details in Supplementary Information (SI) A.

### 2.2 Model and parameterization

FORMIND is a process-based forest gap model featuring the main processes regeneration, competition, tree growth, and mortality (Fischer et al., 2016). Trees are mainly characterized by their DBH and species. Other properties, such as plant height or crown size, are derived from the DBH via allometric relationships. The model considers $20\,\mathrm{m} \times 20\,\mathrm{m}$ forest patches, for which the vertical leaf distribution and the resulting light climate are computed. The obtained incident radiation is used to compute each tree's GPP. The corresponding NPP is computed by subtracting an individual's respiration and other carbon losses from its GPP. Here, the maintenance respiration is determined by comparing the estimated GPP of trees under unshaded reference conditions with corresponding biomass increments from field data. Growth respiration and other carbon losses are computed as a certain fraction of the difference between GPP and maintenance respiration.

In the past, FORMIND was parameterized for managed European temperate forests (Bohn et al., 2014), but the Changbaishan forest has a different, richer species pool and is old-growth, requiring a correspondingly parameterized regeneration module. Therefore, we needed to develop an adjusted parameterization to apply FORMIND to this site. Below we summarize how we

parameterized the model and highlight changes to the version described before in Fischer et al. (2016). Details can be found in SI B.

**Basic parameterization**

To reduce model complexity in the species-rich Changbaishan setting, we aggregated species into plant functional types (PFTs) based on their maximal DBHs (below / above $30\,\mathrm{cm}$) and light demand (light demanding, mid-tolerant, and shade tolerant). When data necessary for the classification were not available, we assigned species via a likelihood-based cluster analysis based on shade tolerance (Niinemets and Valladares, 2006; Wang et al., 2010) and observed tree growth (SI B2). Because *Quercus mongolica* had a significantly different size structure than the other light-demanding species, we divided the large light demanding into two PFTs, one with all other large light demanding species and one for *Q. mongolica* only. We obtained six PFTs: small light demanding, large light demanding 1 and 2, large mid-tolerant, small shade tolerant, and large shade tolerant species. There were no small mid-tolerant species.

We estimated mean traits and allometric relationships for the PFTs based on the trait and allometry data. When computing the means, we weighted species according to their shares in the inventory to best reflect the species composition in the study area. Details can be found in SI B3 and B4. We modelled the forest under constant climatic conditions, which we derived based on data from the literature (evapotranspiration: Sun et al., 2004; temperature: Wang et al., 2020) and the WFDEI forcing dataset (irradiance, Weedon et al., 2014). See SI B10 for details.

We estimated the DBH-dependent base mortality for each PFT applying a likelihood-based approach to the inventory data (SI B9). To parameterize tree growth, we focused on the carbon use efficiency ($\mathrm{CUE} = \mathrm{NPP}/\mathrm{GPP}$) of trees under optimal growth conditions (SI B7). We modelled the CUE based on the following observations and assumptions: (1) the CUE decreases as plants grow in size, (2) the CUE under optimal conditions suffices for the observed DBH increments, (3) the CUE of trees in the inventory suffices to satisfy their respiratory needs, and (4) the order of magnitude of the CUE on stand level matches field measurements approximately (see SI B7.4).

With the modelled CUE under optimal conditions and FORMIND's submodel for primary production, we computed the GPP and NPP of trees under optimal conditions. We then used corresponding estimates of optimal DBH increments from the census data (SI B7.1) along with allometric relationships for stem dimensions to derive how much biomass trees allocate to their stem and their crown, respectively (SI B7.5). Finally, we adjusted the primary production model until enough biomass was allocated to the crowns that FORMIND's estimate of the Changbaishan forest biomass matched an estimate based on DBH-biomass relationships from the literature for each PFT (Chojnacky et al., 2014; Piponiot et al., 2022; see SI B7.5). Parameters that could not be determined via this approach were fitted so that the model best reproduced the inventory data (see below).

We assumed that trees compete for light only, but included crown defoliation as an additional process to account for the limited capacity of a forest. Trees whose GPP is insufficient to satisfy their respiratory needs loose crown biomass until all remaining parts can be maintained. Here, we assumed that – for a tree of given DBH – the maintenance respiration is proportional to the biomass. We decreased the leaf area index (LAI) of stressed trees along with their crown completeness, i.e., the ratio between current (reduced) and healthy crown biomass. Trees that have lost all their crown biomass die.

To compute the soil respiration required to determine the NEE, FORMIND uses the submodel for deadwood composition described by Sato et al. (2007), which involves a pool of fast and slowly decomposing deadwood, respectively (Paulick et al., 2017). The corresponding decomposition rates and the transition rates between the pools are derived from the mean actual evapotranspiration (Sato et al., 2007), for which we assumed a value of $600\frac{\mathrm{mm}}{\mathrm{yr}}$, in line with independent estimates for the Changbaishan region (Sun et al., 2004) and earlier parameterizations of the model for temperate forests (Bohn et al., 2014).

**Model fitting**

Some of the modelled processes depend on parameters not directly inferable from the available data. This included the following PFT-specific parameters: (1) the external influx of new seeds, (2) the saturation parameters of the light response curves, (3) the magnitudes of carbon losses other than maintenance respiration, and (4) the light required for seedling establishment. Furthermore, we fitted a parameter controlling the magnitude of DBH growth under optimal conditions and the sharpness of the light threshold for seedling input.

We fitted these $26$ parameters using a likelihood-based approach maximizing the approximate likelihood of the inventory data, estimated from a sample of simulation results. We determined each PFT's biomass and stem count in $20\,\mathrm{m} \times 20\,\mathrm{m}$ forest patches. The combined information of stem count and biomass yields basic insight into the size distribution of trees: a large stem count with small biomass indicates a young forest with many small trees, and a small stem count with high biomass indicates an old forest with few large trees. Using these summary statistics instead of the full tree size distribution reduced the dimension of the considered state space, allowing us to estimate the joint distribution of the highly stochastic small-scale forest states based on a reasonable sample of simulation results. The inventory covered $625$ forest patches, providing us with a similarly-sized sample of forest states.

To generate a forest state sample from the model, we first simulated $1\,\mathrm{ha}$ of forest for a burn-in period of $2000\,\mathrm{yr}$. Then, we sampled the forest $500$ times in $5\,\mathrm{yr}$ intervals. We repeated this procedure $67$ times in parallel, equivalent to simulating $67\,\mathrm{ha}$ of forest, obtaining a sample of $837,500$ forest states for each tested parameter combination.

We estimated the likelihood of the field data via kernel density estimation (KDE; Wand and Jones, 1995). In KDE, the probability density of an observation is estimated based on how many model-generated sample points are similar to the observation. Here, similarity is measured via kernel functions, which depend on bandwidth parameters. We used Gaussian kernels with bandwidths chosen corresponding to the scales of the stem counts and biomasses in the inventory data (see Table S10 in SI B11). To correct for the bias introduced when log-transforming the KDE so as to compute the log-likelihood, we applied a bias correction function derived via a first-order Taylor approximation (SI B11).

The resulting likelihood estimate converges to the true likelihood as the size of the generated sample increases and the bandwidth parameters decrease. Hence, optimizing the KDE likelihood yields consistent parameter estimates and avoids potential biases arising if the model was fitted via a deterministic modelling framework (e.g. Lehmann and Huth, 2015; Rödig et al., 2017). However, as the log-likelihood estimate is based on a sample of stochastic model results, it is stochastic as well, making it difficult to optimize. We reduced the stochasticity by decreasing the dimension of the sample space, avoiding the "curse of

dimensionality" (Wand and Jones, 1995) by considering the different PFTs as mutually independent. The parameter estimates remain consistent despite this composite likelihood approach (Varin, 2008).

We maximized the likelihood by repeatedly applying a derivative-free optimization algorithm based on non-local quadratic approximations (Cartis et al., 2019). To avoid getting stuck in local minima, we used the basin-hopping algorithm (Wales and Doye, 1997), which applies multiple local optimizations with randomly perturbed initial conditions. Throughout the fitting process, we constrained the parameters to ecologically reasonable ranges. Details on model fitting can be found in SI B11. The fitted parameter values are provided in SI B.

**Size limitations**

We assumed that each tree has a maximal DBH at which it stops growing. As this maximal DBH may depend on local conditions and the tree's species, we drew the DBH limit randomly for each tree individually (details below). Trees that have reached their DBH limit are called "mature" below and are assumed to use their entire primary production for respiration.

We constructed the distributions of the DBH limits based on the maximal DBHs of the species in each PFT: for each species, we assumed that the site-dependent DBH limits are uniformly distributed between the overall maximal DBH and a value $20\%$ below this maximum. We aggregated these species-specific distributions, weighted according to the species' respective shares in the basal area of the inventory. That way, we obtained the joint distribution of DBH limits for each PFT. In SI B4.1, we describe the approach in greater detail.

## 2.3 Model validation

We validated the fitted model by visually comparing the respective marginal and joint distributions of the biomass and stem count values for the considered PFTs with the corresponding distributions observed in the field data. We created corresponding one- and two-dimensional histograms based on both samples generated via simulations and computed based on the forest inventory data. We observed that the simulated trajectory and distribution of biomass and stem count matched the values from the inventory (Fig. 2, SI D).

To ensure the fitting algorithm did not terminate at a suboptimal local likelihood maximum, we repeated the model fitting procedure three times. We compared the resulting parameter estimates to assess how well the individual parameters are estimable. The differences between the corresponding parameter were moderate for most parameters except the light threshold for seedling establishment (SI D).

To validate the results on a broader scale ($25\,\mathrm{ha}$), we furthermore compared the modelled biomass, NPP, GPP, and LAI with values obtained for the same forest plot in independent studies (Piponiot et al., 2022). The simulated forest had a mean biomass of $270.5\,^{\mathrm{t\,ODM}}/_{\mathrm{ha}}$ (estimated standard deviation for $25\,\mathrm{ha}$: $4.38\,^{\mathrm{t\,ODM}}/_{\mathrm{ha}}$). Our biomass estimates from the allometric equations by Chojnacky et al. (2014) were $270.52\,^{\mathrm{t\,ODM}}/_{\mathrm{ha}}$ if we only considered the major stems and $284.48\,^{\mathrm{t\,ODM}}/_{\mathrm{ha}}$ for all stems in the inventory. This is below the estimate by Piponiot et al. (2022): $302\,^{\mathrm{t\,ODM}}/_{\mathrm{ha}}$. The simulated forest had an aboveground wood production of $2.22\,^{\mathrm{t\,ODM}}/_{\mathrm{ha\cdot yr}}$ (standard deviation: $0.07\,^{\mathrm{t\,ODM}}/_{\mathrm{ha}}$; Piponiot et al., 2022: $3.55\,^{\mathrm{t\,ODM}}/_{\mathrm{ha\cdot yr}}$) and GPP of

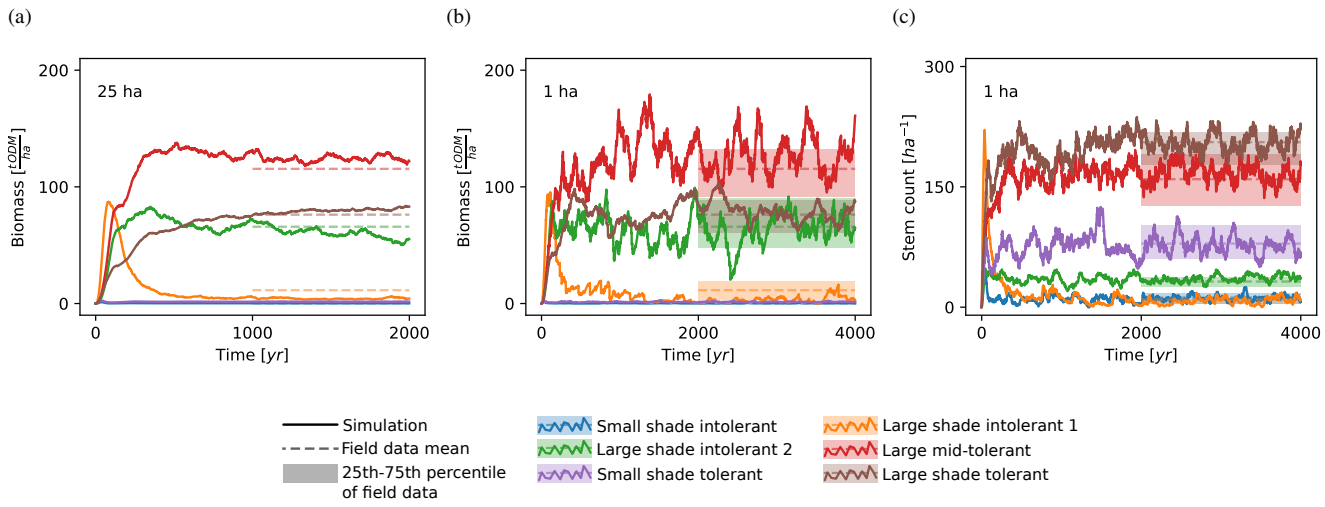


**Figure 2.** Temporal evolution of (a, b) biomass and (c) stem count of the six PFTs on (a) the $25\,\mathrm{ha}$ scale and (b, c) the $1\,\mathrm{ha}$ scale. The solid lines show the trajectory of the model simulation. For comparison, the shaded areas depict the ranges between the 25th and the 75th percentiles of the biomasses and stem counts from the inventory data. The dashed lines represent the corresponding mean values.

$23.39\,{}^{\mathrm{t\,ODM}}/_{\mathrm{ha\cdot yr}}$ (standard deviation: $0.2\,{}^{\mathrm{t\,ODM}}/_{\mathrm{ha}}$; Wu et al., 2009: 29.82-33.86 ${}^{\mathrm{t\,ODM}}/_{\mathrm{ha\cdot yr}}$). The LAI of the simulated forest was $5.18$ (standard deviation $0.05$; Liu et al., 2007: $5.08$). See SI D for details.

### 2.4 Analysis

To analyze the effect of mature trees on forest productivity, we simulated $1\,\mathrm{ha}$ of the Changbaishan forest and sampled forest characteristics and forest productivity over time on the $0.04\,\mathrm{ha}$ and the $1\,\mathrm{ha}$ scale. After a burn-in period of $2000\,\mathrm{yr}$, we analyzed the forest $1000$ times in $5\,\mathrm{yr}$ time intervals. We obtained a sample of $25,000$ forest states on the smaller and $1,000$ states on the larger scale, corresponding to $1000\,\mathrm{ha}$.

To measure forest productivity, we computed the GPP, NPP, NEE, and carbon use efficiency (CUE $=$ NPP/GPP) of the considered forest areas. We characterized the corresponding forest states by determining the basal area $A_{\mathrm{all}}$ of all trees in the forest area and the basal area $A_{\mathrm{grow}}$ of only those trees that had not reached their individual DBH limits. Based on these measures, we also determined the basal area proportion $A_{\mathrm{grow}}/A_{\mathrm{all}}$ of immature trees and the corresponding proportion of mature trees. Furthermore, we computed the DBH entropy (a measure for the diversity of DBH values; detailed explanation in section 2.5), basal-area-weighted height standard deviation, and the Shannon diversity of PFTs on the two considered scales. We weighted the plant heights by the basal areas when computing the height standard deviation so as to account for small plants having a minor impact on forest productivity.

For both considered spatial scales ($0.04\,\mathrm{ha}$ and $1\,\mathrm{ha}$), we plotted GPP, NPP, and NEE against the mentioned forest characteristics and computed the respective coefficients of determination ($R^2$) to quantify the strengths of the relationships. In a similar

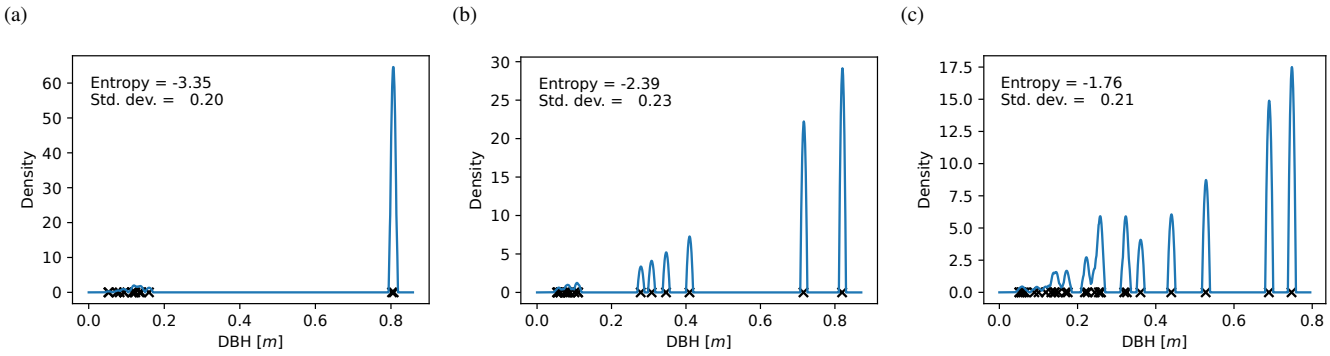


**Figure 3.** Basal-area-weighted DBH distributions for $0.04\,\mathrm{ha}$ forest patches with (a) low, (b) intermediate, and (c) high entropy. Each black cross depicts the DBH of a plant. The height of the corresponding spike in the density function (blue line) corresponds to the plant's share in the basal area; the contributions of trees with similar DBH add up. The width of the spikes ($2h$; here: $2\mathrm{cm}$) is the scale on which different plants are considered similarly sized. The entropy is higher the more uniformly the basal area is distributed across plants with different DBHs. In (a), two similarly large plants dominate the forest patch, whereas in (c), there are many medium-sized plants with different DBHs. Note that the standard deviation of the DBH distribution is not related to the DBH entropy.

manner, we analyzed the relationship between the basal area proportion of mature trees and the CUE. To understand the role of the DBH entropy, we furthermore assessed its relationship with the basal area of mature and immature trees.

To assess how sensitive our results are to the assumption that mature trees stop growing completely, we computed the NPP in hypothetical scenarios in which the CUE of trees is reduced by only $50\%$, $25\%$, or $0\%$, respectively, when they enter the mature stage. To avoid refitting the model for each of these validation scenarios, we adjusted only the intrinsic carbon fluxes and held the sizes of the mature trees constant. We then analyzed the relationship of the obtained NPP values with the covariates given above.

### 2.5 DBH entropy as a proxy for the prevalence of mature trees

It is difficult to know which trees have reached their site-dependent growth limits in field studies. Hence, a proxy for the prevalence of mature trees is needed in practice. Such a proxy should be easy to compute from inventory data and may account for the following working hypotheses: (1) forest patches dominated by mature trees consist of a small number of large individuals preventing the existence of medium-sized trees; (2) in old-growth forests, individuals typically differ in age and size, but mature individuals of the same species may have similar DBH values. The proxy should also reflect that large trees have a higher impact on forest dynamics than small trees.

As a proxy satisfying these requirements, we propose the basal-area-weighted DBH entropy $S_{\mathrm{DBH}}$ (below simply "DBH entropy"), defined as the entropy of the distribution of DBHs in a forest patch (cf. Staudhammer and LeMay, 2001; Park et al., 2019). If we split the range of occurring DBH values into equally sized intervals $I$ and determined the basal area share $p_I$ of

trees in each size class $I$ relative to the total total basal area, the DBH entropy could be approximated via

$$S_{\mathrm{DBH}} = -\sum_{I \in \mathcal{I}} p_I \ln(p_I). \tag{1}$$

Here, $\mathcal{I}$ is the set of DBH classes and

$$p_I = \frac{\sum_{d \in I} d^2}{\sum_{I \in \mathcal{I}} \sum_{d \in I} d^2} \tag{2}$$

is the basal area share of trees in size class $I$.

The weights $p_I$ can be interpreted as probabilities indicating how likely we would obtain a tree from size class $I$ if we randomly selected trees from the forest patch with probabilities proportional to their basal areas. The entropy is higher the more evenly the the DBHs are distributed (Fig. 3). If the forest patch is dominated by one or a few large trees, it is likely that we draw one of their size classes, making the entropy small. Similarly, if two trees have a similar DBH, the probability to pick a tree from their size class increases, decreasing the entropy. Since we weight the DBH distribution by the basal areas, adding small trees to the forest patch does not change the entropy significantly.

As the approach presented above is sensitive to the specific choice of interval bounds, we used a more robust definition of the DBH entropy in our analysis (SI C1). We applied kernel smoothing (Wand and Jones, 1995) with an Epanechnikov kernel to obtain a continuous estimate of the DBH distribution instead of discrete probabilities $p_I$ (cf. Fig. 3), and we exchanged the sum in equation (1) with an integral. Kernel smoothing requires a bandwidth parameter (here: $1\mathrm{cm}$), which is comparable to the width of the DBH intervals $I$ and defines the scale on which two trees are regarded similar.

## 3 Results

The basal area of the forest stand was strongly correlated with the GPP, irrespective of the spatial scale ($R^2 \geq 0.65$; Figs. 4a and 5a). For the NEE, these correlations were much weaker ($R^2 \leq 0.1$; Figs. 4f, 5f) and for the NPP merely existent ($R^2 = 0$; Figs. 4k, 5k). This contrasts with the basal area of immature trees: here, the correlations were small for the GPP ($R^2 \leq 0.15$; Figs. 4b, 5b) but large for the NPP ($R^2 \geq 0.74$; Figs. 4g, 5g) and the NEE ($R^2 \geq 0.59$; Figs. 4l, 5l). We obtained a similar but slightly weaker result for the DBH entropy. On the small scale ($0.04\,\mathrm{ha}$), it was weakly correlated with the GPP ($R^2 = 0.11$; Fig. 4c) but strongly correlated with NPP ($R^2 = 0.47$; Fig. 4h) and NEE ($R^2 = 0.39$; Fig. 4m). These correlations decreased on the larger scale ($1\,\mathrm{ha}$; $R^2 \leq 0.26$; Figs. 5c, h, m).

The weighted tree height standard deviation was strongly negatively correlated with the GPP ($R^2 \geq 0.56$; Figs. 4d, 5d) but almost uncorrelated with NPP and NEE ($\left|R^2\right| \leq 0.03$; Figs. 4/5i, n) on both spatial scales. The Shannon diversity of PFTs was moderately correlated with the NPP ($R^2 \in [0.17, 0.19]$; Figs. 4j, 5j), weakly correlated with the NEE ($R^2 \leq 0.04$; Figs. 4o, 5o), and weakly negatively correlated with the GPP ($R^2 \leq 0.07$; Figs. 4e, 5e).

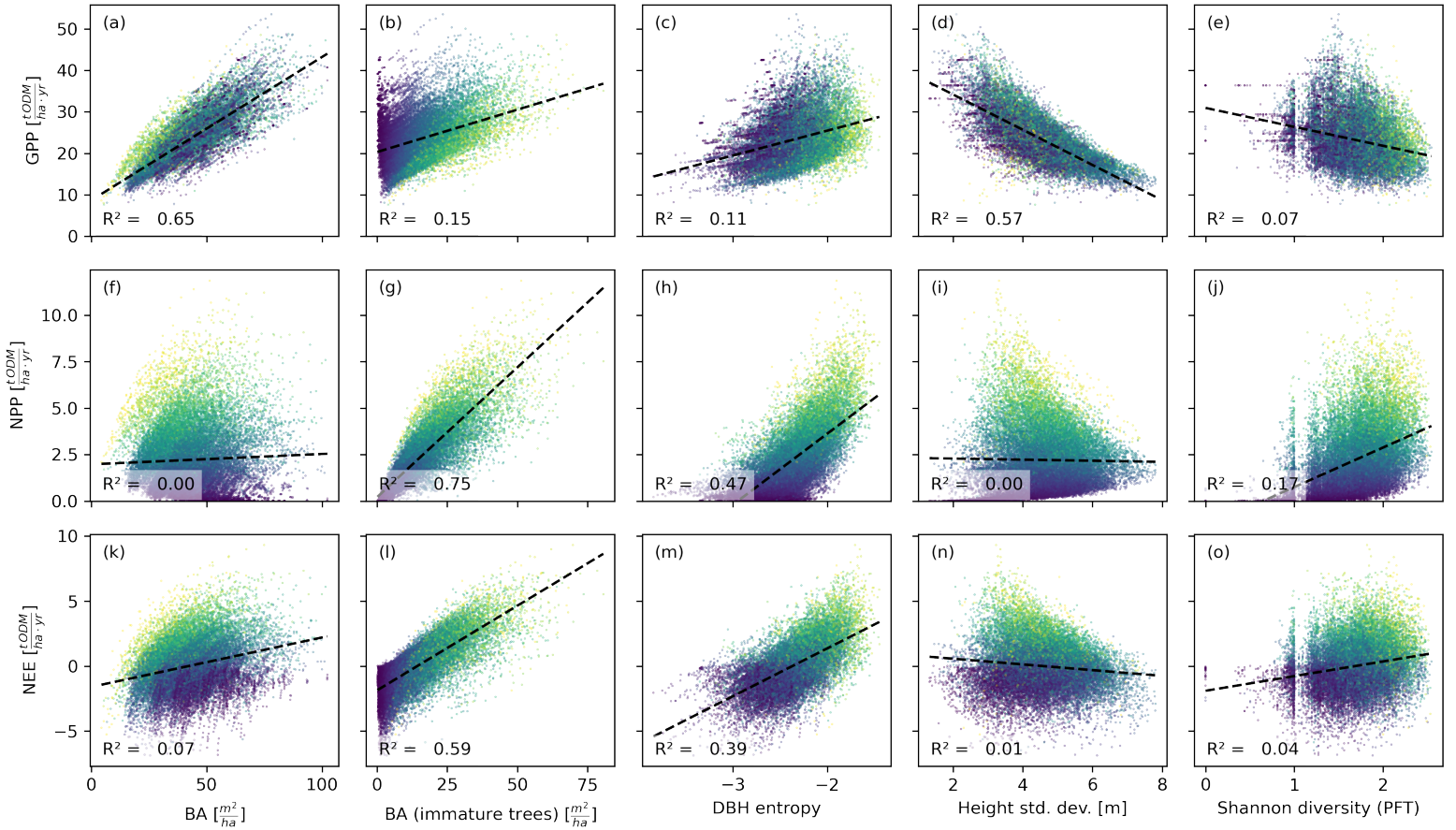


**Figure 4.** Productivity measures (GPP, NPP, and NEE) dependent on different measures of basal area (BA) and heterogeneity. Each dot corresponds to a $0.04\,\mathrm{ha}$ forest patch (sample size: $25,000$). The colour indicates the basal area proportion of mature trees (blue: only mature trees; yellow: no mature trees). The GPP is mainly driven by the basal area, whereas NPP and NEE are driven by the basal area of immature trees. The heterogeneity measures are generally poorer predictors than the basal area measures. Among the former, the DBH entropy has the best predictive capacity for NPP and NEE and may serve as a valuable proxy if distinguishing mature and immature trees is not possible.

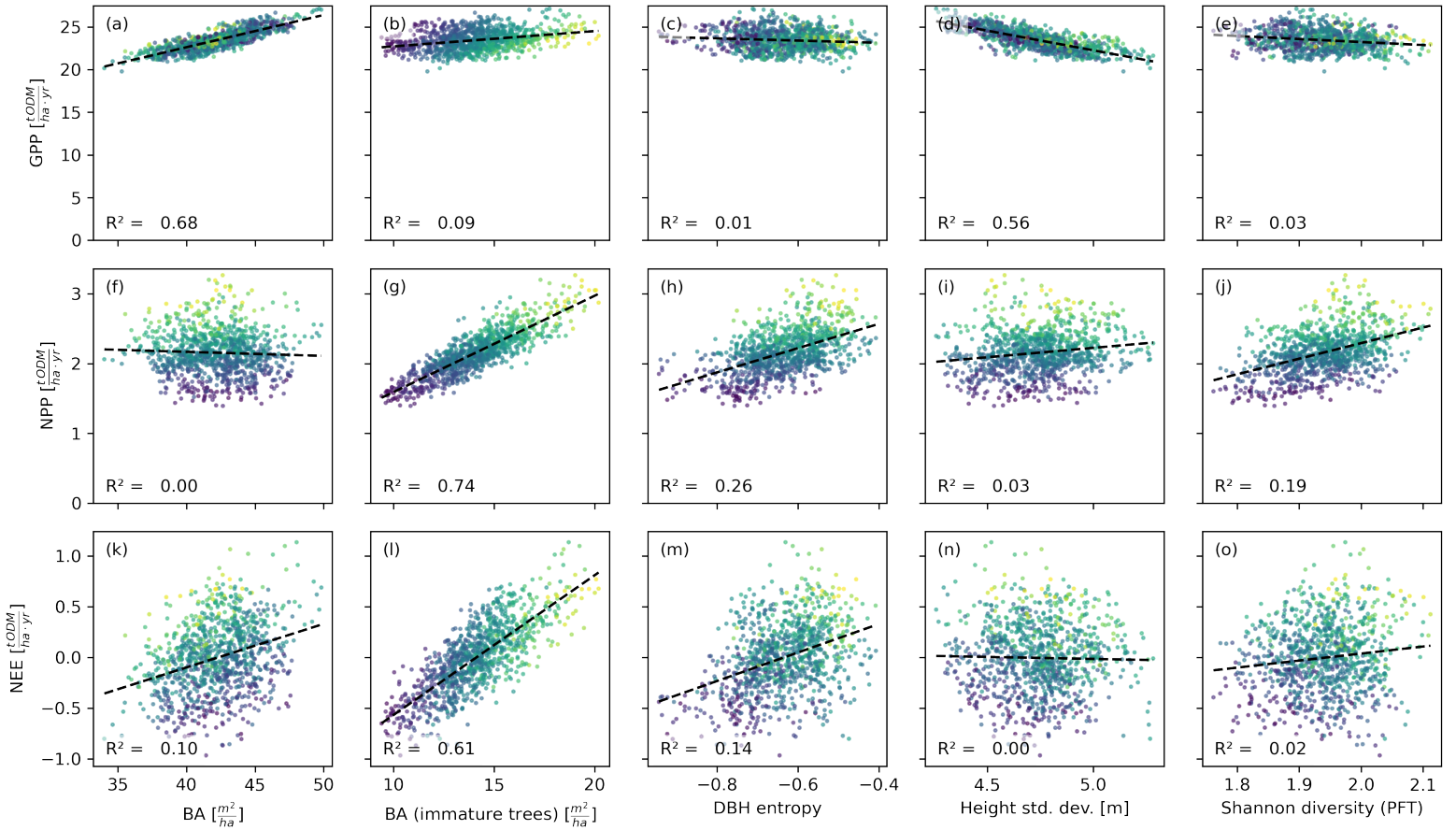


**Figure 5.** Productivity measures dependent on different measures for basal area and heterogeneity. Each dot corresponds to a 1 ha forest patch (sample size: 1,000). The colour indicates the basal area proportion of mature trees (blue: only mature trees; yellow: no mature trees). The correlation patterns resemble those observed on the finer scale (Fig. 4). Only the DBH entropy looses predictive power.

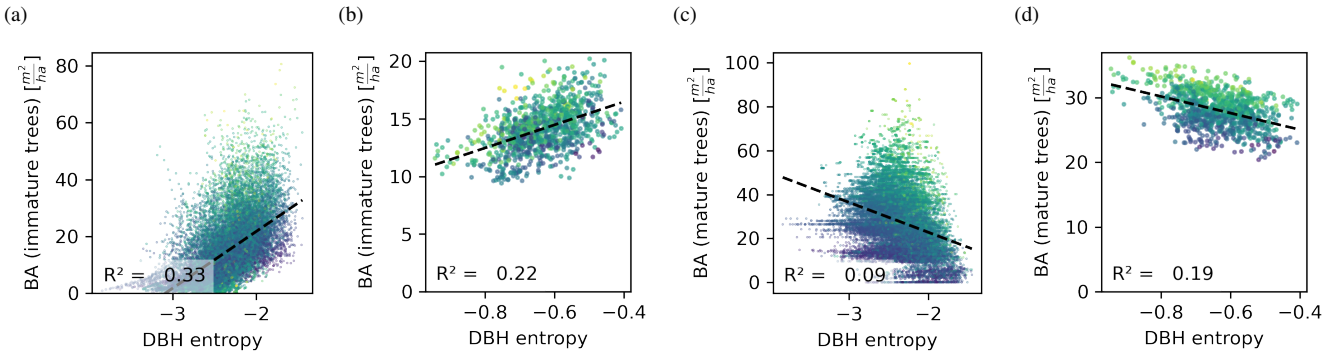


**Figure 6.** Relationship between the DBH entropy and (a, b) the basal area of immature and (c, d) mature trees,depicted on (a, c) the $0.04\,\mathrm{ha}$ and (b, d) the $1\,\mathrm{ha}$ scale. Each dot corresponds to a forest patch of the respective scale. The colour corresponds to the total basal area (dark: low, light: high). The DBH entropy correlates positively with the basal area of immature trees, which drive the NPP, and correlates negatively with the basal area of mature trees, which do not contribute to the NPP and compete with immature trees. The relationships are stronger on the small scale.

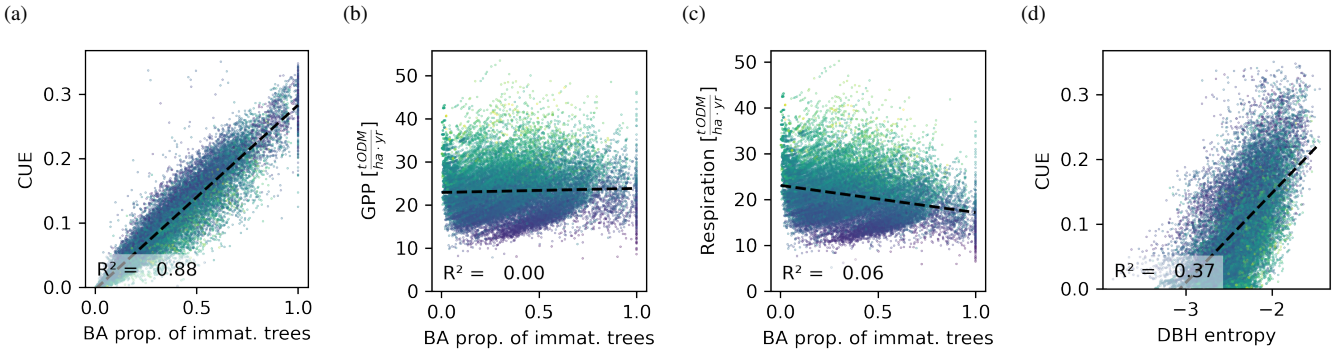


**Figure 7.** Relationship between the basal area proportion of immature trees and (a) the CUE, (b) the GPP, and (c) the tree respiration / carbon losses. The CUE is proportional to the basal area of immature trees. Though the CUE can be directly computed from the GPP and respiration, a similar relationship is not visible for these, indicating that they are not the drivers behind the proportionality. (d) Relationship between the DBH entropy and the CUE. Though this relationship is weaker than that between the proportion of immature trees and and CUE, the DBH entropy may serve as a proxy for the CUE.
Each dot corresponds to a $0.04\,\mathrm{ha}$ forest patch. The colour corresponds to the basal area (dark: low, light: high).

The DBH entropy was positively correlated to the basal area of immature trees ($R^2 = 0.33$ on the small scale; Fig. 6a) and weakly negatively correlated to the basal area of mature trees ($R^2 = 0.09$; Fig. 6c). For the latter, the DBH entropy was a poor predictor in forest patches with large overall basal area. On the hectare scale, the relationships became weaker for immature trees ($R^2 = 0.23$; Fig. 6b) but stronger for mature trees ($R^2 = 0.19$; Fig. 6d).

The CUE was proportional to the proportion of immature trees in the forest (Fig. 7a). The regression analysis yielded an intercept of $3.16{\cdot}10^{-3}$ on the small and $2.182{\cdot}10^{-4}$ on the large scale, with $R^2$ values of $0.88$ and $0.82$, respectively. The proportionality constants (slopes of the fitted curves) were $0.29$ and $0.28$. The relationship between CUE and DBH entropy

was also significant, but weaker ($R^2 = 0.3$ on the small and $R^2 = 0.28$ on the large scale; Fig. 7). The GPP and tree respiration / carbon losses did not show a strong correlation with the proportion of immature trees ($R^2 = 0$ and $R^2 = 006$, respectively on the small scale; Figs. 7b, c).

~~Reducing~~ Decreasing the CUE reduction of mature trees in comparison to similar immature trees decreased the correlation between the basal area of immature trees and the NPP. However, the predictive performance remained high ($R^2 \geq 0.53$) even if the CUE of ~~immature~~ mature trees was only reduced by $25\%$ (Fig. S1). The DBH entropy was even less sensitive to a change in the CUE reduction. However, when the CUE was reduced by less than $50\%$, the DBH entropy computed with cubic DBH weights had a stronger correlation with NPP than the basal-area-weighted version and achieved an even higher $R^2$ of $0.57$ and $0.55$ when the CUE was reduced by only $25\%$ and $0\%$, respectively. Details and further results regarding the CUE reduction scenarios are presented in SI E.

## 4 Discussion

We suggested a simple framework of "mature" and "immature" trees to disentangle the impact of competition and intrinsic growth limitations on forest productivity in old-growth forests. Thereby, we found that the drivers of NPP and NEE were distinct from those determining GPP. While the latter was strongly correlated with the total basal area, NPP and NEE were related to the basal area of immature trees only. This indicates that the increased respiratory losses of mature trees play the major role in forests' carbon balance: despite having a significant GPP, mature trees contribute less to wood production but rather reduce the productivity of other trees via competition. Hence, tree maturity may be a major driver of the difference between NPP and GPP, making GPP-related covariates such as light competition insufficient to explain local variations in NPP and NEE.

This conclusion is supported by the observed proportionality between the CUE and the basal area share of immature trees: carbon usage was more efficient the more the forest was dominated by immature trees. The proportionality can be explained by noting that (1) the individual-level GPP is strongly positively correlated with basal area, irrespective of the maturity stage, and (2) only immature trees contribute to the NPP. On the stand level, neither the GPP nor the respiration were correlated with the proportion of immature trees, showing that the proportionality was not driven by the decreased GPP or increased respiration of forests with a high share of mature trees.

These findings are based on a maturity definition considering the individual trees' growth potential in the absence of competition. This potential can be challenging to determine in field studies, as it requires to identify the causes of individuals' growth limitations. Hence, alternative maturity definitions, based on tree size or signs of senescence may be used (Gibbons et al., 2008). Applying such alternative maturity definitions will yield qualitatively similar results if the considered characteristics are strongly correlated with the trees' growth potential. Otherwise, other structural forest attributes may be considered.

To that end, we suggested the DBH entropy as a proxy for the prevalence of immature trees and thereby NPP and NEE. The DBH entropy was positively correlated with the basal area of immature trees and negatively correlated with the basal area of mature trees, but its relationships to NPP and NEE were even stronger. This indicates that the predictive capacity of the DBH

entropy stems not only from its correlation with the prevalence of immature trees but also from other mechanisms. In line with this observation, the DBH entropy remained a good predictor for NPP even in the validation scenario where we did not reduce the CUE of mature trees (SI E). These findings support previous studies identifying structural diversity as a major driver of forest productivity (Dănescu et al., 2016; Bohn and Huth, 2017; Silva Pedro et al., 2017; Bohn et al., 2018; Park et al., 2019; LaRue et al., 2023). Note that our DBH entropy index differs from the classic entropy-based measures for structural diversity (Staudhammer and LeMay, 2001) by the basal-area-based weighting (Park et al., 2019), which improved its predictive power (SI C2).

Remarkably, the height standard deviation, another measure for structural diversity, did not have a significant positive correlation to any of the productivity measures. The height standard deviation depends on the width of the height spectrum, i.e., the difference between the height of the smallest and the largest tree. Hence, forests can exhibit a high standard deviation even if their diversity of tree heights is low. This contrasts with the entropy, which measures how many different tree sizes there are without regarding their actual values. The strong negative relationship between the height standard deviation and GPP can be explained by the weighting we applied. Weighting the tree heights by basal area decreases the standard deviation in forest stands with many large trees, which in turn have a large GPP.

The Shannon diversity of PFTs was not strongly related to any of the forest productivity measures. This was due to the differences between stem count and biomass of the PFTs. Four PFTs contributed significantly to the forest's stem count and thus the Shannon diversity. In contrast, the biomass was dominated by two PFTs only, which consequently contributed most to the production. Hence, the Shannon diversity of PFTs was a poor predictor for productivity. However, if the Shannon diversity was computed based on tree species rather than PFTs, it could yield useful information on the diversity of the DBH limits, as these are species dependent. Setting this diversity of limits into relation with the actual diversity (or entropy) of DBH values could hence improve NPP estimates.

Changing the spatial scale from $0.04\,\mathrm{ha}$ to $1\,\mathrm{ha}$ did not alter most of the relationships we considered. By construction, the coefficient of determination is insensitive to the addition of independently identically distributed random variables. As the interactions between forest patches were weak and the basal area, GPP, NPP, and NEE are additive measures, their respective correlations were not affected by the scale. The same applied to the height standard deviation, which is additive if the weighted mean height is approximately constant in all small-scale patches. The Shannon diversity of PFTs did not show strong patterns on any scale. The DBH entropy, however, was most informative on a small scale (e.g. $0.04\,\mathrm{ha}$). On large scales (e.g. $1\,\mathrm{ha}$), the entropy increases and varies less between forest sections, since more trees are considered. This is a significant finding, as many previous studies considered entropy-based diversity indices on larger scales (often $\geq 0.5\,\mathrm{ha}$; Dănescu et al. 2016; Silva Pedro et al. 2017; Park et al. 2019). In line with our results, a loss of information on larger scales was noticed by Chisholm et al. (2013) with respect to the Shannon index. Nonetheless, if the scale is smaller than that of plant interactions, the DBH entropy cannot reflect information on competition and dominance, and the similarities between mature trees cannot be reflected.

### 4.1 Model parameterization and limitations

Being an individual- and process-based model, FORMIND is designed to attain high mechanistic realism while achieving the computational performance required to study forest dynamics on large spatial and temporal scales (Fischer et al., 2016). Hence, some processes such as plant-internal signalling, dynamics of nonstructural carbon, below-ground carbon dynamics, interactions with mycorrhiza, or pest-induced stress are not covered explicitly but implicitly incorporated into high-level processes. As a result, not all aspects of forest community dynamics may be reproducible with the model. Nonetheless, the main carbon fluxes are covered, allowing us to differentiate immature trees from those that have reached their maximal sizes and to analyze carbon fluxes on small spatial scales.

Measuring GPP and NEE on small scales is challenging, since eddy covariance measurements, for example, typically apply to the whole stand level only, are costly and bound to one location due to the immobility of the measurement towers. The model-based approach required some innovations in model design and parameter estimation. For example, the likelihood-based fitting method allowed us to estimate parameters based on small-scale (here: $0.04\,\mathrm{ha}$) forest characteristics despite their stochastic variations. The small-scale distribution of stem counts and biomass contains information on local interactions and consequently the range and diversity of local states a forest can attain. This information is typically lost on larger scales. Circumventing the need to reduce stochasticity via aggregation over several hectares of forest (see e.g. Rödig et al., 2017) enabled us to estimate parameters affecting the small-scale forest dynamics and allowed us optimize $26$ parameters on regeneration, light response, optimal growth, and respiration. Applying a parameterization framework focusing on the tree-level carbon use efficiency guaranteed a balanced parameterization of the individual-level NPP and GPP.

Our fitting approach also circumvented challenges typically arising in the Bayesian framework. Bayesian methods, such as approximate Bayesian computation (ABC; Beaumont et al., 2002; Csilléry et al., 2010), require the evaluation of many parameter combinations. This is computationally costly in models for old-growth forests, as the entire succession has to be simulated. Furthermore, the stochastic search performed in ABC and classical Markov Chain Monte Carlo methods may fail to find good parameter combinations when the parameter space is large. Hence, our methodological advances can also benefit future forest models.

The good match between the biomass and stem count distributions in the simulated forest and the inventory indicates that the model replicates the forest structure well. Further validation via independent estimates of biomass, GPP, NPP, and LAI showed that the model reproduces major forest dynamics. Nonetheless, the model underestimated the mean biomass, GPP, and NPP. The underestimated biomass resulted partially from our focus on the main stems in the inventory, neglecting additional minor stems. Including the secondary stems as separate trees would have led to overestimated LAI values, causing forest thinning and making it difficult to fit the dynamic model to the field data. The biomass bias, along with the assumption that mature trees stop growing, may also have caused the underestimated NPP and GPP. Nonetheless, these quantitative differences do not invalidate the strong qualitative results we obtained.

The strong correlation we observed between basal area and GPP may stem from our assumption that leaf area and basal area are proportional within a PFT. Though this assumption is in line with theoretical and empirical findings (West et al., 1999; Xu

et al., 2021), local conditions and competition can blur this relationship in practice, weakening it in field observations. As an alternative, the GPP could be estimated from stand-level LAI values (see e.g. Xie et al., 2019).

The relationship between basal area and GPP could also be weakened by competition for water and other resources, which might also yield other interactions between mature and immature trees. Added competition may strengthen the negative effect of mature trees on forest productivity. As a result, the relationship between the proportion of immature trees and the CUE would become non-linear, with a disproportionally low CUE in stands dominated by mature trees. Consequently, the basal area of mature trees would need to be considered in addition to the basal area of immature trees to accurately estimate NPP and NEE.

In special cases, mature trees could also have positive effects on smaller trees, for example by providing shelter (Lett and Dorrepaal, 2018) and improving soil conditions (Yunusa and Newton, 2003). In forests whose dynamics are driven by sink limitations (i.e., limitations affecting carbon allocation to growth) rather than source limitations (limitations affecting carbon supply), such effects could induce a positive effect of mature trees on NPP.

Our analysis built on the assumption that trees have maximal sizes. We modelled this via an abrupt transition from the growing to the mature stage, which is a common approach in forest modelling (Shugart et al., 2018). In reality this transition can be gradual, and trees may require minimal DBH increments to maintain the function of their vascular system (Prislan et al., 2013). However, our results remained consistent even if the CUE of mature trees was only reduced by $25\%$ as compared to immature trees of the same size, suggesting that life-stage-dependent carbon losses have a dominant impact on the forest dynamics even if they have a moderate magnitude. Though the concept of growth limitations acting on the individual scale is subject to an ongoing debate (Stephenson et al., 2014; Foster et al., 2016; Sheil et al., 2017; Forrester, 2021; Anderson-Teixeira et al., 2022), there is strong evidence that the NPP and / or CUE decrease with the age of forest stands (Gower et al., 1996; Tang et al., 2014; Collalti et al., 2020a), indicating that tree age or size have a significant effect on individual biomass increment (West, 2020).

We considered a forest under spatially and temporally uniform environmental conditions to study the within-stand productivity variations and their connection with forest structure. Temporal climatic variations and changing occurrence of diseases and pests could increase the variance of GPP, NPP, and NEE, and weaken their correlations with forest attributes. Though the external factors could become a major driver of forest dynamics, temporal averaging could reduce the resulting productivity variations so that data obtained on longer time scales might show patterns similar to those presented here. This could be confirmed via further simulation studies, e.g. with an extended FORMIND parameterization incorporating variable climate.

Similarly, spatial heterogeneity in climate, soil, species composition, and other factors could affect forest productivity on larger scales (Munné-Bosch, 2018; West, 2020; Gea-Izquierdo and Sánchez-González, 2022). To appropriately account for these variations, our results would need to be combined with appropriate stand-level covariates to obtain productivity estimates on regional scales. Nevertheless, our findings may be applicable to extended areas with comparable environmental conditions.

### 4.2 Outlook

Using the concept of the potential CUE to characterize tree maturity could become a useful framework to understand forest productivity on local scales. The identification of mature trees, whose growth is primarily limited by intrinsic factors, may be conducted irrespective of the mechanism behind the limitations, be it increased respiratory losses (O'Leary et al., 2019), sink limitations (Potkay et al., 2022), limited nutrient or water availability (Munné-Bosch, 2018), or even genetic predisposition (Liu et al., 2016). As we used a generic forest model and our results were robust across scales, our observations may hint towards a universal relationship between tree maturity and forest productivity. This connection could be used to develop new theory that could eventually lead to accurate predictions of NPP and NEE based on general forest characteristics. Such predictions have proven difficult in the past (Chisholm et al., 2013; Rödig et al., 2018) but could be highly relevant for a broad spectrum of applied and theoretical questions in forest ecosystem science. Here, the DBH entropy could prove particularly useful, as it can be easily obtained from inventory data and may serve both as a measure for forests' structural diversity on the local scale and as a proxy for net forest productivity in old-growth forests.

Confirming and generalizing the observed relationships between tree maturity, DBH entropy, NPP, and NEE is a promising endeavour for both theoretical and field studies. Further modelling studies could assess the expected strength of the relationships in forests in different successional stages, under varying environmental conditions, and in the presence of additional stressors such as competition for nutrients and water. Field studies could attempt to validate these findings. Typical DBH maxima are documented for many species from temperate forests and could serve as a first proxy for maturity (Aiba and Kohyama, 1997; Kohyama et al., 2003; Russell and Weiskittel, 2011; del Río et al., 2019). Combining the gained insights with large-scale predictors for forest productivity could then lead to a unified theory of forest productivity.

## 5 ~~Conclusion~~

## 5 Conclusions

We applied a modelling approach to investigate how the prevalence of mature (full-grown) trees and forest structure explain within-stand variations of forest productivity. We found that NPP and NEE are mainly driven by the basal area of immature trees, whereas the GPP depends on the total basal area. This suggests that loss-induced limitations rather than variations in GPP determine NPP and NEE.

The forest stand CUE was proportional to the basal area share of immature trees. We suggested and tested the basal-area-weighted DBH entropy as an easy-to-compute proxy for both the prevalence of mature trees and NPP and NEE. Other measures for structural diversity, namely the height standard deviation and the Shannon entropy of functional types, had much smaller predictive power. Our results were robust across spatial scales, and due to their solid mechanistic foundation and our generic model, our findings yield promising hypotheses for field studies and new theoretical work.

~~Understanding the drivers of forest productivity is key for an accurate assessment of forests' role in the global carbon cycle. Yet, despite significant research effort, it is not fully understood how the productivity of a forest can be deduced from its~~

stand structure. This is partially due to the challenge of accounting for increased carbon losses of mature trees in For example, we hypothesize that within-stand NPP increases with the DBH entropy and that focusing on immature (not full-grown) trees could yield more accurate structure-productivity relationships. We suggest to tackle this problem by identifying the share and structure of immature trees within mature forests and show that this approach could significantly improve estimates of forests' net productivity. As it is challenging to assess tree maturity for each individual in the field, we suggest an easy-to-compute stand-level proxy for the prevalence of mature trees, yielding the theoretical basis for future field studies improving our understanding of structure-productivity relationships.

## Acknowledgements

*Author contributions.* SMF and AH jointly conceived the study. XW contributed the field data. SMF parameterized the model with substantial input by AH and conducted the data analysis. SMF and AH jointly conceived the manuscript; SMF wrote the manuscript; AH revised the manuscript. All authors approved the manuscript.

*Competing interests.* The authors declare no competing interest.

*Acknowledgements.* The authors would like to thank the members of the vegetation modelling group at the UFZ and two anonymous reviewers for helpful discussions and feedback. This research was conducted as part of the project "The role of species traits and forest structure on spatial carbon dynamics of temperate forests" (ForCTrait), established within the cooperation "China-NSFC-DFG 2019" between the Deutsche Forschungsgemeinschaft (DFG, German Research Foundation) and the Natural Science Foundation of China (NSFC). This work was funded by the Deutsche Forschungsgemeinschaft (DFG) – 43150473.

## Author contributions

SMF and AH jointly conceived the study. XW contributed the field data. SMF parameterized the model with substantial input by AH and conducted the data analysis. SMF and AH jointly conceived the manuscript; SMF wrote the manuscript; AH revised the manuscript. All authors approved the manuscript.

## References


Aiba, S.-I. and Kohyama, T.: Crown Architecture and Life-History Traits of 14 Tree Species in a Warm- Temperate Rain Forest: Significance of Spatial Heterogeneity, The Journal of Ecology, 85, 611, https://doi.org/10.2307/2960532, 1997.

Anav, A., Friedlingstein, P., Beer, C., Ciais, P., Harper, A., Jones, C., Murray-Tortarolo, G., Papale, D., Parazoo, N. C., Peylin, P., Piao, S., Sitch, S., Viovy, N., Wiltshire, A., and Zhao, M.: Spatiotemporal Patterns of Terrestrial Gross Primary Production: A Review: GPP Spatiotemporal Patterns, Reviews of Geophysics, 53, 785–818, https://doi.org/10.1002/2015RG000483, 2015.

Anderson-Teixeira, K. J., Herrmann, V., Rollinson, C. R., Gonzalez, B., Gonzalez-Akre, E. B., Pederson, N., Alexander, M. R., Allen, C. D., Alfaro-Sánchez, R., Awada, T., Baltzer, J. L., Baker, P. J., Birch, J. D., Bunyavejchewin, S., Cherubini, P., Davies, S. J., Dow, C., Helcoski, R., Kašpar, J., Lutz, J. A., Margolis, E. Q., Maxwell, J. T., McMahon, S. M., Piponiot, C., Russo, S. E., Šamonil, P., Sniderhan, A. E., Tepley, A. J., Vašíčková, I., Vlam, M., and Zuidema, P. A.: Joint Effects of Climate, Tree Size, and Year on Annual Tree Growth Derived from Tree-ring Records of Ten Globally Distributed Forests, Global Change Biology, 28, 245–266, https://doi.org/10.1111/gcb.15934, 2022.

Beaumont, M. A., Zhang, W., and Balding, D. J.: Approximate Bayesian Computation in Population Genetics, Genetics, 162, 2025–2035, https://doi.org/10.1093/genetics/162.4.2025, 2002.

Binkley, D.: Acorn Review: The Persistent Mystery of Declining Growth in Older Forests, Forest Ecology and Management, 538, 121 004, https://doi.org/10.1016/j.foreco.2023.121004, 2023.

Bohn, F. J. and Huth, A.: The Importance of Forest Structure to Biodiversity–Productivity Relationships, Royal Society Open Science, 4, 160 521, https://doi.org/10.1098/rsos.160521, 2017.

Bohn, F. J., Frank, K., and Huth, A.: Of Climate and Its Resulting Tree Growth: Simulating the Productivity of Temperate Forests, Ecological Modelling, 278, 9–17, https://doi.org/10.1016/j.ecolmodel.2014.01.021, 2014.

Bohn, F. J., May, F., and Huth, A.: Species Composition and Forest Structure Explain the Temperature Sensitivity Patterns of Productivity in Temperate Forests, Biogeosciences, 15, 1795–1813, https://doi.org/10.5194/bg-15-1795-2018, 2018.

Bugmann, H. and Seidl, R.: The Evolution, Complexity and Diversity of Models of Long-term Forest Dynamics, Journal of Ecology, 110, 2288–2307, https://doi.org/10.1111/1365-2745.13989, 2022.

Cartis, C., Fiala, J., Marteau, B., and Roberts, L.: Improving the Flexibility and Robustness of Model-Based Derivative-Free Optimization Solvers, ACM Transactions on Mathematical Software, 45, 1–41, https://doi.org/10.1145/3338517, 2019.

Chisholm, R. A., Muller-Landau, H. C., Abdul Rahman, K., Bebber, D. P., Bin, Y., Bohlman, S. A., Bourg, N. A., Brinks, J., Bunyavejchewin, S., Butt, N., Cao, H., Cao, M., Cárdenas, D., Chang, L.-W., Chiang, J.-M., Chuyong, G., Condit, R., Dattaraja, H. S., Davies, S., Duque, A., Fletcher, C., Gunatilleke, N., Gunatilleke, S., Hao, Z., Harrison, R. D., Howe, R., Hsieh, C.-F., Hubbell, S. P., Itoh, A., Kenfack, D., Kiratiprayoon, S., Larson, A. J., Lian, J., Lin, D., Liu, H., Lutz, J. A., Ma, K., Malhi, Y., McMahon, S., McShea, W., Meegaskumbura, M., Mohd. Razman, S., Morecroft, M. D., Nytch, C. J., Oliveira, A., Parker, G. G., Pulla, S., Punchi-Manage, R., Romero-Saltos, H., Sang, W., Schurman, J., Su, S.-H., Sukumar, R., Sun, I.-F., Suresh, H. S., Tan, S., Thomas, D., Thomas, S., Thompson, J., Valencia, R., Wolf, A., Yap, S., Ye, W., Yuan, Z., and Zimmerman, J. K.: Scale-Dependent Relationships between Tree Species Richness and Ecosystem Function in Forests, Journal of Ecology, 101, 1214–1224, https://doi.org/10.1111/1365-2745.12132, 2013.

Chojnacky, D. C., Heath, L. S., and Jenkins, J. C.: Updated Generalized Biomass Equations for North American Tree Species, Forestry, 87, 129–151, https://doi.org/10.1093/forestry/cpt053, 2014.

Collalti, A., Ibrom, A., Stockmarr, A., Cescatti, A., Alkama, R., Fernández-Martínez, M., Matteucci, G., Sitch, S., Friedlingstein, P., Ciais, P., Goll, D. S., Nabel, J. E. M. S., Pongratz, J., Arneth, A., Haverd, V., and Prentice, I. C.: Forest Production Efficiency Increases with Growth Temperature, Nature Communications, 11, 5322, https://doi.org/10.1038/s41467-020-19187-w, 2020a.

Collalti, A., Tjoelker, M. G., Hoch, G., Mäkelä, A., Guidolotti, G., Heskel, M., Petit, G., Ryan, M. G., Battipaglia, G., Matteucci, G., and Prentice, I. C.: Plant Respiration: Controlled by Photosynthesis or Biomass?, Global Change Biology, 26, 1739–1753, https://doi.org/10.1111/gcb.14857, 2020b.

Conn, A. R., Gould, N. I. M., and Toint, P. L.: Trust-Region Methods, MPS-SIAM Series on Optimization, Society for Industrial and Applied Mathematics, Philadelphia, PA, ISBN 978-0-89871-460-9, 2000.

Costanza, R., d'Arge, R., de Groot, R., Farber, S., Grasso, M., Hannon, B., Limburg, K., Naeem, S., O'Neill, R. V., Paruelo, J., Raskin, R. G., Sutton, P., and van den Belt, M.: The Value of Ecosystem Services: Putting the Issues in Perspective, Ecological Economics, 25, 67–72, https://doi.org/10.1016/S0921-8009(98)00019-6, 1998.

Csilléry, K., Blum, M. G., Gaggiotti, O. E., and François, O.: Approximate Bayesian Computation (ABC) in Practice, Trends in Ecology & Evolution, 25, 410–418, https://doi.org/10.1016/j.tree.2010.04.001, 2010.

Dănescu, A., Albrecht, A. T., and Bauhus, J.: Structural Diversity Promotes Productivity of Mixed, Uneven-Aged Forests in Southwestern Germany, Oecologia, 182, 319–333, https://doi.org/10.1007/s00442-016-3623-4, 2016.

del Río, M., Bravo-Oviedo, A., Ruiz-Peinado, R., and Condés, S.: Tree Allometry Variation in Response to Intra- and Inter-Specific Competitions, Trees, 33, 121–138, https://doi.org/10.1007/s00468-018-1763-3, 2019.

Dislich, C., Günter, S., Homeier, J., Schröder, B., and Huth, A.: Simulating Forest Dynamics of a Tropical Montane Forest in South Ecuador, ERDKUNDE, 63, 347–364, https://doi.org/10.3112/erdkunde.2009.04.05, 2009.

Fischer, R., Bohn, F., Dantas de Paula, M., Dislich, C., Groeneveld, J., Gutiérrez, A. G., Kazmierczak, M., Knapp, N., Lehmann, S., Paulick, S., Pütz, S., Rödig, E., Taubert, F., Köhler, P., and Huth, A.: Lessons Learned from Applying a Forest Gap Model to Understand Ecosystem and Carbon Dynamics of Complex Tropical Forests, Ecological Modelling, 326, 124–133, https://doi.org/10.1016/j.ecolmodel.2015.11.018, 2016.

Forrester, D. I.: Does Individual-Tree Biomass Growth Increase Continuously with Tree Size?, Forest Ecology and Management, 481, 118 717, https://doi.org/10.1016/j.foreco.2020.118717, 2021.

Forrester, D. I. and Bauhus, J.: A Review of Processes Behind Diversity—Productivity Relationships in Forests, Current Forestry Reports, 2, 45–61, https://doi.org/10.1007/s40725-016-0031-2, 2016.

Foster, J. R., Finley, A. O., D'Amato, A. W., Bradford, J. B., and Banerjee, S.: Predicting Tree Biomass Growth in the Temperate–Boreal Ecotone: Is Tree Size, Age, Competition, or Climate Response Most Important?, Global Change Biology, 22, 2138–2151, https://doi.org/10.1111/gcb.13208, 2016.

Gea-Izquierdo, G. and Sánchez-González, M.: Forest Disturbances and Climate Constrain Carbon Allocation Dynamics in Trees, Global Change Biology, 28, 4342–4358, https://doi.org/10.1111/gcb.16172, 2022.

Gibbons, P., Lindenmayer, D. B., Fischer, J., Manning, A. D., Weinberg, A., Seddon, J., Ryan, P., and Barrett, G.: The Future of Scattered Trees in Agricultural Landscapes, Conservation Biology, 22, 1309–1319, https://doi.org/10.1111/j.1523-1739.2008.00997.x, 2008.

Gower, S. T., McMurtrie, R. E., and Murty, D.: Aboveground Net Primary Production Decline with Stand Age: Potential Causes, Trends in Ecology & Evolution, 11, 378–382, https://doi.org/10.1016/0169-5347(96)10042-2, 1996.

Jha, S., Das, J., and Goyal, M. K.: Assessment of Risk and Resilience of Terrestrial Ecosystem Productivity under the Influence of Extreme Climatic Conditions over India, Scientific Reports, 9, 18 923, https://doi.org/10.1038/s41598-019-55067-0, 2019.

Jones, E., Oliphant, T., and Peterson, P.: SciPy: Open Source Scientific Tools for Python, https://scipy.org/, 2001.

Kohyama, T., Suzuki, E., Partomihardjo, T., Yamada, T., and Kubo, T.: Tree Species Differentiation in Growth, Recruitment and Allometry in Relation to Maximum Height in a Bornean Mixed Dipterocarp Forest: *Tree Species Differentiation*, Journal of Ecology, 91, 797–806, https://doi.org/10.1046/j.1365-2745.2003.00810.x, 2003.

LaRue, E. A., Knott, J. A., Domke, G. M., Chen, H. Y., Guo, Q., Hisano, M., Oswalt, C., Oswalt, S., Kong, N., Potter, K. M., and Fei, S.: Structural Diversity as a Reliable and Novel Predictor for Ecosystem Productivity, Frontiers in Ecology and the Environment, 21, 33–39, https://doi.org/10.1002/fee.2586, 2023.

Lehmann, S. and Huth, A.: Fast Calibration of a Dynamic Vegetation Model with Minimum Observation Data, Ecological Modelling, 301, 98–105, https://doi.org/10.1016/j.ecolmodel.2015.01.013, 2015.

Lett, S. and Dorrepaal, E.: Global Drivers of Tree Seedling Establishment at Alpine Treelines in a Changing Climate, Functional Ecology, 32, 1666–1680, https://doi.org/10.1111/1365-2435.13137, 2018.

Liu, Q.-J.: Nested regression for establishing tree biomass equations, Chinese Journal of Plant Ecology, 33, 331, 2009.

Liu, R., Chen, J., Liu, J., Deng, F., and Sun, R.: Application of a New Leaf Area Index Algorithm to China's Landmass Using MODIS Data for Carbon Cycle Research, Journal of Environmental Management, 85, 649–658, https://doi.org/10.1016/j.jenvman.2006.04.023, 2007.

Liu, X., Swenson, N. G., Lin, D., Mi, X., Umaña, M. N., Schmid, B., and Ma, K.: Linking Individual-level Functional Traits to Tree Growth in a Subtropical Forest, Ecology, 97, 2396–2405, https://doi.org/10.1002/ecy.1445, 2016.

McElhinny, C., Gibbons, P., Brack, C., and Bauhus, J.: Forest and Woodland Stand Structural Complexity: Its Definition and Measurement, Forest Ecology and Management, 218, 1–24, https://doi.org/10.1016/j.foreco.2005.08.034, 2005.

Merganičová, K., Merganič, J., Lehtonen, A., Vacchiano, G., Sever, M. Z. O., Augustynczik, A. L. D., Grote, R., Kyselová, I., Mäkelä, A., Yousefpour, R., Krejza, J., Collalti, A., and Reyer, C. P. O.: Forest Carbon Allocation Modelling under Climate Change, Tree Physiology, 39, 1937–1960, https://doi.org/10.1093/treephys/tpz105, 2019.

Munné-Bosch, S.: Limits to Tree Growth and Longevity, Trends in Plant Science, 23, 985–993, https://doi.org/10.1016/j.tplants.2018.08.001, 2018.

Niinemets, Ü. and Valladares, F.: Tolerance to Shade, Drought, and Waterlogging of Temperate Northern Hemisphere Trees and Shrubs, Ecological Monographs, 76, 521–547, https://doi.org/10.1890/0012-9615(2006)076[0521:TTSDAW]2.0.CO;2, 2006.

O'Leary, B. M., Asao, S., Millar, A. H., and Atkin, O. K.: Core Principles Which Explain Variation in Respiration across Biological Scales, New Phytologist, 222, 670–686, https://doi.org/10.1111/nph.15576, 2019.

Park, J., Kim, H. S., Jo, H. K., and Jung, I. B.: The Influence of Tree Structural and Species Diversity on Temperate Forest Productivity and Stability in Korea, Forests, 10, 1113, https://doi.org/10.3390/f10121113, 2019.

Paulick, S., Dislich, C., Homeier, J., Fischer, R., and Huth, A.: The Carbon Fluxes in Different Successional Stages: Modelling the Dynamics of Tropical Montane Forests in South Ecuador, Forest Ecosystems, 4, 5, https://doi.org/10.1186/s40663-017-0092-0, 2017.

Piponiot, C., Anderson-Teixeira, K. J., Davies, S. J., Allen, D., Bourg, N. A., Burslem, D. F. R. P., Cárdenas, D., Chang-Yang, C.-H., Chuyong, G., Cordell, S., Dattaraja, H. S., Duque, Á., Ediriweera, S., Ewango, C., Ezedin, Z., Filip, J., Giardina, C. P., Howe, R., Hsieh, C.-F., Hubbell, S. P., Inman-Narahari, F. M., Itoh, A., Janík, D., Kenfack, D., Král, K., Lutz, J. A., Makana, J.-R., McMahon, S. M., McShea, W., Mi, X., Bt. Mohamad, M., Novotný, V., O'Brien, M. J., Ostertag, R., Parker, G., Pérez, R., Ren, H., Reynolds, G., Md Sabri, M. D., Sack, L., Shringi, A., Su, S.-H., Sukumar, R., Sun, I.-F., Suresh, H. S., Thomas, D. W., Thompson, J., Uriarte, M., Vandermeer, J., Wang, Y., Ware, I. M., Weiblen, G. D., Whitfeld, T. J. S., Wolf, A., Yao, T. L., Yu, M., Yuan, Z., Zimmerman, J. K., Zuleta, D., and

Muller-Landau, H. C.: Distribution of Biomass Dynamics in Relation to Tree Size in Forests across the World, New Phytologist, 234, 1664–1677, https://doi.org/10.1111/nph.17995, 2022.

Potkay, A., Hölttä, T., Trugman, A. T., and Fan, Y.: Turgor-Limited Predictions of Tree Growth, Height and Metabolic Scaling over Tree Lifespans, Tree Physiology, 42, 229–252, https://doi.org/10.1093/treephys/tpab094, 2022.

Prislan, P., Gričar, J., De Luis, M., Smith, K. T., and Čufar, K.: Phenological Variation in Xylem and Phloem Formation in Fagus Sylvatica from Two Contrasting Sites, Agricultural and Forest Meteorology, 180, 142–151, https://doi.org/10.1016/j.agrformet.2013.06.001, 2013.

Rödig, E., Cuntz, M., Heinke, J., Rammig, A., and Huth, A.: Spatial Heterogeneity of Biomass and Forest Structure of the Amazon Rain Forest: Linking Remote Sensing, Forest Modelling and Field Inventory, Global Ecology and Biogeography, 26, 1292–1302, https://doi.org/10.1111/geb.12639, 2017.

Rödig, E., Cuntz, M., Rammig, A., Fischer, R., Taubert, F., and Huth, A.: The Importance of Forest Structure for Carbon Fluxes of the Amazon Rainforest, Environmental Research Letters, 13, 054 013, https://doi.org/10.1088/1748-9326/aabc61, 2018.

Russell, M. B. and Weiskittel, A. R.: Maximum and Largest Crown Width Equations for 15 Tree Species in Maine, Northern Journal of Applied Forestry, 28, 84–91, https://doi.org/10.1093/njaf/28.2.84, 2011.

Sato, H., Itoh, A., and Kohyama, T.: SEIB-DGVM: A New Dynamic Global Vegetation Model Using a Spatially Explicit Individual-Based Approach, Ecological Modelling, 200, 279–307, https://doi.org/10.1016/j.ecolmodel.2006.09.006, 2007.

Sheil, D. and Bongers, F.: Interpreting Forest Diversity-Productivity Relationships: Volume Values, Disturbance Histories and Alternative Inferences, Forest Ecosystems, 7, 6, https://doi.org/10.1186/s40663-020-0215-x, 2020.

Sheil, D., Eastaugh, C. S., Vlam, M., Zuidema, P. A., Groenendijk, P., Sleen, P., Jay, A., and Vanclay, J.: Does Biomass Growth Increase in the Largest Trees? Flaws, Fallacies and Alternative Analyses, Functional Ecology, 31, 568–581, https://doi.org/10.1111/1365-2435.12775, 2017.

Shugart, H. H., Wang, B., Fischer, R., Ma, J., Fang, J., Yan, X., Huth, A., and Armstrong, A. H.: Gap Models and Their Individual-Based Relatives in the Assessment of the Consequences of Global Change, Environmental Research Letters, 13, 033 001, https://doi.org/10.1088/1748-9326/aaaacc, 2018.

Silva Pedro, M., Rammer, W., and Seidl, R.: Disentangling the Effects of Compositional and Structural Diversity on Forest Productivity, Journal of Vegetation Science, 28, 649–658, https://doi.org/10.1111/jvs.12505, 2017.

Staudhammer, C. L. and LeMay, V. M.: Introduction and Evaluation of Possible Indices of Stand Structural Diversity, Canadian Journal of Forest Research, 31, 1105–1115, https://doi.org/10.1139/x01-033, 2001.

Stephenson, N. L., Das, A. J., Condit, R., Russo, S. E., Baker, P. J., Beckman, N. G., Coomes, D. A., Lines, E. R., Morris, W. K., Rüger, N., Álvarez, E., Blundo, C., Bunyavejchewin, S., Chuyong, G., Davies, S. J., Duque, Á., Ewango, C. N., Flores, O., Franklin, J. F., Grau, H. R., Hao, Z., Harmon, M. E., Hubbell, S. P., Kenfack, D., Lin, Y., Makana, J.-R., Malizia, A., Malizia, L. R., Pabst, R. J., Pongpattananurak, N., Su, S.-H., Sun, I.-F., Tan, S., Thomas, D., van Mantgem, P. J., Wang, X., Wiser, S. K., and Zavala, M. A.: Rate of Tree Carbon Accumulation Increases Continuously with Tree Size, Nature, 507, 90–93, https://doi.org/10.1038/nature12914, 2014.

Sun, R., Chen, J. M., Zhu, Q., Zhou, Y., Liu, J., Li, J., Liu, S., Yan, G., and Tang, S.: Spatial Distribution of Net Primary Productivity and Evapotranspiration in Changbaishan Natural Reserve, China, Using Landsat ETM+ Data, Canadian Journal of Remote Sensing, 30, 731–742, https://doi.org/10.5589/m04-040, 2004.

Tang, J., Luyssaert, S., Richardson, A. D., Kutsch, W., and Janssens, I. A.: Steeper Declines in Forest Photosynthesis than Respiration Explain Age-Driven Decreases in Forest Growth, Proceedings of the National Academy of Sciences, 111, 8856–8860, https://doi.org/10.1073/pnas.1320761111, 2014.

Varin, C.: On Composite Marginal Likelihoods, AStA Advances in Statistical Analysis, 92, 1–28, https://doi.org/10.1007/s10182-008-0060-7, 2008.

Waide, R. B., Willig, M. R., Steiner, C. F., Mittelbach, G., Gough, L., Dodson, S. I., Juday, G. P., and Parmenter, R.: The Relationship Between Productivity and Species Richness, Annual Review of Ecology and Systematics, 30, 257–300, https://doi.org/10.1146/annurev.ecolsys.30.1.257, 1999.

Wales, D. J. and Doye, J. P. K.: Global Optimization by Basin-hopping and the Lowest Energy Structures of Lennard-Jones Clusters Containing up to 110 Atoms, The Journal of Physical Chemistry A, 101, 5111–5116, https://doi.org/10.1021/jp970984n, 1997.

Wand, M. P. and Jones, M. C.: Kernel Smoothing, no. 60 in Monographs on Statistics and Applied Probability, Chapman & Hall, London ; New York, 1st ed edn., ISBN 978-0-412-55270-0, 1995.

Wang, H., Xu, J., Sheng, L., Ma, L., and Liu, X.: Study on the Characteristics of Climate Change in Changbai Mountain National Natural Reserve from 1958 to 2017, Arabian Journal of Geosciences, 13, 777, https://doi.org/10.1007/s12517-020-05808-7, 2020.

Wang, X., Ye, J., Li, B., Zhang, J., Lin, F., and Hao, Z.: Spatial Distributions of Species in an Old-Growth Temperate Forest, Northeastern China, Canadian Journal of Forest Research, 40, 1011–1019, https://doi.org/10.1139/X10-056, 2010.

Weedon, G. P., Balsamo, G., Bellouin, N., Gomes, S., Best, M. J., and Viterbo, P.: The WFDEI Meteorological Forcing Data Set: WATCH Forcing Data Methodology Applied to ERA-Interim Reanalysis Data, Water Resources Research, 50, 7505–7514, https://doi.org/10.1002/2014WR015638, 2014.

West, G. B., Brown, J. H., and Enquist, B. J.: A General Model for the Structure and Allometry of Plant Vascular Systems, Nature, 400, 664–667, https://doi.org/10.1038/23251, 1999.

West, P. W.: Do Increasing Respiratory Costs Explain the Decline with Age of Forest Growth Rate?, Journal of Forestry Research, 31, 693–712, https://doi.org/10.1007/s11676-019-01020-w, 2020.

Wiley, E. and Helliker, B.: A Re-evaluation of Carbon Storage in Trees Lends Greater Support for Carbon Limitation to Growth, New Phytologist, 195, 285–289, https://doi.org/10.1111/j.1469-8137.2012.04180.x, 2012.

Wu, J. B., Xiao, X. M., Guan, D. X., Shi, T. T., Jin, C. J., and Han, S. J.: Estimation of the Gross Primary Production of an Old-growth Temperate Mixed Forest Using Eddy Covariance and Remote Sensing, International Journal of Remote Sensing, 30, 463–479, https://doi.org/10.1080/01431160802372143, 2009.

Xie, X., Li, A., Jin, H., Tan, J., Wang, C., Lei, G., Zhang, Z., Bian, J., and Nan, X.: Assessment of Five Satellite-Derived LAI Datasets for GPP Estimations through Ecosystem Models, Science of The Total Environment, 690, 1120–1130, https://doi.org/10.1016/j.scitotenv.2019.06.516, 2019.

Xu, Z., Liu, Q., Du, W., Zhou, G., Qin, L., and Sun, Z.: Modelling Leaf Phenology of Some Trees with Accumulated Temperature in a Temperate Forest in Northeast China, Forest Ecology and Management, 489, 119 085, https://doi.org/10.1016/j.foreco.2021.119085, 2021.

Yunusa, I. A. M. and Newton, P. J.: Plants for Amelioration of Subsoil Constraints and Hydrological Control: The Primer-Plant Concept, Plant and Soil, 257, 261–281, https://doi.org/10.1023/A:1027381329549, 2003.

# Supplementary Information



## Appendix A: Data availability by species

The table below displays basic information and data availability for each species in the inventory of 2014. The rows are sorted by the species' respective basal areas (including minor stems). The column "PFT" indicates the plant functional types the species were assigned to; the PFT numbers correspond to those provided in SI B2. The column "Allometry data available" shows whether DBH-dependent data on allometric properties, such as tree height or crown length, were available. The column

"Biomass equation available" indicates whether we found a suitable DBH biomass relationship in Chojnacky et al. (2014). Species not present in the inventory of 2014 were omitted.

The allometry dataset contained DBH values, heights, crown diameters, and crown lengths for individual trees. On average, the dataset contained 73 individuals per species covered in the dataset.

Note that when fitting allometric equations for plant functional types (PFTs), the species were weighted according to their share in the inventory (SI B3). Hence, missing data are not expected to impact the fitted relationships significantly if the corresponding species have a small share of basal area in the inventory. Furthermore, the biomass equations were only used to approximate the relative share of each PFT in the inventory and estimate a single parameter per PFT based on this information (SI .B4.5). Therefore, missing data are not expected to impact the model results significantly.

| Species | Basal area in inventory $\left[\frac{\mathrm{m}^2}{\mathrm{ha}}\right]$ | PFT | Shade tolerance | Allometry data available | Biomass equation available |
|---|---|---|---|---|---|
| *Tilia amurensis* | 12.556 | 6 | Shade tolerant | ✓ | ✓ |
| *Pinus koraiensis* | 9.870 | 4 | Midtolerant | ✓ | ✓ |
| *Quercus mongolica* | 6.748 | 3 | Light demanding | ✓ | ✓ |
| *Fraxinus mandshurica* | 6.098 | 4 | Midtolerant | ✓ | ✓ |
| *Acer mono* | 2.552 | 6 | Shade tolerant | ✓ | ✓ |
| *Ulmus japonica* | 1.867 | 4 | Midtolerant | ✓ | ✓ |
| *Acer pseudo-sieboldianum* | 1.254 | 5 | Shade tolerant | ✓ | ✓ |
| *Populus ussuriensis* | 1.212 | 2 | Light demanding | ✓ | ✓ |
| *Tilia mandshurica* | 0.345 | 6 | Shade tolerant | ✓ | ✓ |
| *Maackia amurensis* | 0.285 | 4 | Midtolerant | ✓ | – |
| *Populus koreana* | 0.203 | 2 | Light demanding | ✓ | ✓ |
| *Acer barbinerve* | 0.199 | 5 | Shade tolerant | – | – |
| *Betula platyphylla* | 0.179 | 2 | Light demanding | ✓ | ✓ |
| *Corylus mandshurica* | 0.151 | 5 | Shade tolerant | – | – |
| *Acer triflorum* | 0.120 | 6 | Shade tolerant | ✓ | – |
| *Acer tegmentosum* | 0.120 | 5 | Shade tolerant | ✓ | – |
| *Syringa reticulata* | 0.110 | 1 | Light demanding | ✓ | – |
| *Malus baccata* | 0.103 | 6 | Shade tolerant | ✓ | – |
| *Phellodendron amurense* | 0.100 | 2 | Light demanding | ✓ | – |
| *Acer mandshuricum* | 0.083 | 6 | Shade tolerant | ✓ | – |
| *Prunus padus* | 0.073 | 6 | Shade tolerant | ✓ | – |

| Species | Basal area in inventory $\left[\frac{\mathrm{m}^2}{\mathrm{ha}}\right]$ | PFT | Shade tolerance | Allometry data available | Biomass equation available |
|---|---|---|---|---|---|
| *Ulmus laciniata* | 0.068 | 4 | Midtolerant | ✓ | – |
| *Betula costata* | 0.053 | 2 | Light demanding | ✓ | – |
| *Populus davidiana* | 0.031 | 2 | Light demanding | ✓ | – |
| *Pyrus ussuriensis* | 0.026 | 2 | Light demanding | ✓ | – |
| *Abies nephrolepis* | 0.026 | 4 | – | ✓ | – |
| *Rhamnus ussuriensis* | 0.017 | 5 | Shade tolerant | – | – |
| *Cerasus maximowiczii* | 0.010 | 1 | Light demanding | – | – |
| *Acer ginnala* | 0.009 | 5 | Shade tolerant | – | – |
| *Sorbus alnifolia* | 0.006 | 5 | Shade tolerant | ✓ | – |
| *Philadelphus schrenkii* | 0.004 | 5 | Shade tolerant | – | – |
| *Rhamnus davurica* | 0.004 | 5 | Shade tolerant | – | – |
| *Crataegus maximowiczii* | 0.002 | 1 | – | – | – |
| *Euonymus pauciflorus* | 0.001 | 5 | Shade tolerant | – | – |
| *Euonymus alatus* | 0.001 | 5 | Shade tolerant | – | – |
| *Acanthopanax senticosus* | 0.000 | 5 | Shade tolerant | – | – |
| *Sambucus williamsii* | 0.000 | 1 | Light demanding | – | – |
| *Lonicera chrysantha* | 0.000 | 5 | – | – | – |
| *Viburnum sargenti* | 0.000 | 5 | Shade tolerant | – | – |
| *Actinidia kolomikta* | 0.000 | 5 | – | – | – |
| *Viburnum bureiaeticum* | 0.000 | 5 | Shade tolerant | – | – |
| *Rhamnus diamantiaca* | 0.000 | 5 | Shade tolerant | – | – |
| *Euonymus macropterus* | 0.000 | 5 | Shade tolerant | – | – |
| *Vitis amurensis* | 0.000 | 5 | – | – | – |
| *Aralia elata* | 0.000 | 5 | Shade tolerant | – | – |
| *Deutzia amurensis* | 0.000 | 5 | – | – | – |
| *Sorbaria sorbifolia* | 0.000 | 4 | – | – | – |

## Appendix B: Parameterization of the forest model FORMIND

The forest model FORMIND is described in detail by Bohn et al. (2014) and Fischer et al. (2016). Below we focus on those aspects of the model that deviate from this description, and we provide details about the parameter choice and model fitting procedure. We based our analysis on forest inventory data from an old-growth temperate forest in the Changbaishan National Nature Reserve in northeastern China. The surveyed area consists of $25\,\mathrm{ha}$ of conifer/broad-leaf mixed forest with $47$ species, a total biomass of $302\,{}^{\mathrm{t\,ODM}}/_{\mathrm{ha}}$ (Piponiot et al., 2022). The inventory data contain the position, diameter at breast height (DBH) and species of each tree with $\mathrm{DBH} \geq 1\mathrm{cm}$ for the census years $2004$, $2009$, and $2014$. Each tree is uniquely identified with an ID number. For trees that had multiple stems at breast height, we focused on the main stem (maximal DBH) in our analysis and we disregarded minor stems.

Below we provide an overview of the parameterization procedure before describing each step in detail.

### Overview

We started by assigning species to PFTs, which aggregate species dependent on their shade tolerance and sizes (SI B2). Where no shade tolerance data were available, we assigned species to a PFT based on the light demand of their saplings and their median observed DBH increment. Next, we derived environmental parameters from the literature and public data sets (SI B10).

To incorporate species traits and allometric relationships into the model, we computed mean trait values / allometries for each PFT based on independent species-specific data sets or the literature, weighting the species according to their basal area share in the inventory. For size-dependent traits / allometries, we fitted simple functions mapping the DBH to the corresponding trait value. We considered the following DBH-dependent traits: Tree height (SI B3.1), crown length (SI B3.2), crown diameter (SI B3.3), stem from factor (SI B3.4), and LAI (SI B4.3). Furthermore, we considered the following constant traits: maximal DBH (SI B4.1), wood density (SI B4.2), light extinction coefficient (SI B4.4), and mean stem biomass proportion (mean taken over DBH values; SI B4.5).

To parameterize the modelled processes, we used a combination of approaches. Where possible, we derived parameters by comparing inventory data from two consecutive censuses. This applied to the parameters of the optimal potential growth of trees (SI B7.1) and tree mortality (SI B9). Some further parameters could be derived by considering the light climate that FORMIND obtains for the forest state observed in the inventory. That way, we could estimate the maximal incident radiation of trees in the inventory (SI B7.2) and constrain the carbon use efficiency (CUE) of trees (SI B7.4). The remaining process-related parameters were determined by fitting the results from dynamic model simulations to the observed inventory data. With this approach, we obtained the parameters for the seed influx (SI B5), ingrowth of saplings (SI B6), photosynthesis (SI B7.3), carbon losses other than maintenance respiration (SI B7.4), as well as another parameter controlling the optimal growth of trees (SI B7.1).

To fit the model to the inventory data by optimizing the latter parameters, we used a likelihood-based approach, maximizing the likelihood with which the collected inventory data are observed according to the model (SI B11). This method has the advantage that it can be applied on small scales (here: $0.04\,\mathrm{ha}$), where forest data are highly stochastic and can have strongly

skewed distributions. The approach fits the model not only to spatially aggregated forest attributes but considers their entire distribution. That is, it seeks to reproduce the frequency of each possible forest state, including uncommon or extreme states. By considering the complete state distribution, more information is used in the fitting stage, and parameters can be estimated with higher precision and accuracy.

Though we largely applied the same FORMIND version used in previous studies (Fischer et al., 2016), we also adjusted some submodels to achieve higher realism and to assert that fitted parameters do not lead to unreasonable model behaviour. We made the following procedural adjustments:

**Individual-specific size limits (SI B4.1):** We allowed each individual tree to have a different DBH limit. That way, we could account for (1) different size limits of the species within the PFTs and (2) heterogeneity in local conditions constraining tree height. Without individual-specific size limits, all mature trees in a PFT would have had the same size, potentially introducing model artifacts to the relationships between forest structure and tree maturity and hence forest productivity.

**Ingrowth (SI B6):** Rather than using sharp light thresholds to decide whether seeds can establish to saplings, we used sigmoid curves that allow a small fraction of seeds to establish even under unfavourable conditions. This approach avoids sudden strong changes in ingrowth dynamics, potentially leading to greater heterogeneity in forest patches.

**Optimal DBH increment (SI B7.1):** We estimated the optimal growth of trees as a certain quantile of the DBH increment distribution. This approach is more robust than simply considering maximal observed DBH increments, as it is insensitive to outliers and avoids the statistical bias that could occur if the tree size distribution is not uniform.

**Reference light conditions (SI B7.2):** We assumed that the maximal DBH increments observed in the inventory were achieved under shaded conditions for small trees. In earlier parameterizations of FORMIND, it was typically assumed that the fastest-growing trees in the inventory were not shaded, irrespective of their size. For the Changbaishan forest, this was not in line with the light climate that FORMIND estimated based on the inventory data.

**CUE under optimal conditions (SI B7.4) / size-dependent biomass allocation (SI B7.5):** We introduced a submodel for the optimal CUE of trees and used this along with biomass data to derive DBH-dependent stem and crown biomass proportions and to scale the light response curve (c.f. the introduction of section B7). Without this approach, GPP and respiration would have had to be parameterized independently of one antother, making it likely (sometimes inevitable) to run into situations where for some trees either (1) the parameterized GPP does not suffice for the biomass increment observed in the inventory, resulting in zero-estimates for the maintenance respiration of these trees or (2) the parameterized GPP exceeds the observed biomass increment by orders of magnitude, resulting in maintenance respiration estimates so high that even moderately shaded trees cannot satisfy their respiratory needs and die. These situations cannot occur if the optimal CUE is fixed to reasonable values.

**Defoliation (SI B7.6):** We created a new submodel for stress situations in which trees' maintenance respiration exceeds their GPP. In the new model, trees loose leaves and biomass until their remaining respiratory needs can be satisfied. As the

loss of leaves leads to a further decline of GPP, stress can result in a feedback loop leading to tree death. Hence, the defoliation mechanism constrains the forest density in a mechanistic manner. The previous approach to model space competition was based on stochastic crowding mortality and would have capped the forest density even if all trees had a positive NPP and thus growth potential. By linking the maximal forest density to productivity and respiration, the defoliation approach also helped to obtain realistic parameters for the corresponding submodels.

After providing an overview of the parameterization procedure, we list all parameterization details required to reproduce the study results.

### B1 Time step and simulation area

We ran the model using a yearly time step. We simulated a square-shaped forest area of one hectare, subdivided into $25$ patches of $20\mathrm{m} \times 20\mathrm{m}$, in which light competition occurs. Plants in different patches interact via tree falling only. For this interaction, we assume torus boundary conditions to minimize boundary effects.

### B2 Classification of species to plant functional types (PFTs)

We assigned the $47$ tree species into $6$ plant functional types (PFTs) according to their shade tolerance and their maximal height. In addition, we considered the species Mongolian Oak (*Quercus mongolica*) individually, as it had a unique DBH distribution in the forest, making it difficult to assign it to other PFTs without major information loss. We considered the following $6$ PFTs:

1. Small shade intolerant species (pioneers with maximal diameter at breast height (DBH) below $30\mathrm{cm}$).
2. Large shade intolerant species 1 (pioneers with maximal DBH exceeding $30\mathrm{cm}$).
3. Large shade intolerant species 2 (Mongolian oak).
4. Large mid-tolerant species (intermediate species with maximal DBH exceeding $30\mathrm{cm}$).
5. Small shade tolerant species (climax species with maximal DBH below $30\mathrm{cm}$).
6. Large shade tolerant species (climax species with maximal DBH exceeding $30\mathrm{cm}$).

We did not consider a PFT of small mid-tolerant species, because there were no mid-tolerant species with maximal DBH below $30\mathrm{cm}$.

#### Classification of species with unknown shade tolerance class

We assigned species for which shade tolerance classification data were not readily available to the PFTs via a likelihood-based cluster analysis. For this analysis, we determined the median DBH change after 5 years for each species' individuals observed in the inventory. We used this value along with numerical shade tolerance data (Niinemets and Valladares, 2006; Wang et al.,

2010), indicating the fraction of sunlight that a sapling requires to grow, as covariates. A shade tolerance value of 1 corresponds to a light requirement of $> 50\%$ of the full sunlight; 2 to 25%–50%; 3 to 10%–25%; 4 to 5%–10%; 5 to 2%–5%.

We assumed that the covariates follow a multivariate normal distribution $\mathcal{N}(\mu_i, \Sigma_i)$ for each shade tolerance class $i$. We estimated the means $\mu_i$ and covariance matrices $\Sigma_i$ using the method of moments. For each shade tolerance group $i$, we determined the mean values $\mu_{ij}$ of the covariates $j$ and covariances $\Sigma_{ij_1j_2}$ between covariate $j_1$ and $j_2$. We assigned each species $s$ with unknown shade tolerance type to the class for which the likelihood based on the derived distributions was maximized. That is, with $x_s$ being the covariate vector of species $s$ and $f_{\mathcal{N}}$ the density function of the two-dimensional multivariate normal distribution, we set

$$\text{class}(s) = \underset{\text{classes } i}{\text{argmax}}\, f_{\mathcal{N}}(x_j; \mu_i, \Sigma_i). \tag{S1}$$

Fig. S1 depicts the classification of the species into shade tolerance classes.

### B3 Allometric relationships

We determined allometric relationships for the six PFTs based on allometry data for the individual species. Specifically, we estimated the relationships between DBH and the geometric properties tree height, crown length, and crown radius, respectively. Let $p$ be the index of a geometric property, $i$ the considered PFT, $\theta_{pi}$ a parameter vector and $x_{pi}$ the value of allometric property $p$ for PFT $i$, $d$ be the DBH and $g_p : \mathbb{R}_+ \to \mathbb{R}_+$ an injective function. Then we set

$$x_{pi} = g_p(d; \theta_{pi}). \tag{S2}$$

To estimate the parameter vectors $\theta_{pi}$, we used a dataset containing tuples of tree DBH and tree height, crown length, and crown radius for several species. As we desired to find the allometric relationships that best represent the considered forest in Changbaishan, we weighted the data according to the frequency of trees with similar species and DBH in the inventory (see subsection F1). Then we fitted the parameters $\theta_{pi}$ based on the weighted likelihood, assuming that the data were subject to a normally distributed error with constant variance $\sigma_{pi}^2$:

$$X_{pi} \sim \mathcal{N}\big(g_p(d; \theta_{pi}), \sigma_{pi}^2\big), \tag{S3}$$

where $X_{pi}$ denotes the observed geometry values. This reduces to a weighted least squares method. That is, the objective function can be expressed as

$$\bar{\ell}(\theta_{pi}) = -\sum_{k \in \mathcal{A}_i} \left(x_{pik} - g_p(d_k; \theta_{pi})\right)^2 w_k, \tag{S4}$$

where $\mathcal{A}_i$ is the set of entries in the allometry dataset corresponding to trees of PFT $i$, $x_{pk}$ is the observed value for the geometric property $p$ in entry $k$, $d_k$ is the corresponding DBH value, and $w_k$ is the weight. To maximize the likelihood, we

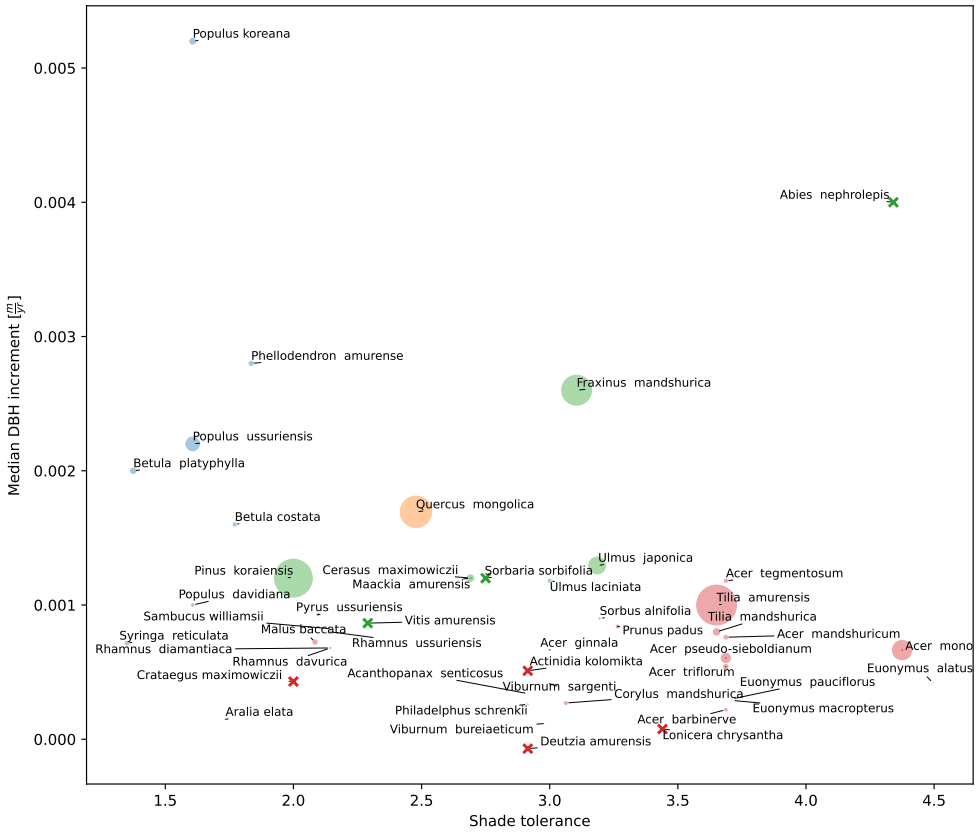


**Figure S1.** Assignment of species to PFTs with unknown shade tolerance based on a cluster analysis. Each colour corresponds to a shade tolerance type: shade intolerant (blue), mid-tolerant (green), shade tolerant (red). *Quercus mongolica* is drawn in a separate colour (orange), as it is a PFT on its own. Circles indicate species with a known shade tolerance type. The size of the circles correspond to the respective species' basal area in the inventory. Crosses depict species for which the shade tolerance type was assigned via the cluster analysis. The shade tolerance values indicate the fraction of sunlight that a sapling of the respective species requires to grow. Here, 1 corresponds to a light requirement of $> 50\%$ of the full sunlight; 2: 25%–50%; 3: 10%–25%; 4: 5%–10%; 5: 2%–5%.

used a Newton-Raphson-type trust region approach (Conn et al., 2000) as provided in the Python library Scipy (Jones et al., 2001).

For some species, no allometry data were available even though they were present in the inventory. Due to the lack of data, these species were not taken into account when fitting the allometric relationships. However, they were responsible for only a small share ($4\%$) of the basal area in the inventory (cf. SI A), so that their impact on the fitted relationships would have been small and we expect the lack of data not to bias the results significantly.

**Table S1.** Parameter values for allometric relationships.

### B3.1 Height

For the relationship between DBH and tree height, we used the model

$$g_{\text{height}}(d;\theta_{\text{height},i}) = \frac{\theta_{\text{height},i,0}\theta_{\text{height},i,1}d}{d\cdot\theta_{\text{height},i,0}+\theta_{\text{height},i,1}}, \tag{S5}$$

where $\theta_{\text{height},i,0}$ is the initial slope of $g_{\text{height}}$ and $\theta_{\text{height},i,1}$ is the height asymptote. The fitted parameter values are displayed in Table S1; the fitted curves are shown in Fig. S2a..

### B3.2 Crown length

We used a linear relationship to model the relationship between tree height and crown length:

$$\tilde{g}_{\text{crown-l}}(h;\theta_{\text{crown-l},i}) = \theta_{\text{crown-l},i}\cdot h, \tag{S6}$$

where $h$ is the tree height. With equation (S5), equation (S6) can also be expressed as a function of the DBH:

$$g_{\text{crown-l}}(d;\theta_{\text{height},i},\theta_{\text{crown-l},i}) = \theta_{\text{crown-l},i}\cdot g_{\text{height}}(d;\theta_{\text{height},i}). \tag{S7}$$

The fitted parameter values are displayed in Table S1; the fitted curves are depicted in Fig. S2b.

### B3.3 (Maximal) crown diameter

For the relationship between DBH and crown diameter, we used a power-law model:

$$g_{\text{crown-d}}(d;\theta_{\text{crown-d},i}) = \theta_{\text{crown-d},0}\cdot d^{\theta_{\text{crown-d},1}}, \tag{S8}$$

where $\theta_{\text{crown-d},0}$ is the scaling factor and $\theta_{\text{crown-d},1}$ is the exponent. The fitted parameter values are displayed in Table S1 and the fitted curves in Fig. S2c.

Typically, the crown diameter of trees varies with height, and the available allometry data represent *maximal* crown diameters. In this parameterization of FORMIND, however, crowns are assumed to have cylindrical shapes, with diameters constant along the vertical axis. Hence, using the observed maximal crown diameters as diameters of the cylindrical shapes used in the model would lead to an overestimation of crown volumes and, as a result, the LAI. To correct for this potential bias, we assumed that the trees from which the data were taken had crowns shaped like ellipsoids, rotationally symmetric around the vertical axis. A cylinder with the same volume and height as this ellipsoid must have a diameter scaled by factor $\sqrt{\frac{2}{3}}$ as compared to the

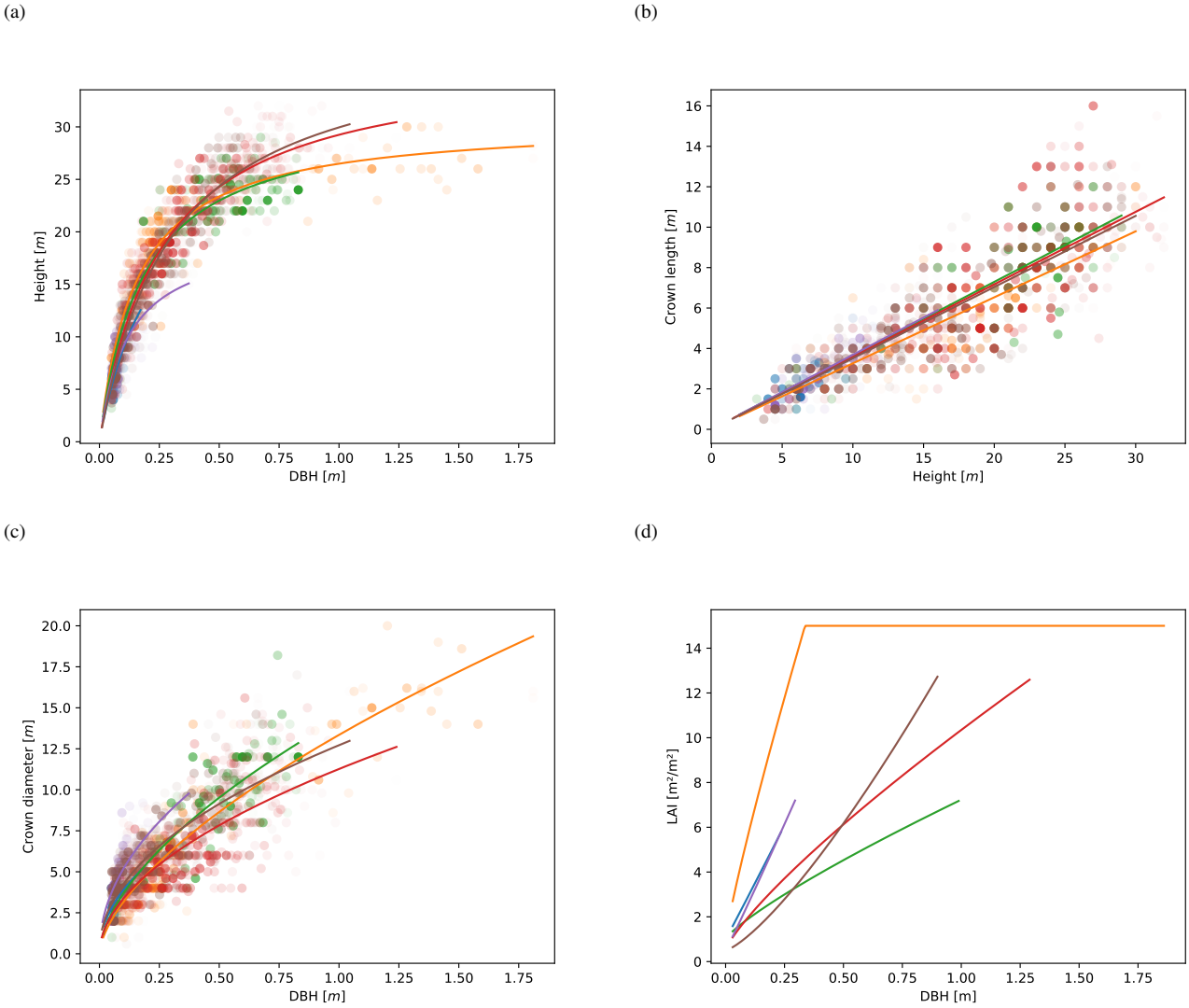


**Figure S2.** Size-dependent plant traits. The circles depict data points from the allometry dataset; their opacity shows their weight. Each colour corresponds to a different PFT: small shade intolerant (blue), large shade intolerant 1 (orange) large shade intolerant 2 (green), large mid-tolerant (red), small shade tolerant (purple), large shade tolerant (brown).

length of the horizontal semi-axis of the ellipsoid. Hence, we parameterized the model with the scaled DBH-crown-diameter relationship

$$g_{\text{crown-d}}(d;\theta_{\text{crown-d},i}) = \sqrt{\frac{2}{3}}\theta_{\text{crown-d},0}\cdot d^{\theta_{\text{crown-d},1}}. \tag{S9}$$

### B3.4 Stem volume and form factor

To compute the stem volume $V_{\mathrm{stem},i}$, we used the formula

$$V_{\mathrm{stem},i}(d) = \frac{\pi}{4} d^2 g_{\mathrm{height}}(d; \theta_{\mathrm{height},i}) \nu_i(d), \tag{S10}$$

where $d$ is the DBH, $g_{\mathrm{height}}(d; \theta_{\mathrm{height},i})$ is the height (see equation (S5)), and $\nu_i(d)$ is a DBH- and PFT-dependent form factor. A form factor $\nu_i(d) = 1$ corresponds to a cylindrical stem shape, $\nu_i(d) = \frac{1}{3}$ to a cone, $\nu_i(d) \in \left(1, \frac{1}{3}\right)$ to a convex cone-like shape, and $\nu_i(d) \in \left(1, \frac{1}{3}\right)$ to a concave cone-like shape of the stem. In line with earlier parameterizations of FORMIND (Dislich et al., 2009), we chose

$$\nu_i(d) = \theta_{\mathrm{form},i,0} d^{\theta_{\mathrm{form},i,1}} \tag{S11}$$

with $\theta_{\mathrm{form},i,0} = 0.336\,\mathrm{m}^{-\theta_{\mathrm{form},i,1}}$ and $\theta_{\mathrm{form},i,1} = -0.18$ for all PFTs $i$.

## B4 Plant traits

Besides geometric relationships, the FORMIND model requires information about the maximal size of trees, their wood density, and their leaf area index (LAI).

### B4.1 Maximal DBH

We assumed that each tree $t$ has its own site-dependent maximal DBH $d_t^{\max}$. As this value may depend on the tree's species, which is neglected when species are summarized to PFTs, we constructed the distribution of maximal heights based on each species' maximal DBH and the species' frequency in the inventory. Below we provide a detailed description of our approach.

Let $s$ be a species and $\mathcal{A}_s$ and $\mathcal{I}_s$ the subsets of the allometry and inventory dataset, respectively, that correspond to species $s$. We determine the maximal DBH of species $s$ based on the maximal DBH observed in the allometry dataset and the $99.5$th percentile of the inventory:

$$\bar{d}_s^{\max} = \max\left\{ F^{-1}_{\{d_k, k\in\mathcal{A}_s\}}(0.995), \max_{t\in\mathcal{I}_s} d_t \right\}, \tag{S12}$$

where $F_{\cdot}^{-1}(\cdot)$ is the observed percentile function.

There were some cases in which the maximal DBH from the inventory dataset was more than $10\%$ lower than the corresponding maximum from the allometry dataset (here: $10\% \mathrel{\hat{=}} 15\,\mathrm{cm}$ difference). This may indicate that for these species, local conditions are unfavourable, which in turn should be reflected in the parameterization. In cases where we had enough (more than $1000$) trees in the inventory to suggest that the maximal DBHs in the inventory coincide with the maximal DBH reachable the study site, we therefore used the value $F^{-1}_{\{d_k, k\in\mathcal{A}_s\}}(0.995)/0.9$. These cases are shown in Table S2.

**Table S2.** Maximal DBH values for species where the estimates from the inventory and the allometry data deviate strongly.

We determined the frequency of each species in the inventory based on its total basal area. Based on this, we constructed a discrete probability distribution for the maximal tree height of a tree $t$. Let $\mathcal{S}_i$ be the species belonging to PFT $i$. We obtained the following probability mass function for the maximal height of a tree of PFT $i$:

$$p_i^{\max}(d) = \frac{\sum_{s\in\mathcal{S}_i} \mathrm{I}_{\left\{\bar{d}_s^{\max}\right\}}(d) w_s}{\sum_{s\in\mathcal{S}_i} w_s} \tag{S13}$$

with

$$w_s = \sum_{t\in\mathcal{I}_s} d_t^2 \tag{S14}$$

and the indicator function $\mathrm{I}_{\{X\}}(x)$, which is 1 id $x \in X$ and 0 otherwise.

Since even trees of the same species may have different site-dependent growth limits and to reduce a potential model artifact arising from drawing the maximal DBHs from discrete distributions, we constructed continuous distributions for the maximal diameters by blurring the distribution below the maximal DBH values $\bar{d}_s^{\max}$. That way, we obtained a continuous distribution with probability density function

$$f_i^{\max}(d) = c \sum_{s\in\mathcal{S}_i} \mathrm{I}_{\left[(1-\beta)\bar{d}_s^{\max}, \bar{d}_s^{\max}\right]}(d) \frac{w_s}{2\beta\bar{d}_s^{\max}}, \tag{S15}$$

where $\beta$ is a measure for the relative within-species variation of the maximal diameter and $c$ is a normalization constant. We assumed that the maximal diameter for each species can take values $\beta = 20\%$ below the observed maximum. The resulting probability density functions are displayed in Fig. S3.

For technical reasons, we used a discretized version of distribution (S15). To that end, we considered 200 potential maximal DBH values homogeneously distributed in the interval $\left[\min_{s\in\mathcal{S}_i}(1-\beta)\,\bar{d}_s^{\max}, \max_{s\in\mathcal{S}_i}(1-\beta)\,\bar{d}_s^{\max}\right]$.

### B4.2 Wood density

We computed the wood density of each PFT by taking a weighted average of species-specific wood densities. As weights, we used each species' basal area in the inventory. That is, with weights $w_s$ defined as in equation (S14), we computed the wood density $\rho_i$ of PFT $i$ via

$$\rho_i = \frac{\sum_{s\in\mathcal{S}_i} \rho_s w_s}{\sum_{s\in\mathcal{S}_i} w_s}, \tag{S16}$$

where $\rho_s$ is the wood density of species $s$.

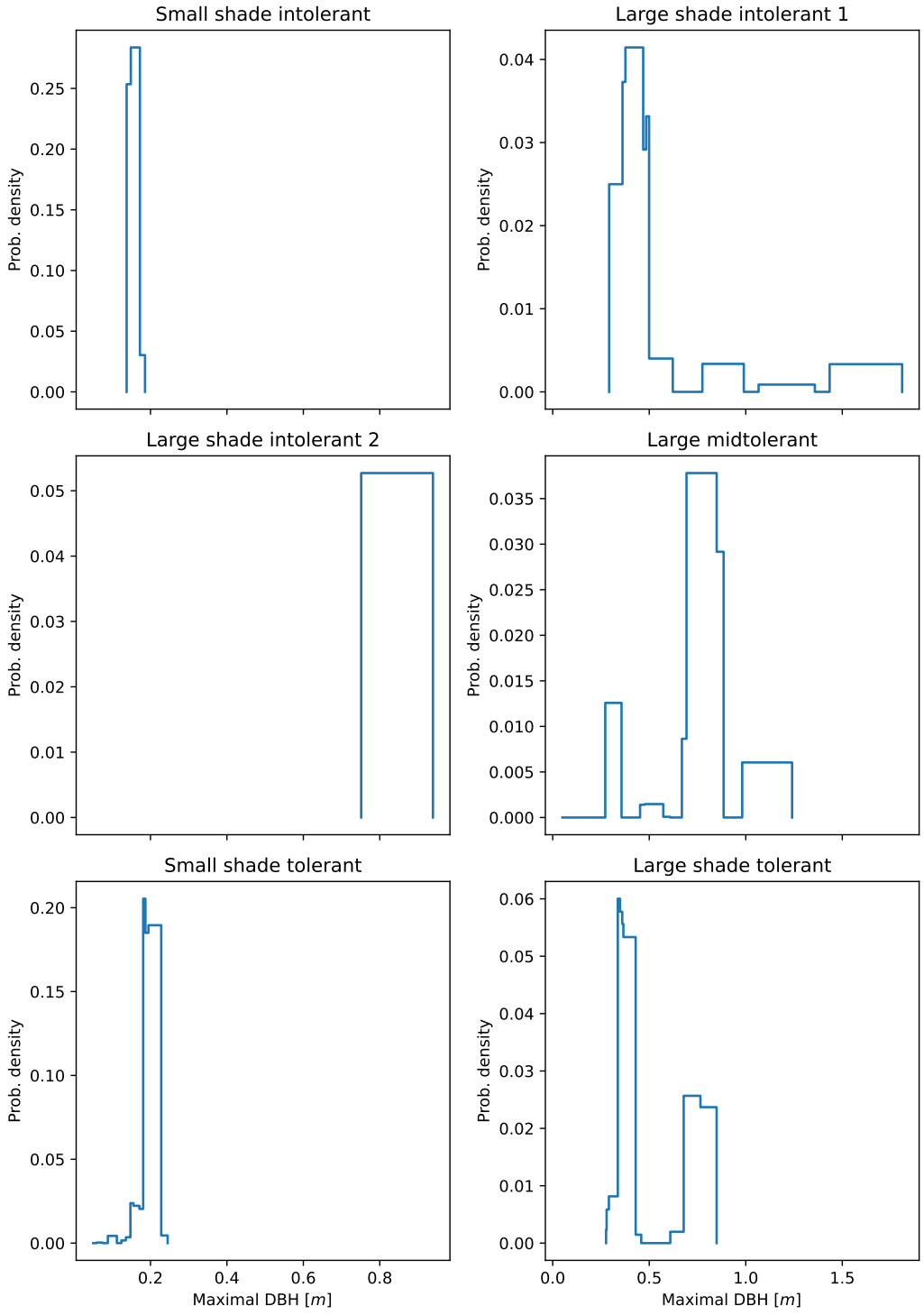


**Figure S3.** Distribution of the maximal DBH for the six PFTs.

**Table S3.** Parameter values for the relationship between DBH and LAI. Values marked with an asterisk (*) were taken from Xu et al. (2021).

### B4.3 LAI

Both theoretical and empirical studies suggest that a tree's leaf area is roughly proportional to its basal area (West et al., 1999; Xu et al., 2021). However, as it is difficult and costly to determine the leaf area of individual trees, empirical individual-level data on leaf area, leaf number, or LAI are sparse. Xu et al. (2021) estimated leaf numbers as functions of the DBH based on measurements on different branch levels (Liu, 2009) for three species common in our study area. In the absence of more direct measurements, we used a simple approximation based on results by Xu et al. (2021) to parameterize the PFTs to which the species they considered belong and used generic estimates for the other PFTs.

As general ansatz for the relationship between DBH $d$ and LAI $L$, we used the following function:

$$L(d) = \theta_{\mathrm{LAI},0,i} + \theta_{\mathrm{LAI},1,i} \frac{d^{\theta_{\mathrm{LAI},2,i}}}{A_i(d)}, \tag{S17}$$

where $\theta_{\mathrm{LAI},0,i}$, $\theta_{\mathrm{LAI},1,i}$, $\theta_{\mathrm{LAI},2,i}$ are parameters for PFT $i$ and

$$A_i(d) = \frac{\pi}{4} g_{\text{crown-d}}(d; \theta_{\text{crown-d},i})^2 \tag{S18}$$

is the corresponding crown projection area (see also equation (S9)). The division by the crown projection area $A_i(d)$ transforms leaf area values to LAI values. The intercept parameter is necessary, because trees require a minimal LAI to growth as much as observed in the field. As the crown projection area is roughly proportional to the DBH, the LAI would converge to $0$ for small trees if $\theta_{\mathrm{LAI},0,i} = 0$.

We used the exponents $\theta_{\mathrm{LAI},2,i}$ reported by Xu et al. (2021) for *Betula platyphylla*, *Pinus koraiensis* and *Tilia amurensis* for the large shade intolerant 1, large mid-tolerant, and large shade tolerant PFT, respectively. For the other PFTs, we assumed a generic value of 2 (West et al., 1999). We computed the remaining parameters $\theta_{\mathrm{LAI},1,i}$ based on mean LAI values $L_{\mathrm{ref},i}$ reported by Xu et al. (2021). For PFTs with unknown mean LAI, we used a generic value of 3. As it was unclear, to which DBH values the reported mean values corresponded, we set reference DBH values $d_{\mathrm{ref},i}$ dependent on the maximal tree sizes: $0.1\mathrm{m}$ for small PFTs and $0.25\mathrm{m}$ for large PFTs. Setting $L(d_{\mathrm{ref},i}) = L_{\mathrm{ref},i}$, we obtained $\theta_{\mathrm{LAI},1,i}$ with a simple manipulation of equation (S17). The resulting parameter values are displayed in Table S3. The resulting curves are visible in Fig. S2d.

### B4.4 Light extinction and transmission

To compute the light climate in the forest, parameters for the light extinction and light transmission of leaves are needed. We assumed that these coefficients are independent of the PFTs. For the light extinction coefficients we assumed a value of $0.5$ and for the light transmission coefficients a value of $0.1$.

**Table S4.** Estimated mean stem biomass proportion for the different PFTs.

**Table S5.** Parameters for seed influx and establishment.

### B4.5 Mean stem biomass proportion

In FORMIND, the biomass of a tree is computed by scaling the stem biomass by an expansion factor, which reflects that some biomass is allocated in branches and leaves. This expansion factor may depend on the tree size and PFT. In our parameterization, we computed the factor based on a submodel described in section B7.5 below. However, to parameterize this submodel, we needed information about the mean stem biomass proportions.

We determined the mean proportions of above-ground biomass in the tree crown (i.e., branches and leaves) by comparing independent biomass estimates (Piponiot et al., 2022) for the Changbaishan forest plot with the biomass estimates obtained via the allometric relationships estimated in the sections above. As the estimates by Piponiot et al. (2022) correspond to the entire forest only, we reimplemented their approach, which is based on the allometric biomass equations presented in Table 5 in Chojnacky et al. (2014). We mapped the species found in the inventory data to the taxa found in the table and used the corresponding biomass equations to estimate the species' respective total biomasses in the study area. For species for which we could not find a matching biomass equation, we used the equation corresponding to Aceraceae with specific gravity below $0.5$. We then adjusted the mean stem biomass proportions until our biomass estimates matched the ones obtained via the equations by Chojnacky et al. (2014). The resulting stem biomass proportions are displayed in Table S4.

### B5 Seed production and seed mortality

We assume that there is a constant external seed influx to the forest. This assumption holds approximately if the considered forest is part of a larger forest area and seed availability does not depend on local species abundances. The seeds are distributed evenly among the patches. Seeds that do not establish to small trees accumulate in a "seed bank" and may establish in later years. However, seeds in the seed bank are subject to a mortality of $50\%$ per year.

We determined the number $n_{\mathrm{seeds},i}$ of incoming seeds of PFT $i$ by fitting the model to forest inventory data (see section B11 for details). The resulting values are displayed in Table S5.

### B6 Ingrowth

Seeds establish to small trees dependent on the light available at the forest's ground and the length of the productive season. The fraction $\phi_{\mathrm{seed},i}$ of seeds of PFT $i$ that establish is computed using a Hill function:

$$\phi_{\mathrm{seed},i}(\phi_{\mathrm{light},j}) = \frac{\phi_{\mathrm{light}}^{\theta_{\mathrm{est},1}}}{\phi_{\mathrm{light}}^{\theta_{\mathrm{est},1}} + \theta_{\mathrm{est},0,i}^{\theta_{\mathrm{est},1}}}, \tag{S19}$$

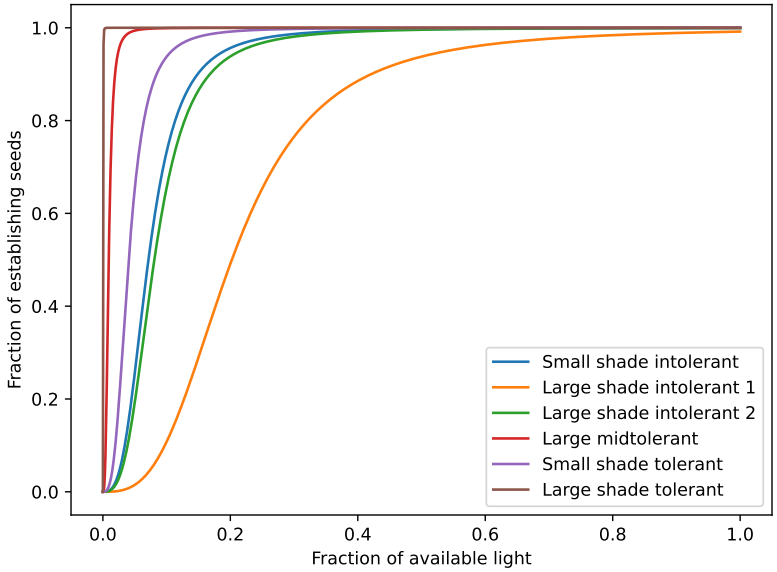


**Figure S4.** Ingrowth functions for the six PFTs. The fraction of seeds in the seedbank that establish depends on the fraction of irradiation reaching the bottom of the forest as compared to the incoming irradiation.

where $\phi_{\text{light},j} \in [0,1]$ is the fraction of the incoming irradiance that reaches the ground in patch $j$, the parameter $\theta_{\text{est},0,i} \in [0,1]$ is the irradiance at which half of the seeds of PFT $i$ germinate, and $\theta_{\text{est},1}$ is a parameter controlling how steep the transition from unfavourable to favourable germination conditions is. We estimated the parameters $\theta_{\text{est},0,i}$ and $\theta_{\text{est},1}$ by fitting the model to forest inventory data (section B11). The resulting values for $\theta_{\text{est},0,i}$ are displayed in Table S5; the threshold sharpness was not fitted PFT-specifically and assumed a value of $\theta_{\text{est},1} = 3$. The resulting curves are shown in Fig. S4.

The number $n_{\text{seedling},i,j}$ of newly establishing trees of PFT $i$ in patch $j$ is computed by rounding the product of the number $n_{\text{seedbank},i,j}$ of seeds in the corresponding seed bank and the number of establishing seeds $\phi_{\text{seed},i}(\phi_{\text{light},j})$:

$$n_{\text{seedling},i,j} := \lfloor n_{\text{seedbank},i,j} \phi_{\text{seed},i}(\phi_{\text{light},j}) + 0.5 \rfloor \tag{S20}$$

All newly established trees have an initial DBH of $0.05\text{m}$ irrespective of the PFT.

### B7 Growth

In FORMIND, the growth of a tree is modelled using multiple interacting submodels, which we calibrated partly jointly and partly independently from one another (see Fig. S5 for an overview). The key idea of our approach was to focus on trees growing under the best possible conditions found on site. Focusing on optimal conditions reduces the complexity while at the same time setting a frame for the possible model behaviour. Below we briefly summarize our approach before providing details in the succeeding sections.

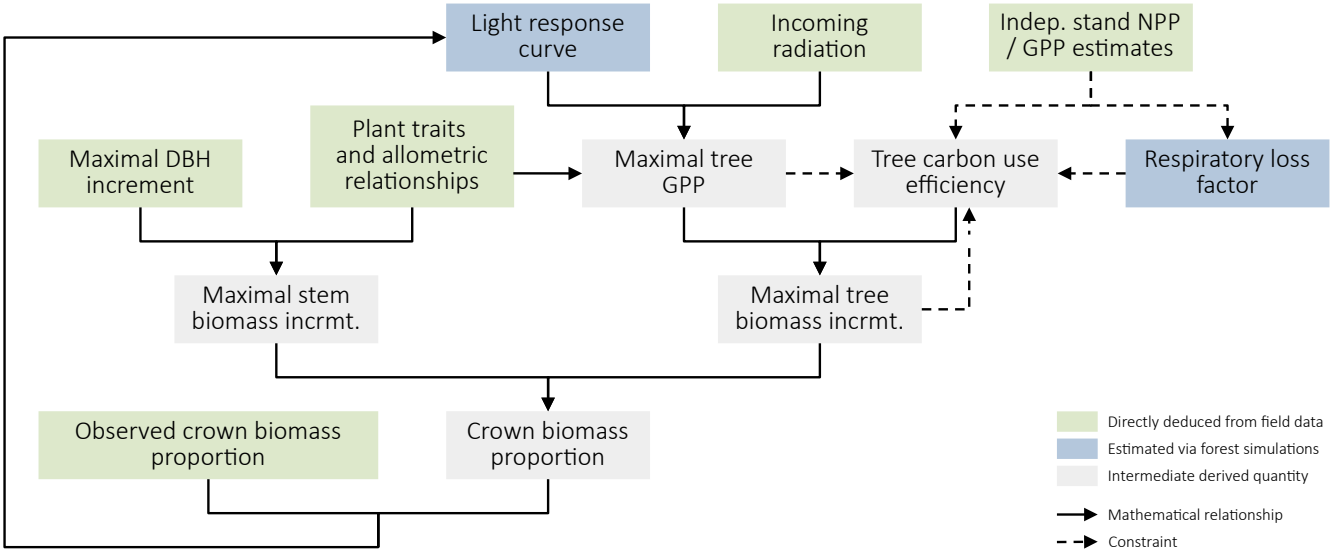


**Figure S5.** Overview of the model components and intermediate results used to fit the submodels for the growth of individual trees. Solid arrows depict direct mathematical relationships, whereas dashed arrows denote constraints. Submodels and quantities that could be estimated independently from the full model are drawn in green. Submodels with parameters that could only be estimated from the full model are shown in blue. Quantities that were derived from other components are depicted in grey.

Based on the forest inventory data, we estimated the PFT- and DBH-dependent DBH increment under optimal conditions (section B7.1) and used this along with the estimated allometric relationships (section B3) and plant traits (section B4) to approximate the stem biomass increment under optimal conditions. At the same time, we used our model to estimate the GPP (section B7.3) and carbon use efficiency (section B7.4) of trees under optimal growth conditions. In a second step, we computed the aboveground wood production, which we could use along with the observed stem biomass increments to deduce the biomass allocated to the crown (section B7.5). We compared these values with field estimates, in turn, to refine the parameters that we used to compute the GPP. Parameters that could not be estimated with this procedure were estimated by fitting the full forest model to the forest inventory data (section B11).

### B7.1 DBH increment under optimal conditions

We estimated the DBH increment under optimal conditions based on the DBH increments observed in consecutive forest inventory data. We modelled the DBH increment as observed in the inventory data via a simple stochastic model and used this as a baseline to derive the optimal DBH increment.

We assumed that the DBH increment $\Delta d_{i_k}(d_k)$ of a tree $k$ with PFT $i_k$ and DBH $d_k$ follows a Gamma distribution. Specifically,

$$\Delta d_i(d) \sim \text{Gamma}\left(\frac{\mu_{\Delta\text{DBH},i}(d)}{\theta_{\Delta\text{DBH}}}, \theta_{\Delta\text{DBH}}\right), \tag{S21}$$

**Table S6.** Parameters for the DBH increment distributions.

where $\mu_{\Delta\mathrm{DBH},i}(d)$ is the DBH-dependent mean DBH increment, and $\theta_{\Delta\mathrm{DBH}}$ is a scale parameter controlling the distributions mean to variance ratio, which we assumed to be independent of the DBH. We assumed that

$$\mu_{\Delta\mathrm{DBH},i}(d) = \theta_{\Delta\mathrm{DBH},i,0} + \theta_{\Delta\mathrm{DBH},i,1} d + \theta_{\Delta\mathrm{DBH},i,2} d^2 + \theta_{\Delta\mathrm{DBH},i,3} d^3 \tag{S22}$$

is a cubic polynomial satisfying the following constraints:

$$\mu_{\Delta\mathrm{DBH},i}(d_i^{\max}) = 0, \tag{S23}$$

$$\mu_{\Delta\mathrm{DBH},i}(0) \geq 0, \tag{S24}$$

$$\mu'_{\Delta\mathrm{DBH},i}(0) \geq 0, \tag{S25}$$

$$\mu'_{\Delta\mathrm{DBH},i}(d_i^{\max}) \leq 0, \tag{S26}$$

where $d_i^{\max}$ is the maximal DBH a tree of PFT $i$ can assume. Constraint (S23) reflects that trees with DBH $d_i^{\max}$ cannot grow even under optimal conditions. Together with constraints (S24)-(S26), it follows that $\mu'_{\Delta\mathrm{DBH},i}$ is always non-negative and at most unimodal in the interval $[0, d_i^{\max}]$. Note that constraint (S23) implies that one of the parameters $\theta_{\Delta\mathrm{DBH},i,0}, \ldots, \theta_{\Delta\mathrm{DBH},i,3}$ can be expressed in terms of the other ones, reducing the degree of freedom when fitting the model.

We estimated the parameters by maximizing the likelihood given data from consecutive forest inventories, conducted in intervals of five years. For each tree $k$ that appeared in two consecutive inventories, we determined the observed DBH difference

$$\Delta d_k^{\mathrm{obs}} = d_{k,t_2} - d_{k,t_1}, \tag{S27}$$

where $d_{k,t}$ is the observed DBH of tree $k$ in year $t$ and $\Delta t = t_2 - t_1 = 5\,\mathrm{yr}$. As empirical data may always be prone to error, we disregarded all data that were more than $5$ standard deviations apart from the mean DBH increment, taken over all individuals of the considered PFT. Afterwards, we also excluded all negative values $\Delta d_k^{\mathrm{obs}} < 0$. We estimated the parameters for the optimal DBH growth by fitting the distribution (S21) to the values

$$\Delta \bar{d}_k^{\mathrm{obs}} = \frac{\Delta d_k^{\mathrm{obs}}}{\Delta t}. \tag{S28}$$

The resulting parameter estimates are displayed in Table S6. In Fig. S6, we show histograms for the observed DBH increments and the density functions of the corresponding fitted Gamma distributions.

The Gamma distribution can take arbitrarily large values. Our goal, however, was to determine some "maximal" DBH increment. We assumed that the maximal DBH increment is given by some (high) quantile $q_{\Delta\mathrm{DBH}}$ of the fitted DBH increment

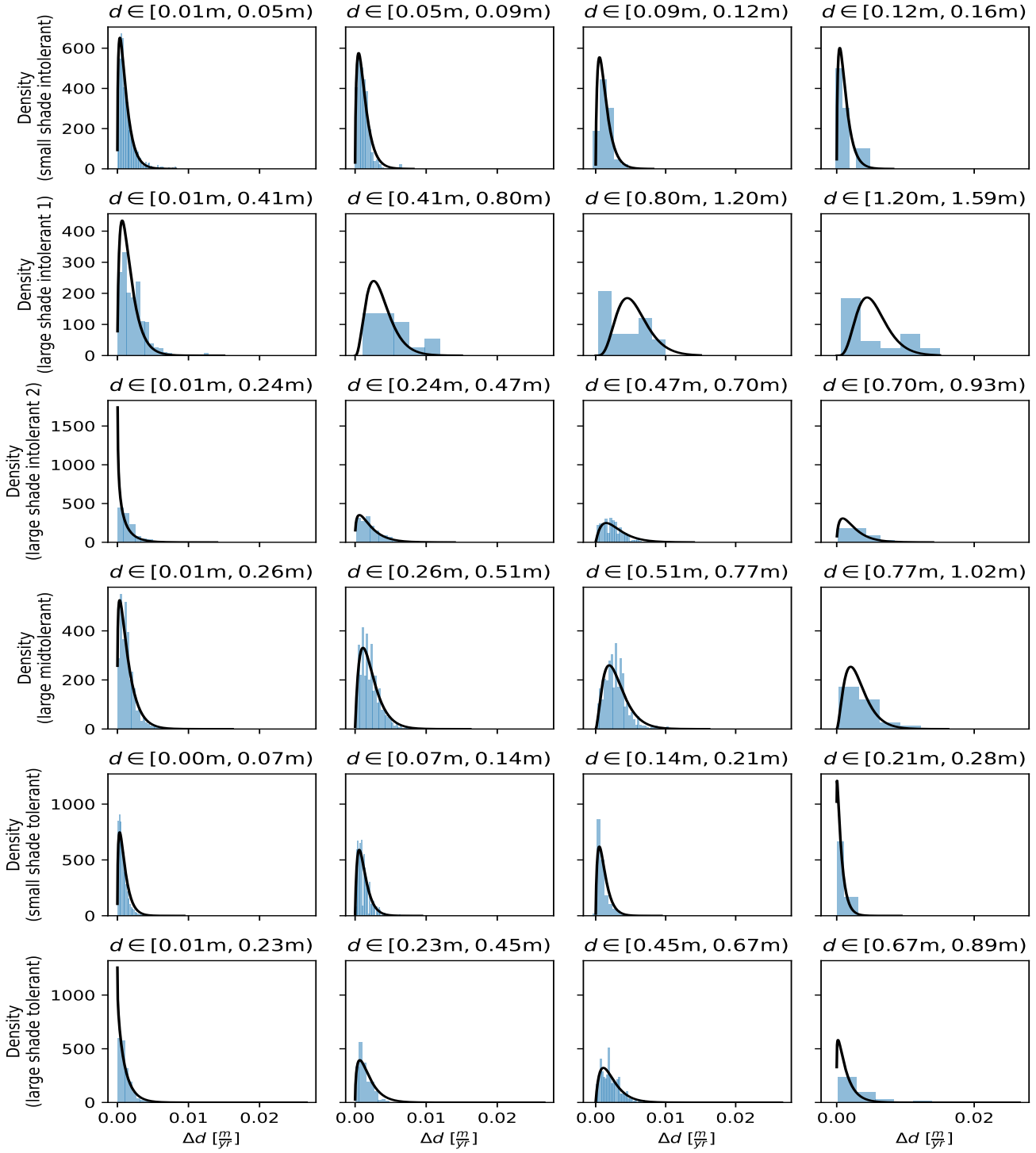


**Figure S6.** Histogram of observed DBH increments (blue histograms) and fitted DBH increment used in the model (black lines) for the six PFTs and plant sizes. Each panel corresponds to a PFT (indicated in the row description) and a size class (range of considered DBH indicated in the panel heading). The observed DBH increments are averages over five year periods. The plotted probability densities correspond to the DBHs in the centre of the respective considered DBH interval.

distribution:

$$\Delta d_{\max,i}(d) = F^{-1}_{\Delta d_i(d)}(q_{\Delta\mathrm{DBH}}), \tag{S29}$$

where $F^{-1}_{\Delta d_i(d)}$ is the inverse cumulative probability density function of $\Delta d_i(d)$. That is, the DBH under optimal conditions is the value chosen so that a fraction of $q_{\Delta\mathrm{DBH}}$ of the DBH increments of similar trees are expected to be lower. Whereas we estimated the distribution of the DBH increments from forest inventory data, we fitted the parameter $q_{\Delta\mathrm{DBH}}$ along with other parameters based on a dynamic forest simulation (see section B11). We obtained a value of $q_{\Delta\mathrm{DBH}} = 0.991$. The resulting curves for the DBH-dependent optimal DBH increment are displayed in Fig. S7.

### B7.2 Reference conditions

We assumed that the estimated optimal DBH increments (section B7.1) were obtained under the best possible conditions found at the Changbaishan site. To link these observed DBH increments to the modelled GPP, we needed to model these reference conditions explicitly. We assumed that the optimal growth conditions correspond to the best light conditions observed in the forest inventory. For large trees, this is equivalent to being unshaded by other trees. However, there may be no unshaded small trees in the inventory for some PFT, requiring us to adjust the reference light conditions accordingly. This issue was not considered in previous paramterizations of FORMIND. This may have led to underestimated growth of small trees.

Here, we made an ad-hoc correction to account for the range of light conditions found for trees in the inventory. We initialized FORMIND with the forest inventory data, computed the incoming light for all trees (Fig. S8), and determined a simple piecewise linear function that yields for each DBH the maximal fraction of incoming radiation observed for trees with this DBH

$$\phi_{\mathrm{light}}(d) = \min(\theta_{\mathrm{light},0} + \theta_{\mathrm{light},1} d, 1)$$

where $\theta_{\mathrm{light},0}$ is the most favourable fraction of irradiance received by small plants and $\theta_{\mathrm{light},1}$ is the initial slope of the reference light fraction. We fitted this curve via visual inspection, observing (1) the approximate maximal irradiance received by small trees and (2) the DBH at which some trees received the full irradiance. We obtained the values $\theta_{\mathrm{light},0} = 0.5$ and $\theta_{\mathrm{light},1} = 1.5625\mathrm{m}^{-1}$. The resulting relation is displayed in Fig. S8.

### B7.3 Light response curve

In FORMIND, a tree's GPP is determined based on the light response curve mapping the incoming radiation $I_{\mathrm{leaf}}$ of a leaf of PFT $i$ to its photosynthetic rate $P_{\mathrm{leaf}}$

$$P_{\mathrm{leaf},i}(I_{\mathrm{leaf}}) = \frac{\theta_{\mathrm{production},i,0} I_{\mathrm{leaf}}}{\theta_{\mathrm{production},i,1} + I_{\mathrm{leaf}}}, \tag{S30}$$

where $\theta_{\mathrm{production},i,0}$ is the maximal possible photosynthetic rate and $\theta_{\mathrm{production},i,1}$ the irradiation at which half of the maximally possible photosynthetic rate is achieved. We fitted the parameters $\theta_{\mathrm{production},i,1}$ based on model simulations and

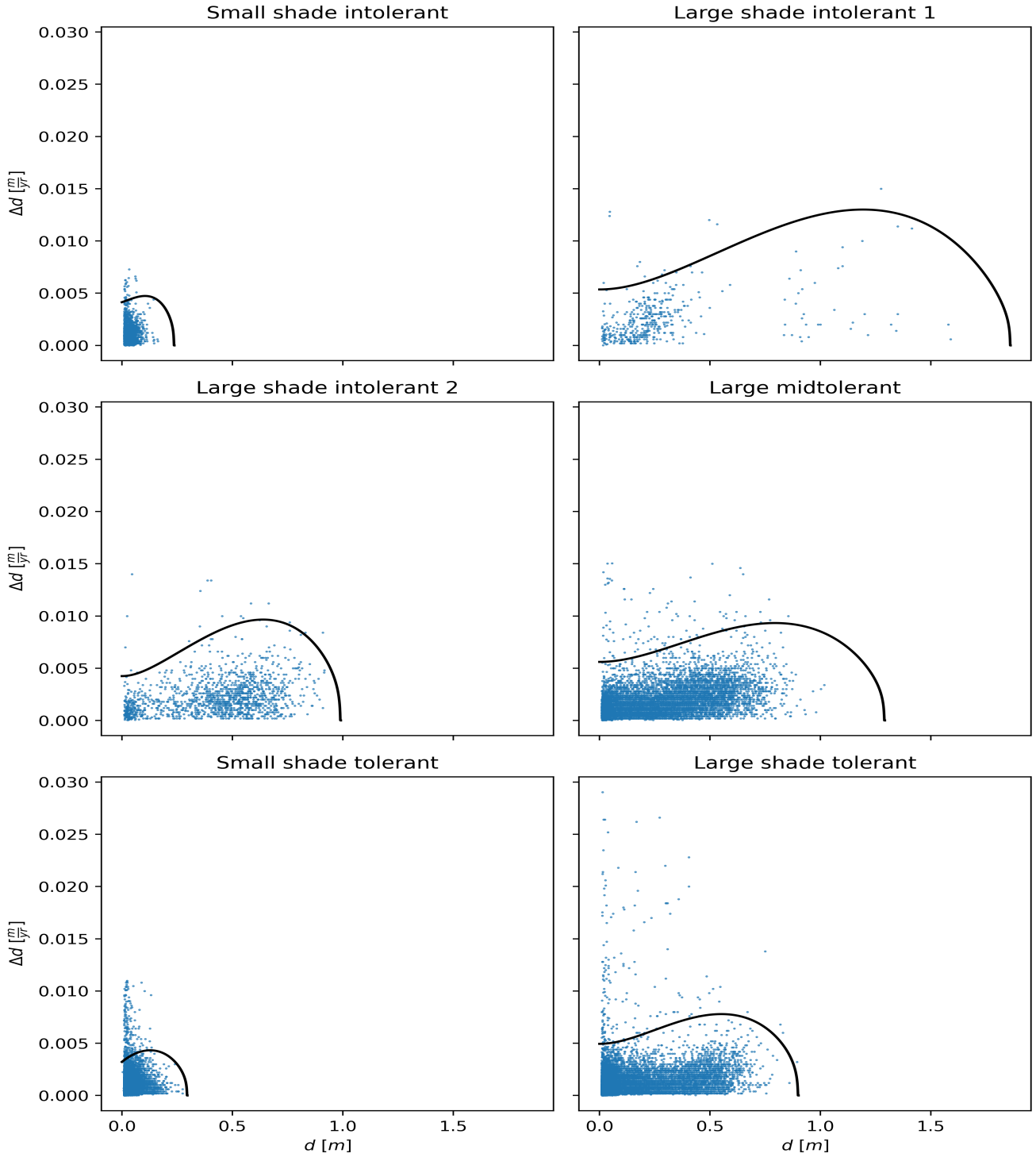


**Figure S7.** Observed yearly DBH increments (blue dots) and maximal DBH increment used in the model (black lines) for the six PFTs.

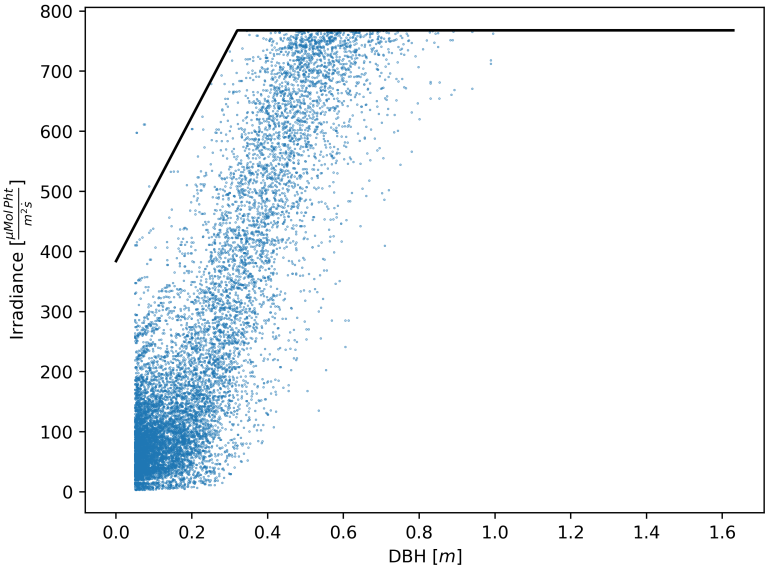


**Figure S8.** Reference light conditions dependent on the DBH. Each blue dot corresponds to a tree in the inventory and shows its DBH and the irradiance that it received according to the shading model in FORMIND. The black line depicts the irradiance that is used as "optimal" reference in the parameterization. As there are no unshaded small trees, the estimated maximal observed DBH increment (section B7.1) does not correspond to unshaded trees. Therefore, the black curve starts at an irradiance $50\%$ below the irradiance received by unshaded trees.

**Table S7.** Parameters for the light response curve.

the forest inventory data (section B11). For each given value of $\theta_{\text{production},i,1}$, we computed the corresponding parameter $\theta_{\text{production},i,0}$ by determining how large the production needs to be to let the trees of PFT $i$ attain their observed crown biomass proportions based on our assumptions on the carbon use efficiency (see section B7.4) and stem biomass allocation. Details are provided in section B7.5.

### B7.4 Carbon use efficiency and respiration

We define the carbon use efficiency (CUE; in formulas $C_k$) of a tree $k$ as the fraction of its primary production (GPP; in formulas $P_k$) that is used for net (aboveground) primary production (NPP, in formulas $\Delta B_k$):

$$C_k = \frac{\Delta B_k}{P_k}. \tag{S31}$$

The NPP, in turn, can be written as the difference of GPP and respiration:

$$\Delta B_k = P_k - R_k. \tag{S32}$$

We considered two types of respiratory losses: the maintenance respiration $R_{\mathrm{maint},i}(d)$, dependent on the tree size but independent of the GPP, and other losses and limitations $R_{\mathrm{loss},k}$, proportional to the NPP but otherwise independent of the tree size:

$$R_k = R_{\mathrm{maint},i}(d_k) + R_{\mathrm{loss},k} = R_{\mathrm{maint},k} + \frac{\gamma_{i_k}}{1-\gamma_{i_k}} \Delta B_k = R_{\mathrm{maint},k} + \gamma_{i_k} \left(P_k - R_{\mathrm{maint},k}\right),$$

where $\gamma_{i_k}$ is a PFT-dependent loss factor, modelling how much of the production not assigned to maintenance can be used for production. It follows

$$\begin{aligned} C_k &= \frac{P_k - R_{\mathrm{maint},k} - \gamma_{i_k}\left(P_k - R_{\mathrm{maint},k}\right)}{P_k} \\ &= \left(1-\gamma_{i_k}\right)\left(1 - \frac{R_{\mathrm{maint},k}}{P_k}\right) \end{aligned} \tag{S33}$$

Note that the maintenance respiration represents the tree's minimal respiratory needs and thus cannot be reduced even if the tree is under stress. Hence, if the maintenance respiration is large compared to the other losses, already a moderate reduction of the GPP (e.g. due to shading) can entail that a tree cannot satisfy its respiratory needs and stops growing or dies.

As no data on the optimal CUE on single-tree level were available to us, we created a phenomenological model for the *optimal* CUE (below: OCUE) based on a number of observations:

1. The OCUE decreases as trees grow in size.
2. The OCUE must be sufficiently large that trees can reach the estimated optimal biomass increment.
3. The CUE must suffice that most trees observed in the inventory can satisfy their minimal respiratory needs.
4. The order of magnitude of the OCUE must be chosen so that the values of GPP and NPP match field measurements on the stand level approximately.
5. The OCUE is subject to additional limitations and carbon losses independent of the maintenance respiration. Hence the OCUE cannot exceed $1-\gamma_i$.

As baseline for the OCUE model, we used the following formula:

$$C_{\mathrm{base},i}(d) = \theta_{\mathrm{OCUE},0,i} - \theta_{\mathrm{OCUE},1,i} d^{\theta_{\mathrm{OCUE},2,i}}, \tag{S34}$$

where $i$ is the PFT, $d$ is the DBH, and $\theta_{\mathrm{OCUE},0,i}$, $\theta_{\mathrm{OCUE},1,i}$, and $\theta_{\mathrm{OCUE},2,i}$ are parameters. However, to guarantee that constraint 2 is satisfied, we also computed the minimal required CUE so that the trees can grow as much as observed under optimal conditions. Let

$$\Delta B^{\mathrm{opt}}_{\mathrm{stem},i}(d) = \rho_i \left(V_{\mathrm{stem},i}(d + \Delta d_{\max,i}(d)) - V_{\mathrm{stem},i}(d)\right) \tag{S35}$$

**Table S8.** Scaling factors relating the NPP to respiratory losses other than the maintenance respiration.

be the stem biomass increment under optimal conditions, where $d$ is the current DBH, $\rho_i$ is the wood density, $V_{\mathrm{stem},i}$ the stem volume, and $\Delta d_{\max,i}$ the DBH increment under optimal conditions. We assumed that, under optimal conditions, at least a factor $\kappa_{\min} = 0.1$ of the NPP is allocated to crown growth. Hence, the NPP under optimal conditions must be at least $\frac{1}{1-\kappa}\Delta B \Delta B^{\mathrm{opt}}_{\mathrm{stem},i}(d)$. Consequently, we adjusted the OCUE correspondingly:

$$C_{\mathrm{opt},i}(d) = \max\left(C_{\mathrm{base},i}(d),\, \frac{1}{1-\kappa_{\min}}\Delta B^{\mathrm{opt}}_{\mathrm{stem},i}(d)\right). \tag{S36}$$

We assumed that the OCUE is monotonously decreasing as trees grow. With constraint 5, we obtain that $\theta_{\mathrm{OCUE},0,i} \leq \gamma_i$. At the same time, constraint 3 requires that $R_{\mathrm{maint},i}(d)$ is small for small trees, as small shaded trees observed in the inventory could not survive otherwise. Hence, we set

$$\theta_{\mathrm{OCUE},0,i} = \gamma_i - 0.01. \tag{S37}$$

Similarly, applying the shading module of FORMIND to the inventory data, we observed that the OCUE must decrease slowly for small trees (Fig. S9), which in turn requires a sufficiently large exponent $\theta_{\mathrm{OCUE},2,i}$. We therefore set $\theta_{\mathrm{OCUE},2,i} = 3$ for all PFTs $i$. Lastly, we determined $\theta_{\mathrm{OCUE},1,i}$ so that the largest possible trees of PFT $i$ have an OCUE of $0$ at their maximal DBH. That is, if

$$d_{\max,i} = \sup\{d;\, f_i^{\max}(d) > 0\} \tag{S38}$$

is the maximal DBH a tree of PFT $i$ can attain (cf. equation (S15)), then

$$\theta_{\mathrm{OCUE},1,i} = \theta_{\mathrm{OCUE},0,i} d_{\max,i}^{-\theta_{\mathrm{OCUE},2,i}}. \tag{S39}$$

We estimated the loss factors $\gamma_i$ by fitting the full model to the inventory data (section B11). However, to satisfy constraint 4, we constrained the loss factors $\gamma_i$ to the interval $[0.6, 1]$ to match the relatively low CUE values observed in the Changbaishan mountain area in independent studies (Piponiot et al., 2022). The resulting parameter estimates are displayed in Table S8

As we assume that the maintenance respiration is independent of a tree's productivity, equation (S33) must in particular hold for trees under optimal growth conditions. Hence, after inserting the fitted OCUE $C_{\mathrm{opt},i}(d)$ and GPP under optimal conditions, equation (S33) can be manipulated to derive the maintenance respiration for a tree of given PFT and DBH.

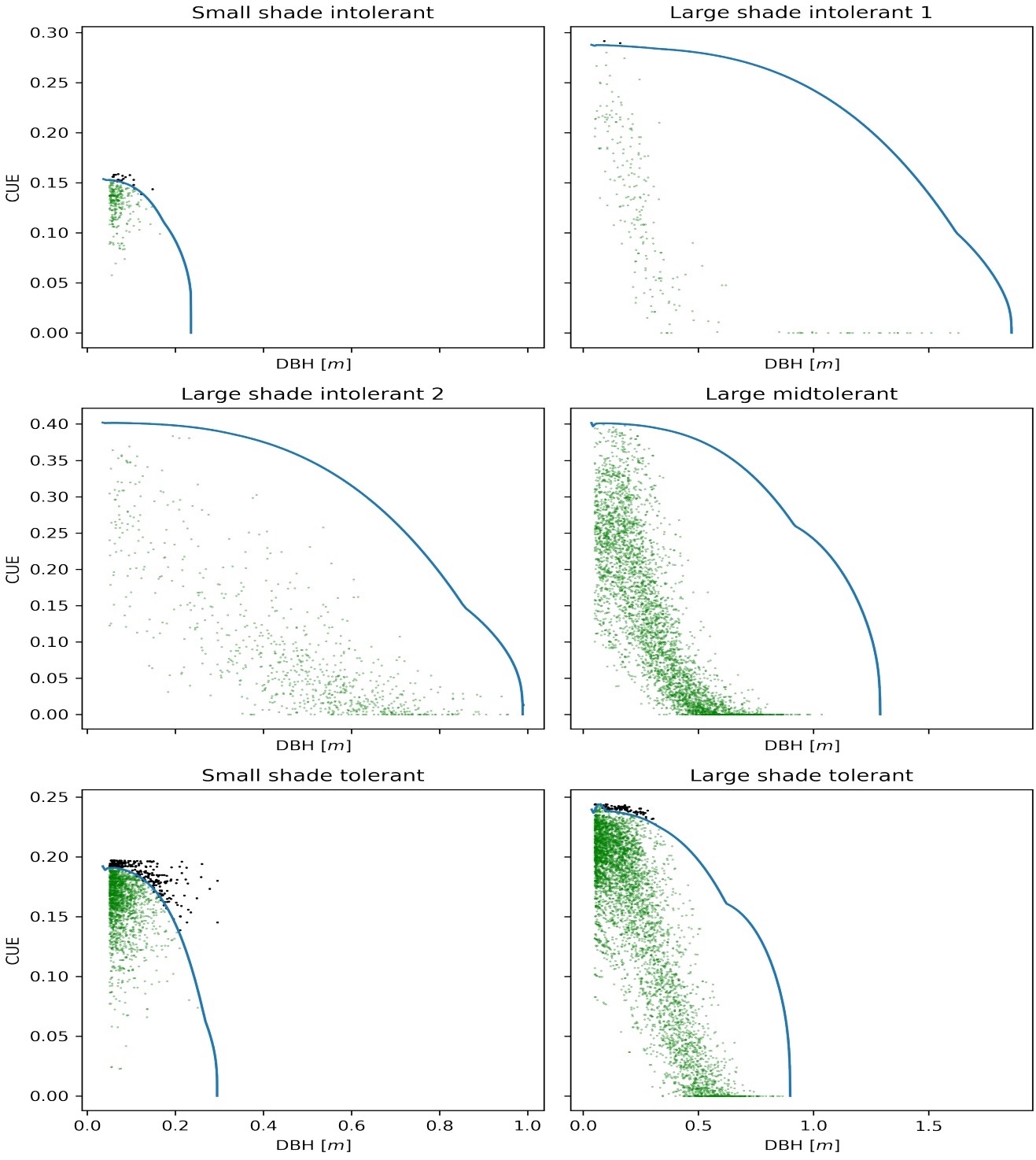


**Figure S9.** The optimal carbon use efficiency OCUE for the different PFTs. The OCUEs used in the model are depicted as solid blue lines. The points show estimated lower bounds for the required CUEs obtained for trees in the inventory via the shading module of FORMIND. Each point corresponds to a tree; the colour shows whether the tree could satisfy its respiratory needs according to the model (green: yes; black: no). The OCUE curves were chosen so that as many of the points are below the blue curves. The sharp transitions between the curve sections are due to constraint 2 imposing a different shape of the curve for large DBH values (see also equation (S36)).

### B7.5 Growth allocation

Based on the OCUE and the GPP under optimal conditions, denoted $C_i$ and $P_i^{\mathrm{opt}}$, respectively, we could compute the corresponding NPP $\Delta B_i^{\mathrm{opt}}(d)$ for trees of a given DBH and PFT. Based on the estimated DBH increment under optimal conditions, determined the respective stem biomass increment $\Delta B_{\mathrm{stem},i}^{\mathrm{opt}}(d)$ (see equation (S35)). If $B_i(d)$ is the biomass of a tree of PFT $i$ with DBH $d$ and $\zeta_i$ is the corresponding stem biomass proportion, then

$$\begin{aligned}\Delta B_i^{\mathrm{opt}}(d) &= C_i(d)P_i^{\mathrm{opt}}(d)\\ &= B_i(d+\Delta d_{\max,i}(d)) - B_i(d)\\ &= \frac{B_{\mathrm{stem},i}(d+\Delta d_{\max,i}(d))}{\zeta_i(d+\Delta d_{\max,i}(d))} - \frac{B_{\mathrm{stem},i}(d)}{\zeta_i(d)} \qquad \text{(S40)}\end{aligned}$$

$$\Longleftrightarrow$$

$$\zeta_i(d+\Delta d_{\max,i}(d)) = \frac{\zeta_i(d)B_{\mathrm{stem},i}(d+\Delta d_{\max,i}(d))}{B_{\mathrm{stem},i}(d)+\zeta_i(d)C_i(d)P_i^{\mathrm{opt}}(d)}. \qquad \text{(S41)}$$

We used this difference equation to compute the stem biomass proportion for all DBHs and PFTs. We provide details below.

Equation (S41) requires knowledge of the previous stem biomass proportion $\zeta_i(d)$. Hence, we needed initial values for the interval $[d_0, d_0+\Delta d_{\max,i}(d)]$ with $d_0$ being the stem diameter of new saplings. These initial values may be chosen arbitrarily. Using a shifted exponential ansatz for the initial condition yielded well-behaved smooth results for $\zeta_i$:

$$\zeta_i(d) = a_{0,i} + a_{1,i}\exp(a_{2,i}\cdot d) \qquad \text{if } d < d_0+\Delta d_{\max,i}(d_0). \qquad \text{(S42)}$$

We chose the coefficients $a_{0i}$, $a_{1i}$, $a_{2i}$ so that the curve $\zeta_i(d)$ is continuous, approximately differentiable, and starts at a given initial value $\zeta_{0i} = \zeta_i(d_0)$.

To see how the coefficients were determined, first note that in practice, the curve $\zeta_i$ is computed numerically and hence evaluated at a discrete set of sampling points only. We chose the sampling points so that they have a constant distance to one another. Intermediate values were obtained via linear interpolation between these points. Now, let $d_{1i} = d_0 + \Delta d_{\max,i}(d_0)$, let $\bar{d}_{1i} > d_{1i}$ be the smallest sampling point larger than $d_{1i}$, and choose $\bar{d}_{0i}$ so that $\bar{d}_{1i} = \bar{d}_{0i} + \Delta d_{\max,i}\big(\bar{d}_{0i}\big)$. Furthermore, define (evaluating equation (S41) at $d_{0i}$ and $\bar{d}_{0i}$)

$$\zeta_{1i} = \frac{\zeta_{0i}B_{\mathrm{stem},i}(d_1)}{B_{\mathrm{stem},i}(d_0)+\zeta_{0i}C_i(d)P_i^{\mathrm{opt}}(d_0)}, \qquad \text{(S43)}$$

$$\bar{\zeta}_{1i} = \frac{\zeta_{0i}B_{\mathrm{stem},i}\big(\bar{d}_1\big)}{B_{\mathrm{stem},i}\big(\bar{d}_{0i}\big)+\zeta_{0i}C_i(d)P_i^{\mathrm{opt}}\big(\bar{d}_{0i}\big)}. \qquad \text{(S44)}$$

Now we imposed the following conditions

$$\zeta_i(d_0) = a_{0i} + a_{1i}\exp(a_{2i}\cdot d_0) = \zeta_{0i}, \tag{S45}$$

$$\zeta_i(d_{1i}) = a_{0i} + a_{1i}\exp(a_{2i}\cdot d_{1i}) = \zeta_{1i}, \tag{S46}$$

$$\zeta_i\big(\bar{d}_{1i}\big) = a_{0i} + a_{1i}\exp\big(a_{2i}\cdot \bar{d}_{1i}\big) = \bar{\zeta}_{1i} \tag{S47}$$

and obtained

$$a_{1i} = \frac{\zeta_{1i} - \zeta_{0i}}{\exp(a_{2i}\cdot d_{1i}) - \exp(a_{2i}\cdot d_0)} \tag{S48}$$

$$a_{0i} = \zeta_{0i} - a_{1i}\exp(a_{2i}\cdot d_0). \tag{S49}$$

We computed the remaining unknown coefficient $a_{2i}$ via a binary search on equation (S47) using the values for $a_{0i}$ and $a_{1i}$ from equations (S48)-(S49).

We approximated the mean of the curves $\zeta_i(d)$ by taking the man of the functions values at $50$ equidistant points in the intervals $[0.1\mathrm{m},\, d_{\max,i}]$, respectively. We then conducted a binary search in the maximal possible photosynthetic rate $\theta_{\mathrm{production},i,0}$ (see section B7.3) until the approximate mean values matched the mean stem biomass proportions estimated from the field data (section B4.5).

### B7.6 Defoliation

If trees are shaded, it can happen that their maintenance respiration exceeds their GPP. In these cases, we assumed that parts of the crown die until the remaining tree can be maintained. Here, we assumed that for a tree of given DBH, the maintenance respiration is proportional to its biomass. That is, a tree $k$ with insufficient production $P_k$, maintenance respiration $R_{\mathrm{maint},k}$, and biomass $B_k$ will reduce its biomass to

$$\tilde{B}_k = B_k \frac{P_k}{R_{\mathrm{maint},k}}, \tag{S50}$$

and its maintenance respiration will be set to $P_k$. As we assume the biomass is lost in the crown only, the stem biomass proportion is adjusted accordingly to a value $\tilde{\zeta}_k$.

We assumed that the loss in crown biomass also affects the tree's number of leaves and thereby the LAI. We reduced the LAI proportional to the crown completeness

$$\begin{aligned}\eta_k &= \frac{\tilde{B}_{\mathrm{crown},k}}{B_{\mathrm{crown},i_k}(d_k)} \\ &= \frac{\tilde{B}_k - B_{\mathrm{stem},i_k}(d_k)}{B_{i_k}(d_k) - B_{\mathrm{stem},i_k}(d_k)},\end{aligned} \tag{S51}$$

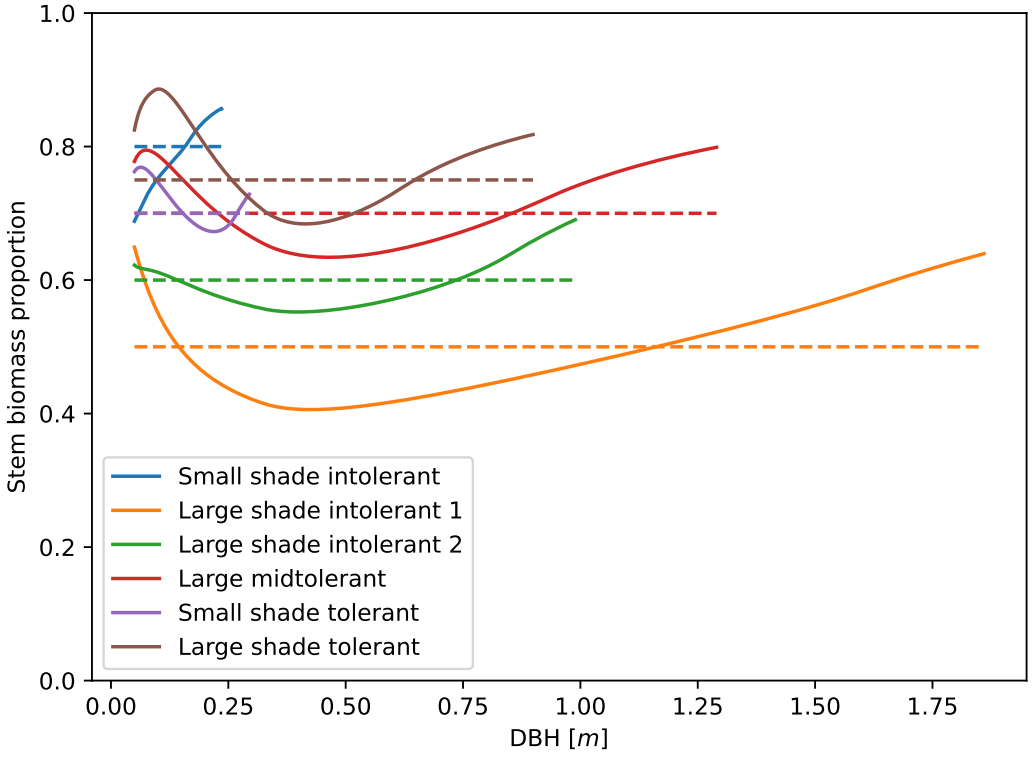


**Figure S10.** Stem biomass proportions of the six PFTs. The solid lines depict the stem biomass proportions used in the model (obtained via the approach described in section B7.5). The dashed lines show the independently estimated mean values (see section B4.5).

where $\tilde{B}_{\mathrm{crown},k}$ is the reduced crown biomass and $B_{i_k}(d_k)$ the biomass of a tree with complete crown and DBH $d_k$. As a result, trees with incomplete crowns have reduced GPP and shade other trees less. Trees without any crown biomass ($\eta_k = 0$) cannot recover and die.

We assumed that if the light conditions for a tree with incomplete crown improve, the new biomass is first allocated to "refill" the crown until $\eta_k = 1$. Any remaining new biomass is allocated to the usual tree growth with corresponding DBH increment.

### B8 Competition

We assumed that trees solely compete for light. In particular, we did not apply crowding mortality. Instead, the forest density is self-regulated via crown defoliation and the resulting tree death. This process has an effect similar to crowding mortality ("full" forests lead to deadly overshadowing of small plants) but a better mechanistic justification. In particular, mortality via light competition incorporates the traits of both the shadowing and the overshadowed trees, since the LAI of larger plants as well as the respiratory demands of smaller plants are parameterized individually for each plant functional type (PFT).

**Table S9.** Parameters for the mortality probabilities.

### B9 Stochastic mortality

We assumed that trees die randomly with probabilities dependent on their PFT and DBH. As model for the mortality, we used a linear combination of exponentials:

$$p_{\mathrm{mort},i}(d) = \theta_{\mathrm{mort},0,\mathrm{i}} + \theta_{\mathrm{mort},1,\mathrm{i}} \exp(\theta_{\mathrm{mort},2,\mathrm{i}} d) + \theta_{\mathrm{mort},3,\mathrm{i}} \exp(\theta_{\mathrm{mort},4,\mathrm{i}} d), \tag{S52}$$

where $p_{\mathrm{mort},i}(d)$ is the probability that a tree of PFT $i$ and DBH $d$ dies within a year. This model may take a variety of shapes including mortality increasing or decreasing with plant size or a "bathtub" shape, where the mortality is lowest for plants with intermediate sizes.

We estimated the parameters in equation (S52) using data from consecutive forest inventories. We determined which trees died in the intermediate time by comparing which trees that were present in the first inventory were also present in the second inventory. For simplicity, we assumed that the tree DBH does not change significantly during the $5$ year period between two censuses and that random mortality is the only death mechanism at play. If $d_{k,t_1}$ is the DBH observed in the inventory in year $t_1$, the probability that the tree survived until the year $t_2$ of the second inventory is approximately

$$p^{\mathrm{obs}}_{\mathrm{mort},i_k} = \left(1 - p_{\mathrm{mort},i_k}(d_{k,t_1})\right)^{t_2 - t_1}. \tag{S53}$$

We used this to construct the likelihood for the observed death and survival events. We then estimated the parameters in equation (S52) for the different PFTs. The resulting parameters are displayed in Table S9 and the resulting curves in Fig. S11.

Besides the random mortality, we trees may die due to strong light competition (see section B7.6) or by falling large trees. We assumed that trees larger than $0.1\,\mathrm{m}$ may fall with a probability of $0.4$ and kill smaller trees. Details of this mechanism are described in Fischer et al. (2016).

### B10 Climate

We used a static climate in our simulations. Advanced features such as the soil water module, temperature effects, and daily changes to the climate were not included. Instead, we used averaged values, which we provide below.

**Evapotranspiration.** For the mean actual evapotranspiration, we used a value of $600\frac{\mathrm{mm}}{\mathrm{yr}}$. This is in line with independent estimates for the Changbaishan region (Sun et al., 2004) and earlier parameterizations of the model for temperate forests (Bohn et al., 2014).

**Growing season.** We defined the growing season as the months with positive mean temperature. This were the months March until October (Wang et al., 2020).

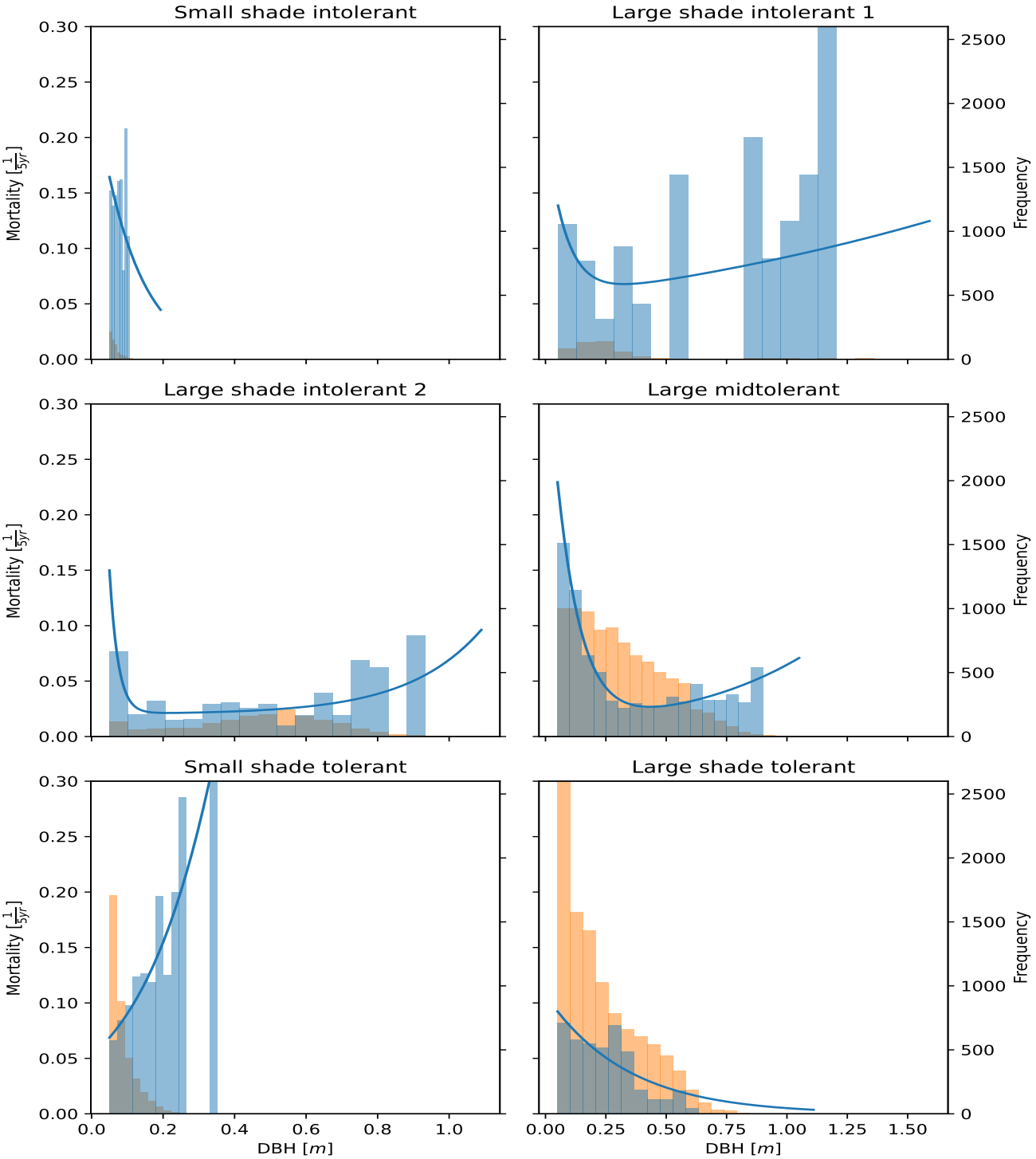


**Figure S11.** Mortality by PFT (field data and model). The blue curves (primary axis) depict the modelled DBH-dependent probabilities that a tree dies within a year. The blue bars correspond to field estimates of the death probabilities (number of dead trees divided by the total number of trees in the inventory). The orange bars (secondary axis) are a histogram for the tree sizes, indicating where the mortality estimates have the strongest empirical support.

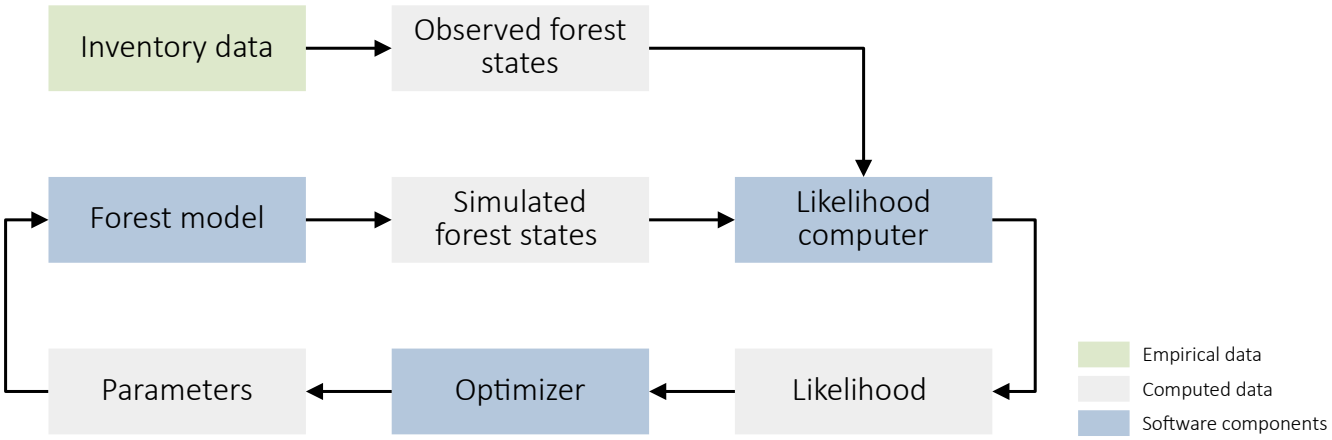


**Figure S12.** Overview of the model fitting procedure.

**Irradiance.** We computed the mean yearly light intensity ("PAR") above the canopy during daytime in the growing season based on the WFDEI forcing dataset (Weedon et al., 2014). We obtained a value of $768 \frac{\mu \mathrm{Mol\,photons}}{\mathrm{m}^2}$.

**Day length.** We computed the average length of a day in the growing season and obtained a value of $13.39\mathrm{h}$.

### B11 Fitting procedure

Some parameters were not available from the literature and could not be determined directly from the available data. We estimated these parameters based on dynamical forest simulations and the inventory data (see Fig. S12). After a burn-in period, we generated a sample of forest states via simulations. Then, we used the generated sample to estimate the likelihood for the parameters given the inventory data via kernel density estimation (KDE). We then optimized the parameters by maximizing the likelihood. Below we provide details for each of the steps involved.

#### B11.1 Forest state characterization

We characterized the forest's state by determining the stem count and the biomass in the considered patch for each PFT. That is, the state space was 12-dimensional. The combined information of stem count and biomass yields basic insight into the size distribution of trees, as a large stem count with small biomass indicates a young forest with many small trees, and a small stem count with high biomass indicates an old forest with few large trees. Hence, these summary statistics provide relatively rich information about the overall forest state.

We considered forest states on the $20\mathrm{m} \times 20\mathrm{m}$ level. For the forest plot in Changbaishan, which has a size of $25\mathrm{ha}$, we therefore obtained a sample of $625$ observed forest states.

### B11.2 Sample generation

To generate a sample of forest states from the model, we first simulated $1\mathrm{ha}$ of forest until it reached its limiting behaviour ($2000\mathrm{yr}$). Then, we generated a sample of forest states on the $20\mathrm{m} \times 20\mathrm{m}$ scale by sampling the forest $500$ times every $5\mathrm{yr}$. Via parallel simulations, we repeated this procedure $67$ times. That way we obtained a sample of forest states with $n_{\mathrm{sample}} = 837,500$ entries.

In FORMIND, the interactions between $20\mathrm{m} \times 20\mathrm{m}$ patches are small (only via tree falling, which is a rare event). Furthermore, taking samples over a relatively long period of $2500\mathrm{yr}$ reduces the temporal correlations between the generated samples. Therefore, and because we also conducted $67$ mutually independent simulations, the generated sample is approximately identically independently distributed.

### B11.3 Likelihood estimation

The distribution of the forest states according to the forest model is not known in closed form and can only be studied via simulations. Therefore, we estimated the probability density, and based on this the likelihood for the parameters given the data, from the model-generated sample of forest states. To this end, we used kernel density estimation (KDE; Wand and Jones, 1995). In KDE, the probability density $f$ of an element $y$ of the state space is estimated as the mean of kernel functions centred at the elements $x_i$ of the generated sample:

$$f\big(y; x_1, \ldots, x_{n_{\mathrm{sample}}}\big) \approx \hat{f}\big(y; x_1, \ldots, x_{n_{\mathrm{sample}}}\big) \quad = \quad \frac{1}{n_{\mathrm{sample}}} \sum_{i=1}^{n_{\mathrm{sample}}} \prod_{j=1}^{n_{\mathrm{dim}}} K(y_j, x_{ij}; h_j), \tag{S54}$$

where $\hat{f}$ is the estimated probability density, $n_{\mathrm{sample}}$ is the number of generated sample points, $n_{\mathrm{dim}}$ is the dimension of the state space, $K$ is the kernel function, and $h_j$ is a bandwidth parameter defining the (marginal) scale on which two points are considered approximately similar. Due to its computational simplicity on the log-scale, we used a Gaussian Kernel. However, since stem counts and biomasses are constrained to the non-negative range, we applied reflecting boundary conditions:

$$K_j(y_j, x_{ij}; h_j) = \begin{cases} \frac{1}{w_j} \left( \exp\left( -\frac{(x_{ij} - y_j)^2}{2h_j^2} \right) + \exp\left( -\frac{(x_{ij} + y_j)^2}{2h_j^2} \right) \right) & \text{if } y_j \geq 0 \\ 0 & \text{else} \end{cases} \tag{S55}$$

with $w_j = \sqrt{2\pi} h_j$. For the stem counts, we furthermore needed to normalized the kernel to correctly account for the discrete nature of the data:

$$K_j(y_j, x_{ij}; h_j) = \begin{cases} \frac{1}{w_j} \left( \exp\left( -\frac{(x_{ij} - y_j)^2}{2h_j^2} \right) + \exp\left( -\frac{(x_{ij} + y_j + 1)^2}{2h_j^2} \right) \right) & \text{if } y_j \geq 0 \\ 0 & \text{else} \end{cases} \tag{S56}$$

with

$$w_j \quad = \quad 2\sum_{k=0}^{\infty}\exp\left(-\frac{k^2}{2h_j^2}\right)-1.$$

The bandwidths we used are displayed in Table S10.

KDE provides unbiased estimate of probability densities. For likelihood optimization, however, we need the log-likelihood, because working with the original likelihood would require us to handle extremely small numbers, which is numerically infeasible. As taking the logarithm of a random variable changes its distribution and, in particular, expected value, we applied a bias correction. First, note that for a Gaussian kernel, the KDE's expected value $\mu_{\mathrm{KDE}}$ and variance $\sigma^2_{\mathrm{KDE}}$ can be approximated as follows (Wand and Jones, 1995):

$$\mu_{\mathrm{KDE}} \approx f(y) \tag{S57}$$

$$\sigma^2_{\mathrm{KDE}} \approx \frac{\mu_{\mathrm{KDE}}}{2\sqrt{\pi}nh}. \tag{S58}$$

We desired to find a bias correction function $g$ so that

$$\mathbb{E}\Big(g\Big(\hat{f}(y)\Big)\Big) = \ln \mu_{\mathrm{KDE}}. \tag{S59}$$

Applying a Taylor expansion about $\mu_{\mathrm{KDE}}$, we find

$$\begin{aligned}\mathbb{E}\Big(g\Big(\hat{f}(y)\Big)\Big) &\approx g(\mu_{\mathrm{KDE}}) + \frac{1}{2}g''(\mu_{\mathrm{KDE}})\underbrace{\mathbb{E}\left(\left(\hat{f}(y)-\mu_{\mathrm{KDE}}\right)^2\right)}_{\sigma^2_{\mathrm{KDE}}} \\ &= g(\mu_{\mathrm{KDE}}) + \frac{\sigma^2_{\mathrm{KDE}}}{2}g''(\mu) \\ &\stackrel{!}{=} \ln \mu_{\mathrm{KDE}}. \end{aligned} \tag{S60}$$

We solved differential equation (S60) to obtain the bias correction function, into which we inserted the original results (S54) from the KDE. To avoid numerical issues, we performed all these steps on the log scale.

To fit the model, we considered a 12-dimensional state space. As a result, the products of the kernel functions in equation (S54) can become very small and very sensitive to stochastic differences between simulation runs. We therefore estimated the probability density for each PFT independently and multiplied the results to obtain the joint density. This is equivalent to assuming that the states of different PFTs are mutually independent. Though this assumption is inaccurate in general, using the resulting composite likelihood still yields consistent parameter estimates (Varin, 2008).

**Table S10.** Ranges and KDE bandwidths for the considered state variables. The bandwidth is the scale in the state space on which a data point in the simulated sample is considered "similar" to a point in the inventory dataset.

**Table S11.** Parameter bounds and initial guesses used for parameter optimization.

### B11.4 Parameter optimization

A challenge when maximizing the kernel density estimate of the likelihood is that this estimate is stochastic. This requires the applied optimizers to be robust against stochastic fluctuations. We applied the algorithm PY-BOBYQA (Cartis et al., 2019) on a preconditioned version of the log-likelihood function. To reduce numerical issues, we optimized all parameters on the log-scale except for $q_{\Delta\mathrm{DBH}}$, for which we applied an inverse logit transform to constrain it to the open interval $(0, 1)$. Then, we evaluated the log-likelihood function $10$ times at the initial parameter guess (Table S11) to estimate its standard deviation. Based on this, we conducted for each parameter individually a rough binary search to find the scale of change on which the log-likelihood function changed by at least $2$ standard deviations but not more than $10$ standard deviations. We scaled the parameters accordingly for an efficient search. This scaling process is called preconditioning.

We constrained the parameters to ecologically reasonable ranges, respectively. The bounds we applied are displayed in Table S11. To avoid getting stuck due to stochastic deviations, we terminated the search algorithm after $200$ likelihood evaluations and restarted the search until a total of $8$ runs was completed. To minimize the risk of converging to a local minimum, we furthermore applied basin-hopping (Wales and Doye, 1997) as implemented in Scipy. This algorithm performs repeated local optimizations with randomly perturbed initial conditions. For the perturbation, we applied a step size of $4$ on the preconditioned parameter scale. We ran the algorithm for $5$ iterations. After finishing this optimization process, we repeated it, using the result as initial value and baseline for preconditioning for the repetition.

## Appendix C: DBH entropy

### C1 Derivation of the DBH entropy

We used the basal-area-weighted DBH entropy as a proxy for the prevalence of large trees in a forest patch. The entropy of the weighted DBH distribution is defined as follows:

$$\tilde{S}_{\mathrm{DBH}} = -\sum_{d \in D} p_d \ln(p_d), \tag{S1}$$

where $D$ is the set of distinct DBH values occurring in the forest patch and

$$p_d = \frac{\sum_{k \in \mathcal{I}: d_k = d} d_k^2}{\sum_{k \in \mathcal{I}} d_k^2}. \tag{S2}$$

is the probability to randomly select a tree with DBH $d$ from the forest patch if the probabilities were proportional to the trees' respective basal areas. Here, $\mathcal{I}$ is the set of trees in the inventory and $d_k$ is the DBH of tree $k$.

Formula (S1) is sensitive to arbitrarily small changes in DBH values, as trees need to have exactly the same DBH values to be considered similar in equation (S2). This is inappropriate, as DBH values come from a continuous domain, and will never be exactly equal in practice. To make the measure more robust, we could consider DBH intervals instead of individual DBH values, as suggested in the main text. However, this approach is sensitive to the choice of interval bounds and can lead to strongly different results for slight changes of DBH values (cf. Wand and Jones, 1995). We therefore used kernel density estimation to obtain a continuous distribution of tree sizes from the inventory. Then, we considered the entropy of the resulting distribution:

$$S_{\mathrm{DBH}} = -\int_0^\infty f_{\mathrm{d}}(\delta) \ln f_{\mathrm{d}}(\delta) \mathrm{d}\delta, \tag{S3}$$

where

$$f_{\mathrm{d}}(\delta) = \sum_{d \in D} w_d K(d, \delta; h) \tag{S4}$$

with weights

$$w_d = \frac{d^\eta}{\sum_{d \in D} d^\eta} \tag{S5}$$

is the smoothed DBH distribution in the forest patch,

$$K(d, \delta; h) = \begin{cases} \frac{3}{4h}\left(1 - \left(\frac{d-\delta}{h}\right)^2\right) & \text{if } |d - \delta| \leq h \\ 0 & \text{else} \end{cases}$$

is the Epanechnikov kernel, $\eta$ is the exponent parameter and $h$ is a bandwidth parameter, defining the scale on which two trees are regarded similar.

### C2 DBH entropy parameterization

The DBH entropy depends on the exponent parameter $\eta$ and the bandwidth parameter $h$. In line with our requirements for a proxy for the prevalence of mature trees, we chose $\eta = 2$ to obtain weights by basal area and $h = 1\,\mathrm{cm}$ for a sufficiently

**Table S1.** Parameter estimates resulting from the three optimization runs. For most of the parameters, the estimates remained in the same order of magnitude, indicating that they are estimable. Only the parameter $\theta_{\mathrm{est},1}$ took on largely different values. This suggests that this parameter is not estimable.

fine-grained resolution to distinguish tree sizes well. To validate this choice of parameters and compare it to parameters used in other studies, we assessed the relationship between GPP, NPP, and NEE and the DBH entropy computed with different parameter values: $\eta = 0$ (no weighting), $\eta = 2$ (weighting by basal area), $\eta = 3$ (higher-order weighting, potentially similar to biomass) with $h = 1\,\mathrm{cm}$, respectively, and $\eta = 0$ and $\eta = 2$ with $h = 10\,\mathrm{cm}$. We used the same methods as for the analysis of the other diversity measures.

The results are displayed in Figs. S1 and S2 for the $0.04\,\mathrm{ha}$ and the $1\,\mathrm{ha}$ scale, respectively. It is visible that weighting the entropy by the basal area strengthened the relationhip with the GPP and NEE on the fine scale; for the $1\,\mathrm{ha}$ scale the relationship to the NEE became slightly weaker compared to the unweighted version of the entropy. However, weighting with a higher exponent ($\eta = 3$) worsened the results. Using a larger bandwidth, i.e., counting more trees as similar, worsened the connection between entropy and NPP and NEE. This is notable, as many studies using the DBH entropy as a measure for structural diversity consider the $1\,\mathrm{ha}$ scale (or larger), use a large bandwidth (e.g. $10\,\mathrm{cm}$; Silva Pedro et al., 2017) and do not weight the trees by basal area (e.g. Dănescu et al., 2016; Silva Pedro et al., 2017; Park et al., 2019).

## Appendix D: Model validation

To verify that our optimization procedure reliably yields good fitting results, we repeated the fitting procedure three times. We obtained estimated log-likelihood values of $-4850.32$, $-4853.39$, and $-4866.18$, respectively. Though already log-likelihood differences of 2 are significant in likelihood ratio tests and for confidence intervals, we consider the fitting procedure successful, because the stochastic optimization problem we needed to solve to fit the model is computationally difficult.

The parameter estimates we obtained in the three optimization runs are displayed in Table S1. For most parameters, the results remained in similar orders of magnitude, suggesting that the parameters are estimable despite remaining uncertainties resulting from the difficulty of the optimization problem. Only the parameter $\theta_{\mathrm{est},1}$ which controls the sharpness of the light threshold for seedling establishment took on vastly different values. This suggests that this parameter may not be estimable and may be set to a predefined value without affecting the goodness of fit significantly.

To validate that our model fits the biomass and stem count distributions from the forest inventory well, we compared a model-generated sample of these values to the sample from the inventory data that was also used in the fitting procedure. We simulated $1\,\mathrm{ha}$ of forest for a burn-in period of $2000\,\mathrm{yr}$ and sampled $25$ patches ($0.04\,\mathrm{ha}$) of the simulated forest $1000$ times in time intervals of $5\,\mathrm{yr}$. We repeated this procedure $8$ times, obtaining a sample with $200,000$ entries, corresponding to a forest of $8000\,\mathrm{ha}$.

Based on the simulated data and the field data, we created one-dimensional histograms of the biomass and stem count for each PFT. Then we plotted these histograms to study how well they overlap. The results are displayed in Figures S1 and S2,

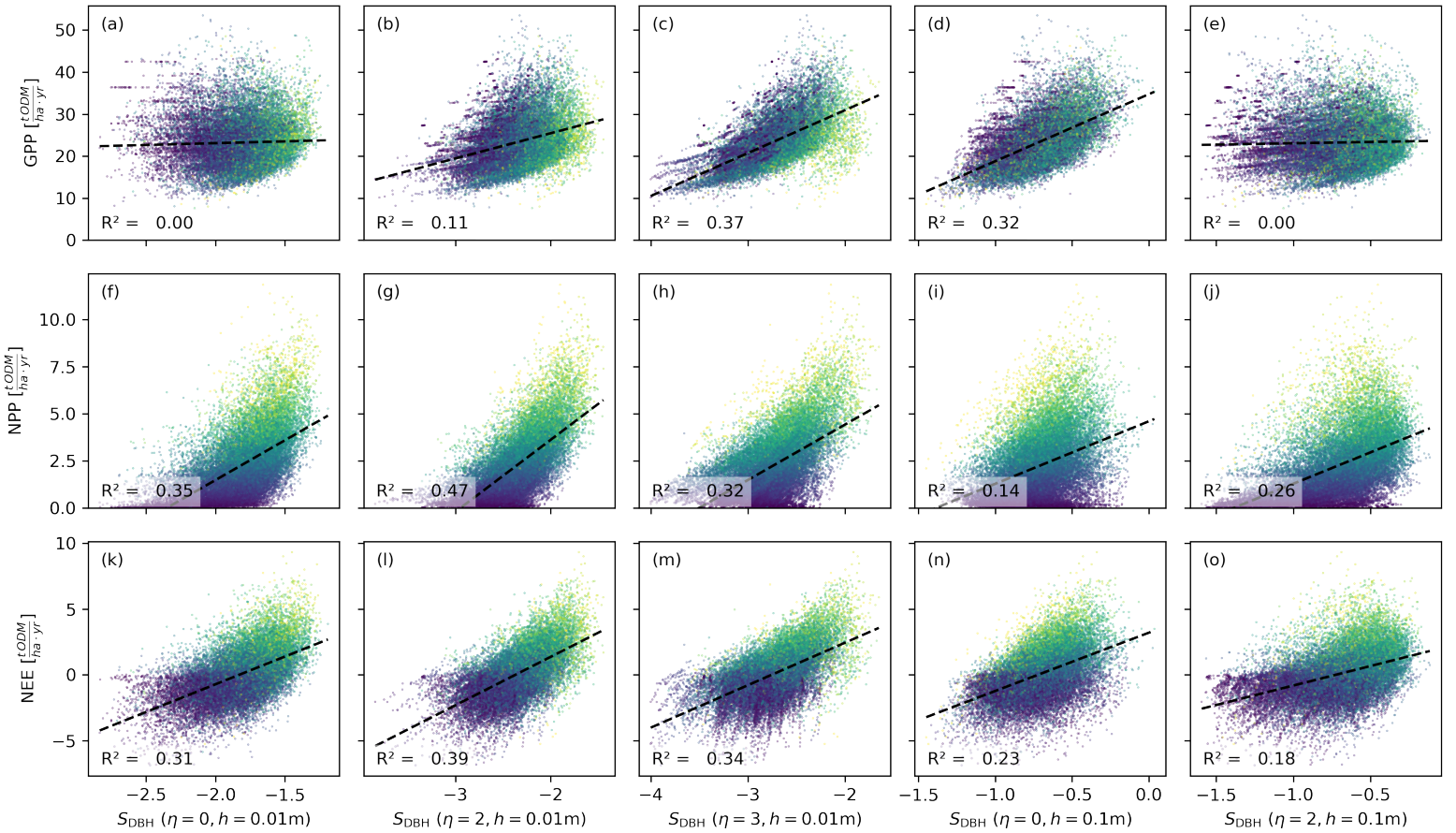


**Figure S1.** Productivity measures (GPP, NPP, and NEE) dependent on different parameters of the DBH entropy $S_{\mathrm{DBH}}$. Each dot corresponds to a $0.04\,\mathrm{ha}$ forest patch. The colour indicates the basal area proportion of mature trees (blue: only mature trees; yellow: no mature trees). The relationship between entropy and NPP or NEE is strongest if the entropy is computed with weights based on the basal area ($\eta = 2$) and a small bandwidth $h = 1\,\mathrm{cm}$, at which trees are considered similar.

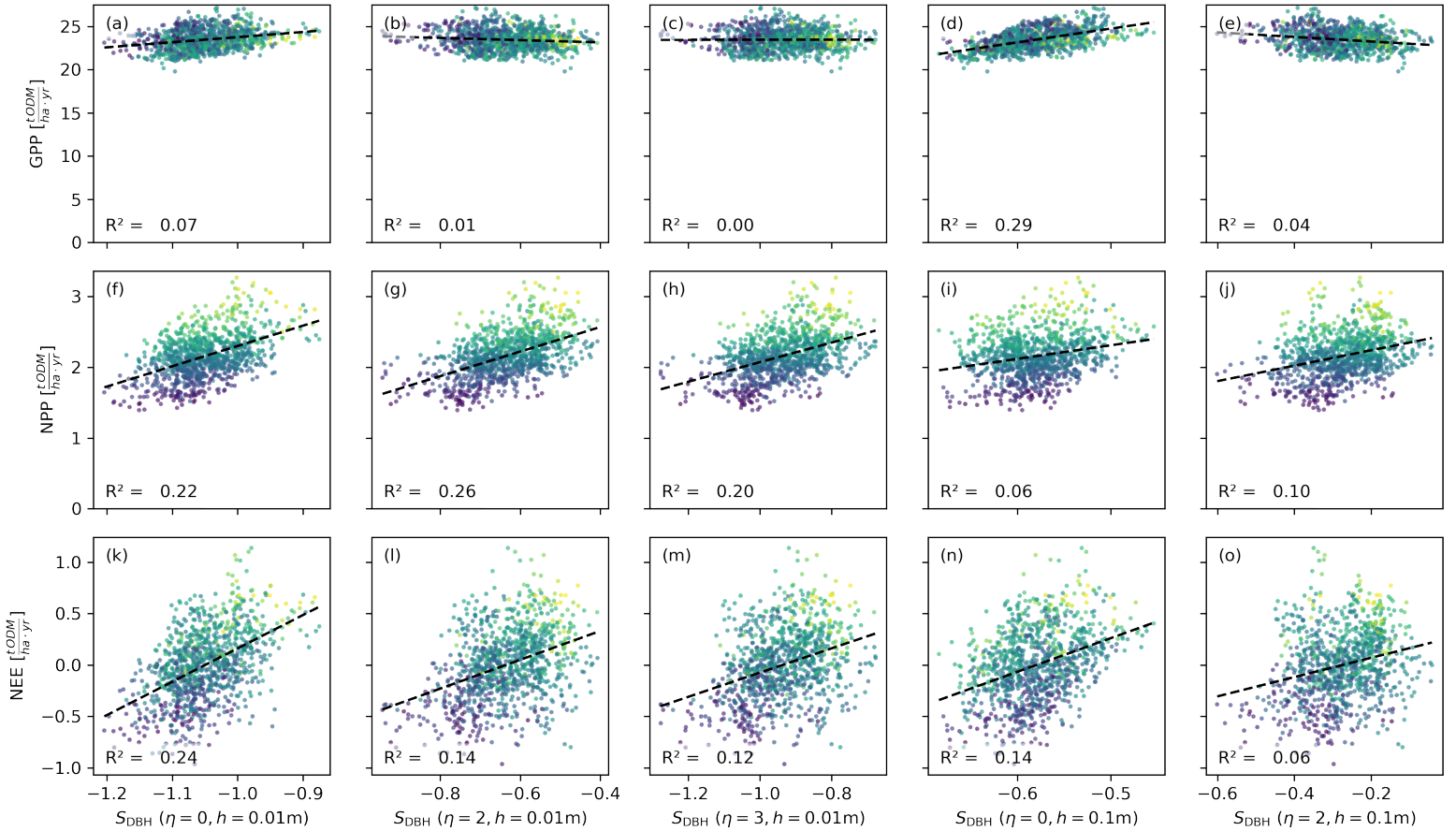


**Figure S2.** Productivity measures (GPP, NPP, and NEE) dependent on different parameters of the DBH entropy $S_{\mathrm{DBH}}$. Each dot corresponds to a 1 ha forest patch. The colour indicates the basal area proportion of mature trees (blue: only mature trees; yellow: no mature trees). The relationship between entropy and NPP is strongest if the entropy is computed with weights based on the basal area ($\eta = 2$) and a small bandwidth $h = 1\,\mathrm{cm}$, at which trees are considered similar. For the NEE, the relationship is stronger if the unweighted DBH distribution is used ($\eta = 0$).

respectively. The distributions match reasonably well, indicating a good model fit in light of the model's complexity and the large number of model features fitted simultaneously.

To also evaluate the model's ability to reproduce the joint distributions of biomass and stem count for the six PFTs, we created corresponding two-dimensional histograms, displayed in Fig. S3. The distributions from the model generally matched the patterns observed in the field data. However, the field data often covered a broader range of values than observed in the model simulation. This indicates that some sources of variation are still missing in the model.

In addition to comparing the simulation results with forest inventory data, we also computed stand-level forest characteristics (biomass, NPP, GPP, and LAI), which we then compared to estimates from independent studies (see main text). We considered a forest area of the same size ($25\,\mathrm{ha}$) as the area where the inventory was conducted. We simulated this forest for a burn-in period of $1,000\,\mathrm{yr}$. Then, we determined the forest characteristics of interest in each year for a simulation period of $3,000\,\mathrm{yr}$, yielding a quasi-independent sample with $3,000$ entries. We then determined the sample mean and standard deviation of each of the considered characteristics and used the resulting values for model validation.

## Appendix E: Variation of the CUE of mature trees

To analyze how much our results depend on the assumption that the CUE of mature trees is reduced by $100\%$, we considered three alternative scenarios, in which the CUE of mature trees was reduced by $50\%$, $25\%$, and $0\%$ compared to immature trees of the same size. For each of the scenarios, we determined how the NPP depends on the covariates considered in the other parts of this paper. Note that as we assumed that a tree's maturity status does not affect its GPP, the considered scenarios would not yield different results with respect to the GPP.

The basal area of immature trees continued to be the best considered predictor, with a reasonable predictive performance ($R^2 \geq 0.53$) even when the CUE of immature trees was only reduced by $25\%$ (Fig. S1). When the CUE was not reduced at all, the complete basal area and the basal area of immature trees had similar predictive capacity ($R^2 \approx 0.35$), and the DBH entropy became the best predictor ($R^2 = 0.4$). When the trees were weighted by their cubic diameter when computing the DBH entropy ($\eta = 3$; see SI C2), the $R^2$ values remained consistently above $0.5$ even when the CUE was not reduced (Fig. S2). The correspondingly adjusted DBH entropy became the best considered predictor if the CUE of mature trees was reduced by $25\%$ or less.

These results suggest that the maturity stage of trees remains significant even if their CUE is only mildly reduced. However, the consistently high predictive capacity of the DBH entropy even in cases where mature trees did not have a reduced CUE shows that the DBH entropy captures more productivity-related forest attributes than just the fraction of mature trees.

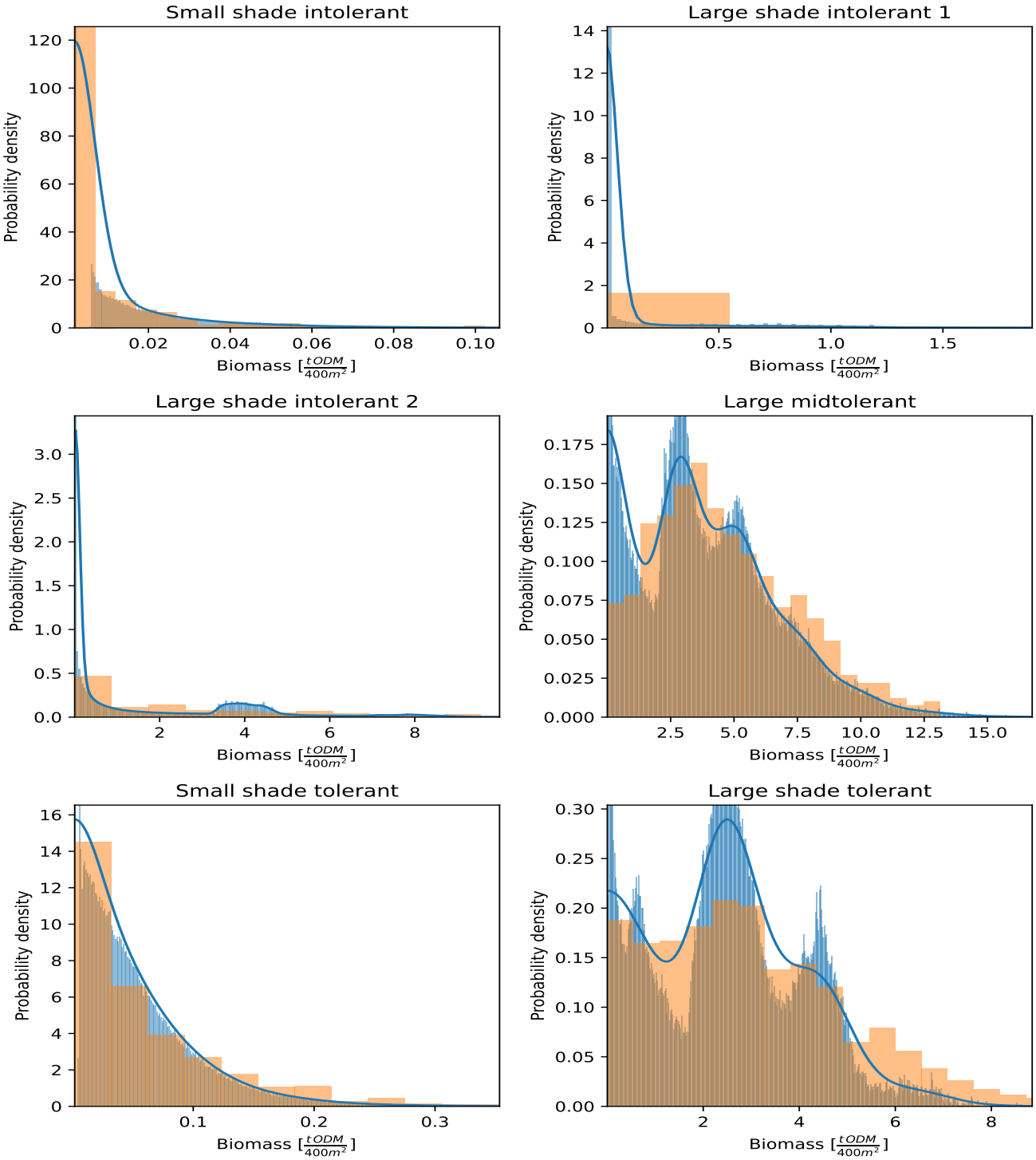


**Figure S1.** Comparison of the simulated biomass distribution with field data. The figure displays the marginal biomass distribution by PFT on the $0.04\,\mathrm{ha}$ scale. The orange bars form histograms of the biomass estimates generated based on the field data from Changbaishan. The blue bars form histograms of the biomass distributions generated from the model. The blue curves depict the kernel-smoothed density of the distribution used to estimate the likelihood. The distributions obtained from the model generally match the corresponding distributions of the field data well.

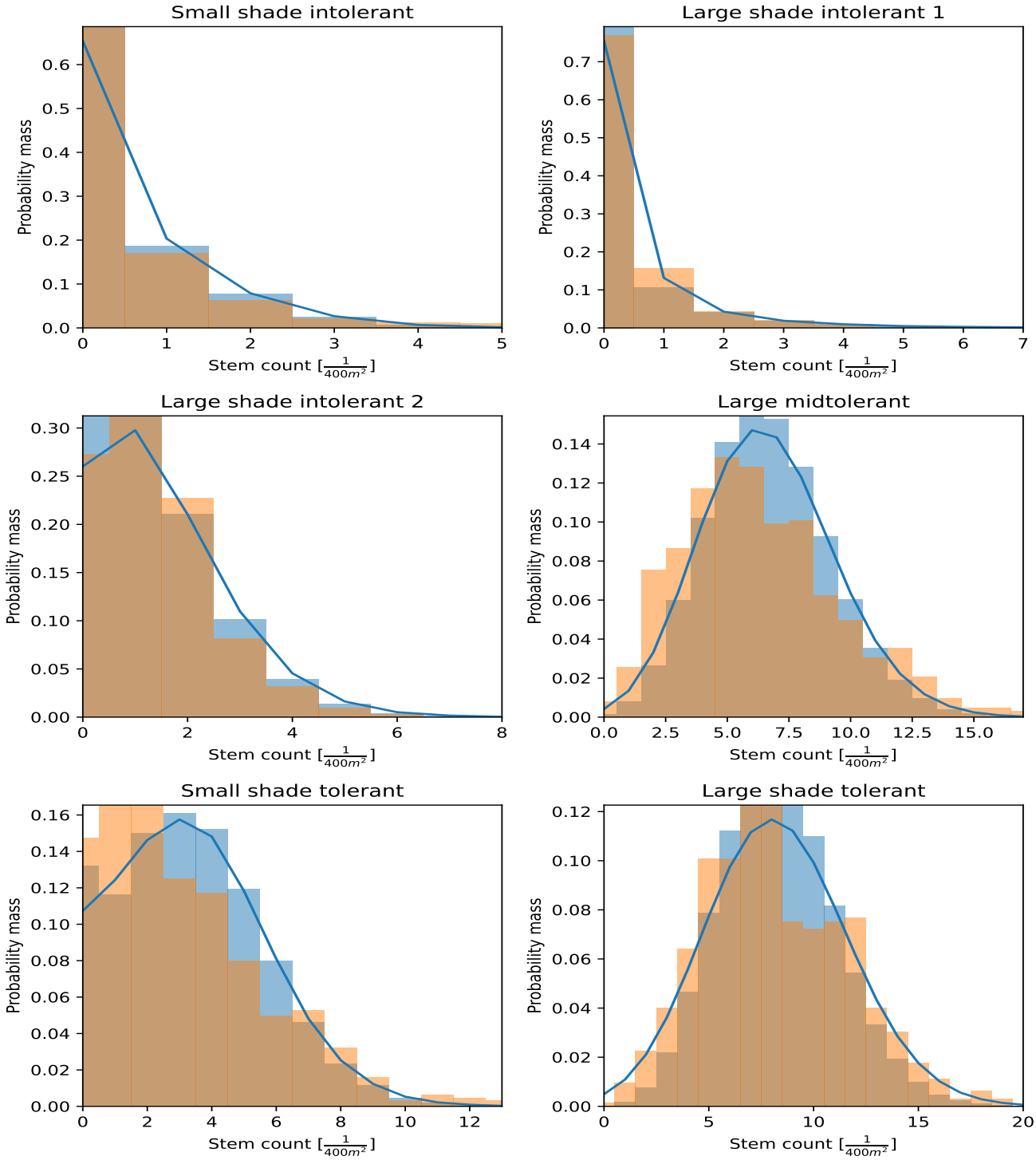


**Figure S2.** Comparison of the simulated stem count distribution with field data. The figure displays the marginal stem count distribution by PFT on the $0.04\,\mathrm{ha}$ scale. The orange bars form histograms of the stem count estimates generated based on the field data from Changbaishan. The blue bars form histograms of the stem count distributions generated from the model. The blue curves depict the kernel-smoothed density of the distribution used to estimate the likelihood. The distributions obtained from the model generally match the corresponding distributions of the field data well.

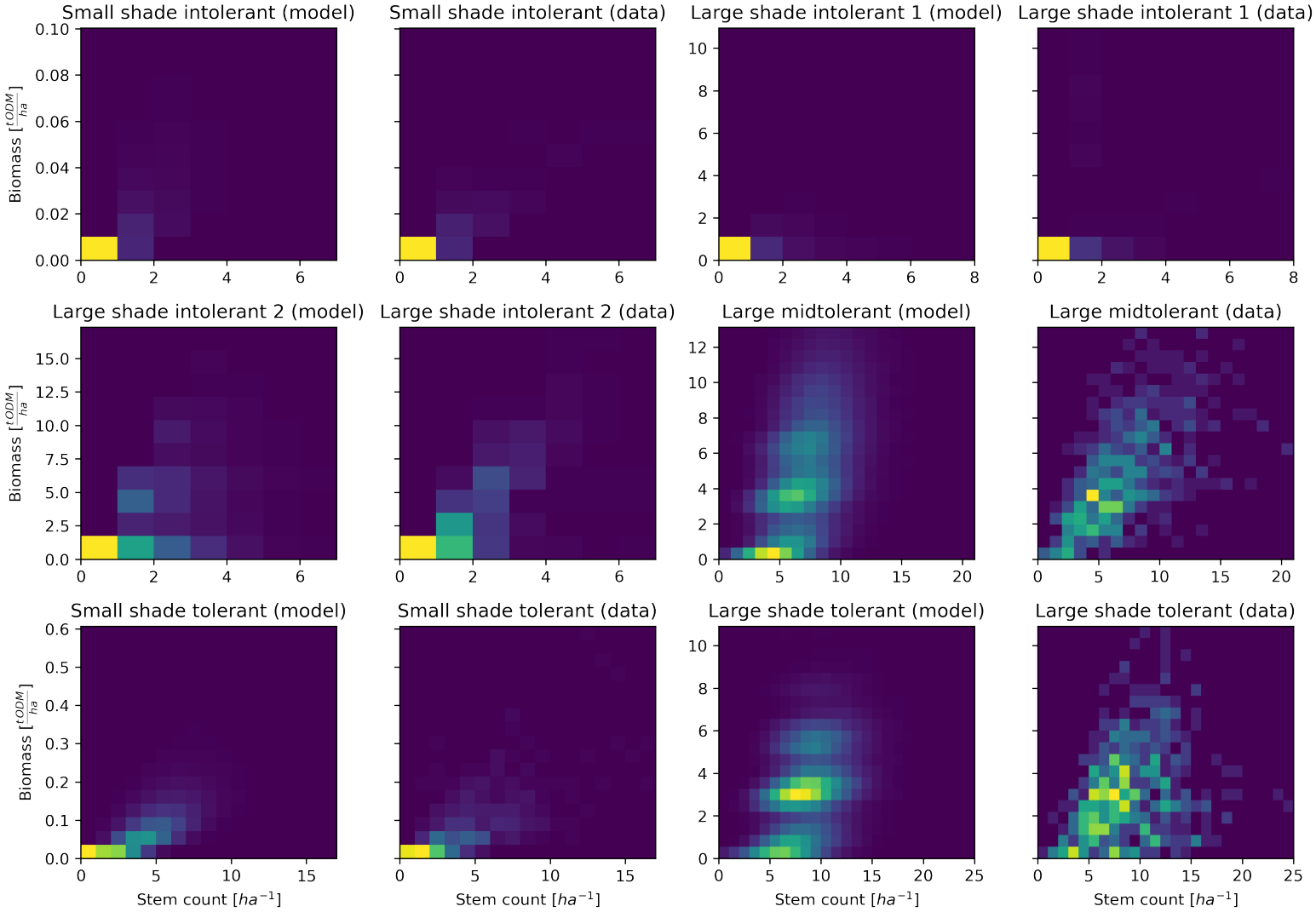


**Figure S3.** Comparison between model- and data-generated histograms of the joint biomass and stem count distributions for the six PFTs. Columns 1 and 3 show histograms obtained from model-generated samples; column 2 and 4 show histograms obtained from the field data. The main features of the histograms from the model and the data match, indicating a reasonable model fit.

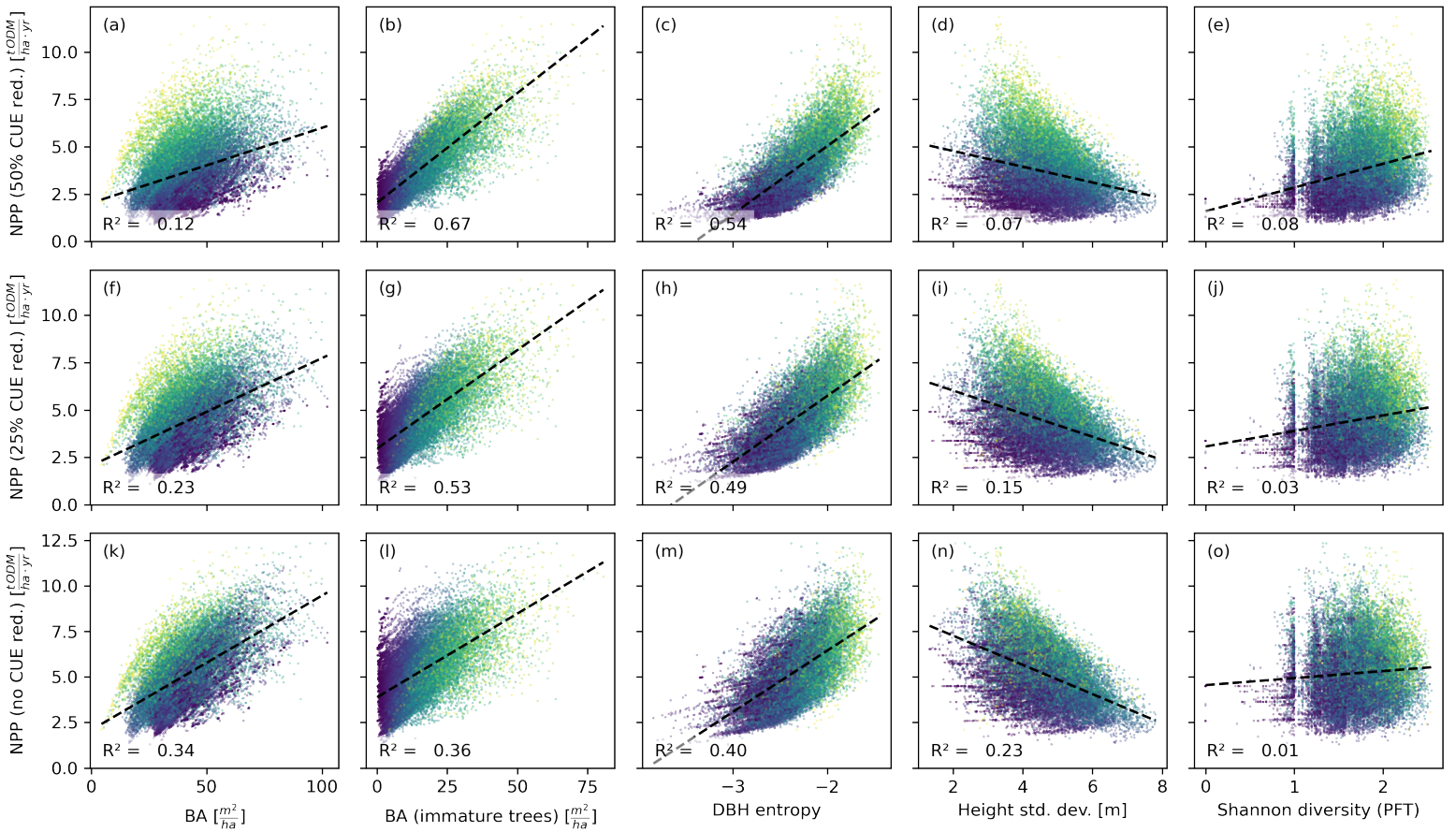


**Figure S1.** NPP dependent on different measures of basal area (BA) and heterogeneity for different CUE reduction scenarios. In the first row, the CUE of mature trees was only reduced by $50\%$ as compared to immature trees of the same size; in the second row, the CUE reduction was $25\%$, and in the third row not existent. Each dot corresponds to a $0.04\,\mathrm{ha}$ forest patch (sample size: $25,000$). The colour indicates the basal area proportion of mature trees (blue: only mature trees; yellow: no mature trees). The basal area of immature trees remains a good predictor of NPP if the CUE is only mildly reduced for mature trees. The DBH entropy is even more robust against changes in the CUE reduction.

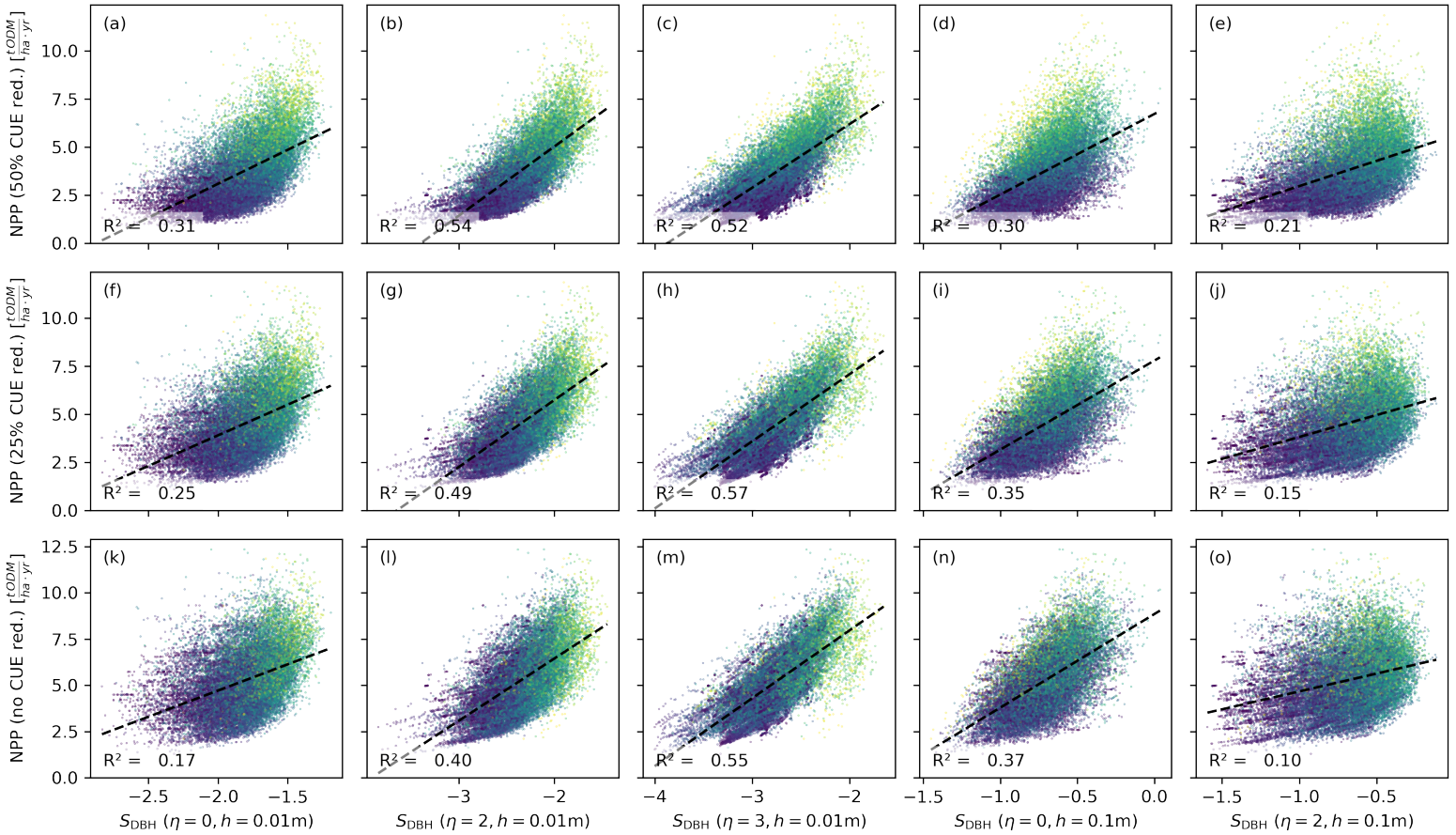


**Figure S2.** NPP dependent on different parameters of the DBH entropy $S_{\mathrm{DBH}}$ in different CUE reduction scenarios. In the first row, the CUE of mature trees was only reduced by $50\%$ as compared to immature trees of the same size; in the second row, the CUE reduction was $25\%$, and in the third row not existent. Each dot corresponds to a $0.04\,\mathrm{ha}$ forest patch. The colour indicates the basal area proportion of mature trees (blue: only mature trees; yellow: no mature trees). For a CUE reduction of $50\%$, the relationship between DBH entropy and NPP or NEE is strongest if the DBH entropy is computed with weights based on the basal area ($\eta = 2$) and a small bandwidth $h = 1\,\mathrm{cm}$; for smaller CUE reductions, computing the weights based on the cubed DBH ($\eta = 3$) and using bandwidth $h = 1\,\mathrm{cm}$ is better and leads to a higher correlation than in any of the configurations with a CUE reduction of $50\%$ and more.

## Appendix F: Further technical details

### F1 Computing the weights of the tree species in the inventory

To derive allometric relationships for the different PFTs, we used data available for individual species, weighted according to their respective prevalence in the inventory. Here we describe how we computed these weights.

For every sufficiently large tree $K$ in the forest inventory, we added one unit of weight to the data points in the allometry dataset that corresponded to trees of the same species with most similar DBH. Trees with DBH below $5\mathrm{cm}$ were ignored, as they are not considered in the model (see section B6). Let $\mathcal{A}$ be an index set for the allometry dataset (ignoring entries with DBH below $5\mathrm{cm}$) and $s_k$ be the species corresponding to $k \in \mathcal{A}$. Let furthermore $\mathcal{A}_k^+ = \left\{\tilde{k} \in \mathcal{A} : \tilde{k} = s_k, d_{\tilde{k}} > d_k\right\}$ the entries in the allometry dataset that correspond to the same species and a larger DBH, and define $\mathcal{A}_k^= = \left\{\tilde{k} \in \mathcal{A} : \tilde{k} = s_k, d_{\tilde{k}} = d_k\right\}$ and $\mathcal{A}_k^- = \left\{\tilde{k} \in \mathcal{A} : \tilde{k} = s_k, d_{\tilde{k}} < d_k\right\}$ correspondingly for entries with equal or smaller DBH, respectively. Define

$$d_k^+ = \begin{cases} \min\limits_{\tilde{k} \in \mathcal{A}_k^+} d_{\tilde{k}} & \text{if } \mathcal{A}_k^+ \neq \emptyset \\ d_k & \text{else} \end{cases} \tag{S1}$$

and

$$d_k^+ = \begin{cases} \max\limits_{\tilde{k} \in \mathcal{A}_k^-} d_{\tilde{k}} & \text{if } \mathcal{A}_k^- \neq \emptyset \\ d_k & \text{else} \end{cases} \tag{S2}$$

as the smallest larger and the largest smaller DBH of an entry in the allometry dataset corresponding to the same species. The contribution $v_{Kk}$ of tree $K$ in the inventory to the weight of entry $k$ in the allometry dataset is given by

$$v_{Kk} = \begin{cases} 1 & \text{if } d_K = d_k, \\ 1 & \text{if } d_K > d_k = d_{s_k}^{\max}, \\ 1 & \text{if } d_K < d_k = d_{s_k}^{\min}, \\ \frac{d_k^+ - d_K}{d_k^+ - d_k} & \text{if } d_K \in \left(d_k, d_k^+\right), \\ \frac{d_K - d_k^-}{d_k - d_k^-} & \text{if } d_K \in \left(d_k^-, d_k\right), \\ 0 & \text{else.} \end{cases} \tag{S3}$$

That is, the contribution is $1$ if the diameters are equal or if the the tree diameter is outside the range of diameters covered in the allometry dataset and the allometry data entry has maximal or minimal diameter, respectively. The weights are then computed

as follows:

$$w_k = c_{\mathrm{class}(s_k)} \sum_{K \in \mathcal{I}_{s_k}} \frac{v_{\kappa k}}{|\mathcal{A}_k^=|}, \tag{S4}$$

where $c_{\mathrm{class}(s_k)}$ is a normalization constant for the PFT $\mathrm{class}(s_k)$ to which species $s_k$ belongs, $\mathcal{I}_{s_k}$ is the subset of trees in the inventory that are of species $s_k$, and $|\cdot|$ denotes the counting norm. The division by the cardinality of $\mathcal{A}_k^=$ distributes the contribution of tree $K$ evenly among all allometry entries with similar species and diameter. As a result, each tree in the inventory makes the same total contribution to the weights.

The normalization constants $c_{\mathrm{class}(s_k)}$ do not affect parameter estimation, but we chose

$$c_j = \frac{|\mathcal{A}_j|}{\sum_{k \in \mathcal{A}_j} \sum_{K \in \mathcal{I}_{s_k}} \frac{v_{\kappa k}}{|\mathcal{A}_k^=|}} \tag{S5}$$

so that the sum of the weights corresponds to the size of the dataset used to fit the allometry curve for PFT $j$. As a result, the likelihood computed using the weights may be of the same order of magnitude as the unweighted likelihood, which can be helpful for model comparison and selection.

To compute the weights efficiently, we sorted both the allometry dataset and the inventory by tree DBH and species. Then, the weights can be computed in linear time of the inventory dataset size (assuming that there are only few entries in the allometry dataset that have both the same species and DBH).

### F2 Assignment of new seeds to patches

Each year, a constant number of seeds is distributed evenly to the different modelled forest patches. If the provided seed number is not an integer divisible by the number of simulated patches, the seed number is rounded stochastically for each patch so that the expected number of seeds per hectare and PFT matches the provided seed number. That is, if $n_{\mathrm{seeds},i}$ is the number of seeds per hectare for PFT $i$ and $n_{\mathrm{patches}}$ the number of simulated patches, then the number of seeds for a patch $j$ is given by

$$n_{\mathrm{seeds},i,j} = \left\lfloor \frac{n_{\mathrm{seeds},i}}{n_{\mathrm{patches}}} \right\rfloor + B_{p_{\mathrm{seed}}}, \tag{S6}$$

where

$$B_{p_{\mathrm{seed}}} \sim \mathrm{Bernoulli}(p_{\mathrm{seed}}) \tag{S7}$$

is a Bernoulli distributed random variable with success probability

$$p_{\mathrm{seed}} = \frac{n_{\mathrm{seeds},i}}{n_{\mathrm{patches}}} - \left\lfloor \frac{n_{\mathrm{seeds},i}}{n_{\mathrm{patches}}} \right\rfloor. \tag{S8}$$